# Moisture movement and drying stresses in wood( Dissertation_全文 )

AUTHOR(S):

Kawai, Shuichi

CITATION:

Kawai, Shuichi. Moisture movement and drying stresses in wood. 京都大学, 1980, 農学博士

ISSUE DATE:

1980-03-24

URL:

https://doi.org/10.14989/doctor.k2380

# MOISTURE MOVEMENT AND DRYING STRESSES IN WOOD

1980

SHUICHI KAWAI

KYOTO UNIVERSITY

# MOISTURE MOVEMENT AND DRYING STRESSES IN WOOD

A DISSERTATION SUBMITTED TO
THE FACULTY OF AGRICULTURE
IN CANDIDACY FOR THE DEGREE OF
DOCTOR OF AGRICULTURE

BY
SHUICHI KAWAI

1980

CONTENTS

CONTENTS -CONTINUED-

PART THREE PREDICTION OF DRYING STRESSES IN WOOD

# INTRODUCTION

Wood, compared with other materials, is not an excellent material which has a special merit in physical properties, but rather a mediocre material: each property of wood such as strength of every kind, decay and chemical resistance, thermal and electrical conductivity, and working qualities, is not significantly superior to that of other materials. However, when evaluated from the point of view of balance among these properties, wood can be regarded as one of the best materials.

One of the characteristic features of wood is that its properties are affected by enviromental conditions such as the humidity and temperature of the atmosphere. Many studies on the relation of water to wood have been made, mainly because wood is an organic and hygroscopic material. There were, for example, studies on water movement in wood, sorption of water by wood, swelling and shrinking owing to water sorption, effect of water on the physical and the mechanical properties of wood, and drying stresses and defects.

Water movement in wood is particularly important in wood science. However, both qualitative and quantitative analysis in this field has not been completely successful so far, because several mechanisms are responsible for this phenomenon. Drying stresses resulting from moisture gradients in wood during drying

have been investigated by use of the slicing technique from the mechanical point of view. However, the quantitative analysis of the drying stresses in relation to water movement in wood has never been studied.

The present study deals with water movement in wood in the hygroscopic range. The moisture content of wood in use usually falls in this range, where the water strongly affects wood properties. The study concerns drying stresses resulting from moisture gradients in wood during drying on the basis of the theory for moisture movement in wood.

The present paper consists of three parts:

PART ONE, where the equation for representing moisture movement in wood is discussed. Based on thermodynamics of irreversible processes, the relationship between flux and the driving force for it is considered. A diffusion equation is proposed and examined by use of experimental data;

PART TWO, where a predictive method for moisture distribution in wood during drying is discussed by use of numerical solutions of the proposed diffusion equation; and

PART THREE, where a computational method and its application for drying stresses resulting from moisture gradients in wood during drying are discussed on the basis of the theory of moisture movement and the predictive method for moisture distribution in wood.

# PART ONE

# MOISTURE MOVEMENT IN WOOD IN THE HYGROSCOPIC RANGE

Fick's law of diffusion has commonly been applied to the moisture movement in wood below the fiber saturation point. However, few reports have discussed the validity of this application; it has been a fundamental postulate.

In this part, the moisture movement in wood is treated by the method of thermodynamics of irreversible processes: a theoretical equation is derived by considering the relationship between mass flux and the driving force. Then the theory is examined on the basis of the experimental data.

## 1-1. *Moisture Distribution*

### 1-1.1. Experimental Method

a) Theory

In order to analyze moisture movement in wood, it is necessary to describe the phenomenon quantitatively. The most direct method is to chart changes in moisture content of wood with time and position,i.e., is to measure moisture distribution as a function of time. Sectioning the specimen as practiced until recently is not a good method because of its inaccuracy; a new method

using soft X-ray densitometry has been developed for this purpose. In wood science, it has been applied to the measurement of density distribution in fiber-board or particle-board[1)-5)] and within growth rings[6)7)]. The theory of moisture distribution measurement by means of X-ray densitometry[8)] is as follows:

When an exposure dose $\Phi_0$ of soft X-ray per unit area is incident on a substance of mass $m$, the transmitted dose $\Phi$ can be expressed as

$$\ln(\Phi/\Phi_0) = -\lambda m \qquad (1\text{-}1.1)$$

where $\lambda$ is the absorption coefficient, i.e., an inherent coefficient of the substance. Wood at a certain moisture content $u$ is considered to be a composite material of wood substance and water. If the absorption coefficient of wood substance and water, and their mass per unit area perpendicular to the emitting axis are denoted in terms of $(\lambda_s, m_s)$ and $(\lambda_w, m_w)$, respectively, and if additivity of Eq.(1-1.1) is assumed for this composite system, the transmitted dose $\Phi$ can be expressed as

$$\ln(\Phi/\Phi_0) = -(\lambda_s m_s + \lambda_w m_w) \qquad (1\text{-}1.2)$$

When $\Phi_0$ is incident on a reference substance, where the thickness parallel to the emitting axis, the specific gravity, the mass, and the absorption coefficient are denoted in terms of $d_0$, $\rho_r$, $m_r$, and $\lambda_r$, respectively, the transmitted dose $\Phi'$ is

$$\ln(\Phi'/\Phi_0) = -\lambda_r m_r = -\lambda_r \rho_r d_0 \qquad (1\text{-}1.3)$$

When the transmitted dose $\Phi'$ of the reference substance at thickness $d_1$ equals the dose $\Phi$ of the specimen at moisture

content $u$, then from Eqs.(1-1.2) and (1-1.3),

$$\lambda_s m_s + \lambda_w m_w = \lambda_r \rho_r d_1 \qquad (1\text{-}1.4)$$

Similarly, when the transmitted dose $\Phi'$ of the reference at thickness $d_2$ equals that of the specimen in the oven-dry state, then

$$\lambda_s m_s = \lambda_r \rho_r d_2 \qquad (1\text{-}1.5)$$

By substitution of Eq.(1-1.5) into Eq.(1-1.4),

$$\lambda_w m_w = \lambda_r \rho_r (d_1 - d_2) \qquad (1\text{-}1.6)$$

When the transmitted dose $\Phi'$ of the reference at thickness $d_3$ equals that of the known amount of water $m_w'$, then

$$\lambda_w m_w' = \lambda_r \rho_r d_3 \qquad (1\text{-}1.7)$$

From Eq.(1-1.6) the mass $m_w$ of the water in wood is given as

$$m_w = \frac{\lambda_r}{\lambda_w} \rho_r (d_1 - d_2) \qquad (1\text{-}1.8)$$

Therefore, by substitution of Eq.(1-1.8) into Eq.(1-1.7)

$$m_w = \frac{m_w'}{d_3} (d_1 - d_2) \qquad (1\text{-}1.9)$$

In practice, the transmitted dose of soft X-ray blackens X-ray film placed under the specimen and the reference during exposure. The radiograph obtained is then scanned with a densitometer. By comparison of the density record of the reference with that of the specimen, the thickness $d_1$, $d_2$, and $d_3$ can be obtained, and $m_w'$ is a known amount. Therefore, the mass $m_w$ of

the water in wood can be estimated. The moisture content $u$ is

$$u = \frac{m_w}{m_s} = \frac{m_w'(d_1-d_2)}{m_s d_3} \qquad (1\text{-}1.10)$$

b) Experimental

In order to measure the changes in moisture distribution in the longitudinal direction of wood during drying, specimens were taken from Hinoki (*Chamaecyparis Obtusa* Endl.) heart wood with oven-dry specific gravity of 0.34 g/cm$^3$. Along the longitudinal direction serial specimens were prepared with dimensions of 10(L)×10(T)×50(R)mm. The radial and the tangential surfaces of the specimens were sealed with adhesive tape in order to limit drying to the end surface so that moisture gradients were formed only in the longitudinal direction. Since the main component of this tape was an acetate film, it was almost nonpermeable, and was readily attached or removed.

Specimens were conditioned to approximately 23% m.c. in moist air at the same temperatures as used in subsequent drying experiments. It was observed that there were no weight changes of the specimens during the last few days of conditioning, and it was confirmed by X-ray densitometry that there was uniform moisture distribution in the specimens.

The drying apparatus consisted of two chambers, as Fig.1.1 shows; the front chamber was for setting up specimens, and the back for controlling temperature and humidity. The front window was made of two sheets of plate glass between which a resistance coil heater was inserted in order to reduce the temperature gradients in the chamber and to avoid condensation on the

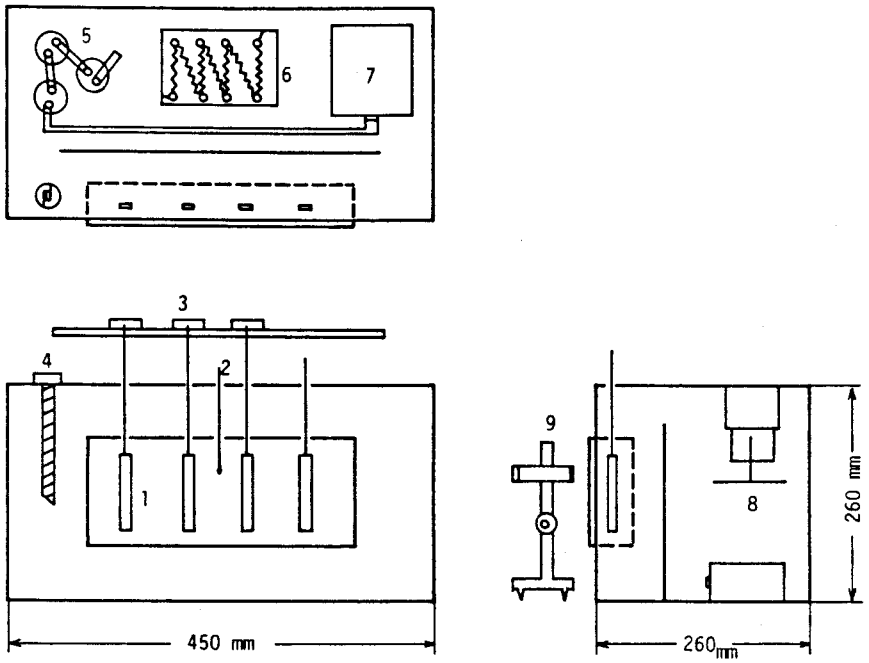


Fig.1.1 Drying apparatus
1. Specimen, 2. Thermistor, 3. Load cell, 4. Thermostat,
5. Vapor source (Saturated salt solutions), 6. Heater,
7. Air pump, 8. Fan, 9. Travelling microscope.

plate glass. An electric heater was used for the main heat source, and the temperature was controlled by use of a thermostat. The humidity was controlled by use of saturated salt solutions in three bottles combined with an air pump. Table 1.1 shows the drying conditions.

The specimens were taken out from the drying apparatus at appropriate time-intervals during drying. Immediately the water in the specimens was fixed by means of dry ice, the specimens were put on X-ray films and were placed directly beneath the X-ray generator, as shown in Fig.1.2. Soft X-ray was then applied to the specimens in a direction normal to the longitudinal direction of the specimens. Then, the specimens were oven-dried,

Table 1.1 Drying conditions used for measuring moisture distributions

| No. | Temp. (°C) | Relative vapor pressure [9] | Salt used | Initial moisture content (g/g) | Final moisture content (g/g) |
|---|---|---|---|---|---|
| 1 | 20 | 0.76 | NaCl | 0.246 | 0.181 |
| 2 | | 0.335 | $MgCl_2$ | 0.246 | 0.141 |
| 3 | 40 | 0.75 | NaCl | 0.260 | 0.082 |
| 4 | | 0.00 | $CaCl_2$ *1 + Silica-gel | 0.230 | 0.024 |
| 5 | 50 | 0.745 | NaCl | 0.225 | 0.084 |
| 6 | | 0.31 | $MgCl_2$ | 0.224 | 0.069 |
| 7 | 60 | 0.74 | NaCl | 0.222 | 0.078 |
| 8 | | 0.30 | $MgCl_2$ | 0.220 | 0.053 |

*1 This is not used in solution, but in the dry condition.

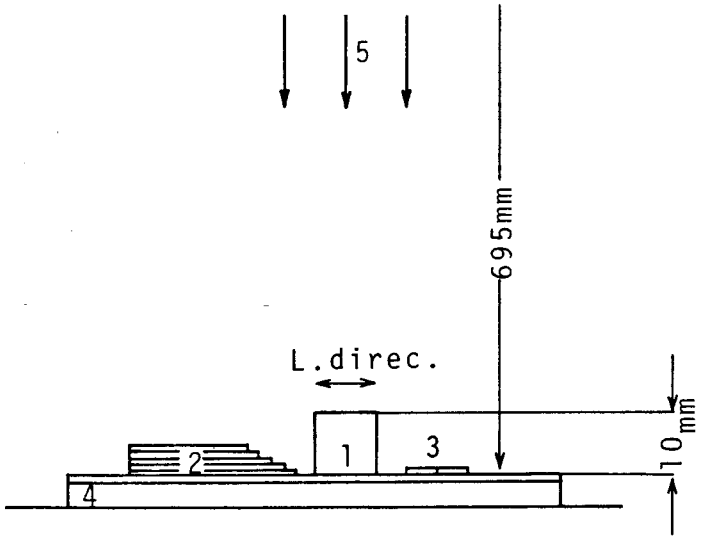


Fig.1.2 Schematic diagram of soft X-ray densitometry
1. Specimen, 2. Reference, 3. Film mark,
4. Soft X-ray film, 5. Soft X-ray beams.

and soft X-ray was again applied to the specimens. The soft X-ray apparatus used was of type EMB made by Softex Co.Ltd., and the films were of fine-grained Fuji Softex film. The exposure settings were the following: 34 kVp and 2 mA, focal spot to film distance 695 mm, and exposure time 75 sec. As a reference, density-calibration wedges were made of polyester films (0.155±0.001 mm thickness) to which silver particles were attached.

The X-ray negatives, obtained by careful development[10], were scanned along the longitudinal direction with a slit width and height of 0.1 and 10 mm, respectively, by means of a Recording Spectrophotometer made by Shimazu Mfg.Co.Ltd., and the density distributions were recorded. Fig.1.3 shows examples of density profiles along the longitudinal direction of wood obtained by soft X-ray densitometry.

The wood specimens shrink when they are oven-dried, and it is necessary to take the effect of shrinkage on density into consideration. As Fig.1.2 shows, soft X-ray is emitted in the direction normal to the radial surface, and the radiograph obtained is scanned along the longitudinal direction. Therefore, the moisture distribution in the longitudinal direction of specimen is corrected as follows:

A small element of wood volume in the slit is considered. On the assumption that the average moisture content of the element is given in terms of $u$ when X-raying, and that the dimensions in the principal directions of the element are $(l_u)_L$, $(l_u)_R$, and $(l_u)_T$, the mass $m_s$ of the wood substance of this element is given by

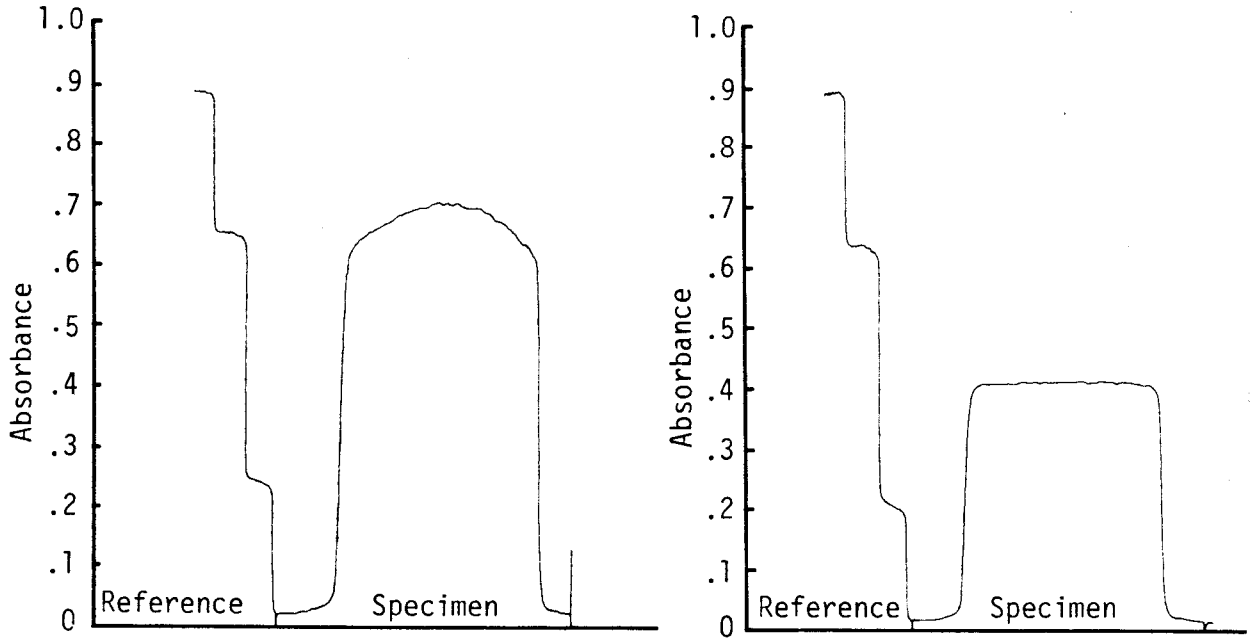


Fig.1.3 Density profile through the longitudinal direction of wood on X-ray film
a) Drying condition: 40°C,74%RH. 0.186 average m.c.
b) Oven-dry condition

$$m_S = \rho_0 (l_u)_L (l_u)_R (l_u)_T (1-\Delta\alpha_L)(1-\Delta\alpha_R)(1-\Delta\alpha_T) \qquad (1\text{-}1.11)$$

where $\rho_0$ is the oven-dry density of the wood element, and $\Delta\alpha_L$, $\Delta\alpha_R$, and $\Delta\alpha_T$ the shrinkage values between the moisture content $u$ and the oven dry state in the three principal directions.*1

---

*1 The dimensions of the specimen in a particular direction in the green state, at the moisture content $u$, and in the oven-dry state are denoted in terms of $l_g$, $l_u$, and $l_0$, respectively. The shrinkage $\alpha_u$ to moisture content $u$ is given as $(l_g-l_u)/l_g$, and the shrinkage $\alpha_0$ to the oven-dry state as $(l_g-l_0)/l_g$. Since $\Delta\alpha=(l_u-l_0)/l_u \simeq \alpha_0-\alpha_u$ ($\because l_u \simeq l_g$), the oven-dry dimension $l_0$ can be expressed as $l_0=l_u(1-\Delta\alpha)$.

On the other hand, the mass $m_w$ of water in the element is expressed as

$$m_w = \beta(l_u)_L(l_u)_R\{d_1-d_2(1-\Delta\alpha_L)(1-\Delta\alpha_R)\} \qquad (1\text{-}1.12)$$

where $\beta = m_w/d_3$, i.e., the mass of water per unit area and per unit film of reference. Therefore, the corrected moisture content $u$ in the element is

$$u = \frac{m_w}{m_s} = \frac{\beta\{d_1-d_2(1-\Delta\alpha_L)(1-\Delta\alpha_R)\}}{\rho_0(l_u)_T(1-\Delta\alpha_L)(1-\Delta\alpha_R)(1-\Delta\alpha_T)} \qquad (1\text{-}1.13)$$

if $1-\Delta\alpha_L \simeq 1$, then

$$u = \frac{m_w}{m_s} = \frac{\beta\{d_1-d_2(1-\Delta\alpha_R)\}}{\rho_0(l_0)_T(1-\Delta\alpha_R)} \qquad (1\text{-}1.14)$$

where $(l_0)_T$ is the oven-dry dimension in the tangential direction. $\beta$ was obtained as 0.0814 g/cm$^2$reference, in comparison to the film of reference with known amount of water. Also, the effect of parallax distortions and of density difference between liquid and solid water on the density distribution were examined by preliminary experiments.

### 1-1.2. Results and Discussion

Fig.1.4 shows drying curves under the various conditions. The same specimen could not be used during the whole drying period, so some scatter is observed in the curves. The degree of scatter is however very small, and the drying may be considered to be well-conducted.

Moisture distribution along the longitudinal direction of wood at each time $t_M$ was measured in each specimen. Fig.1.5

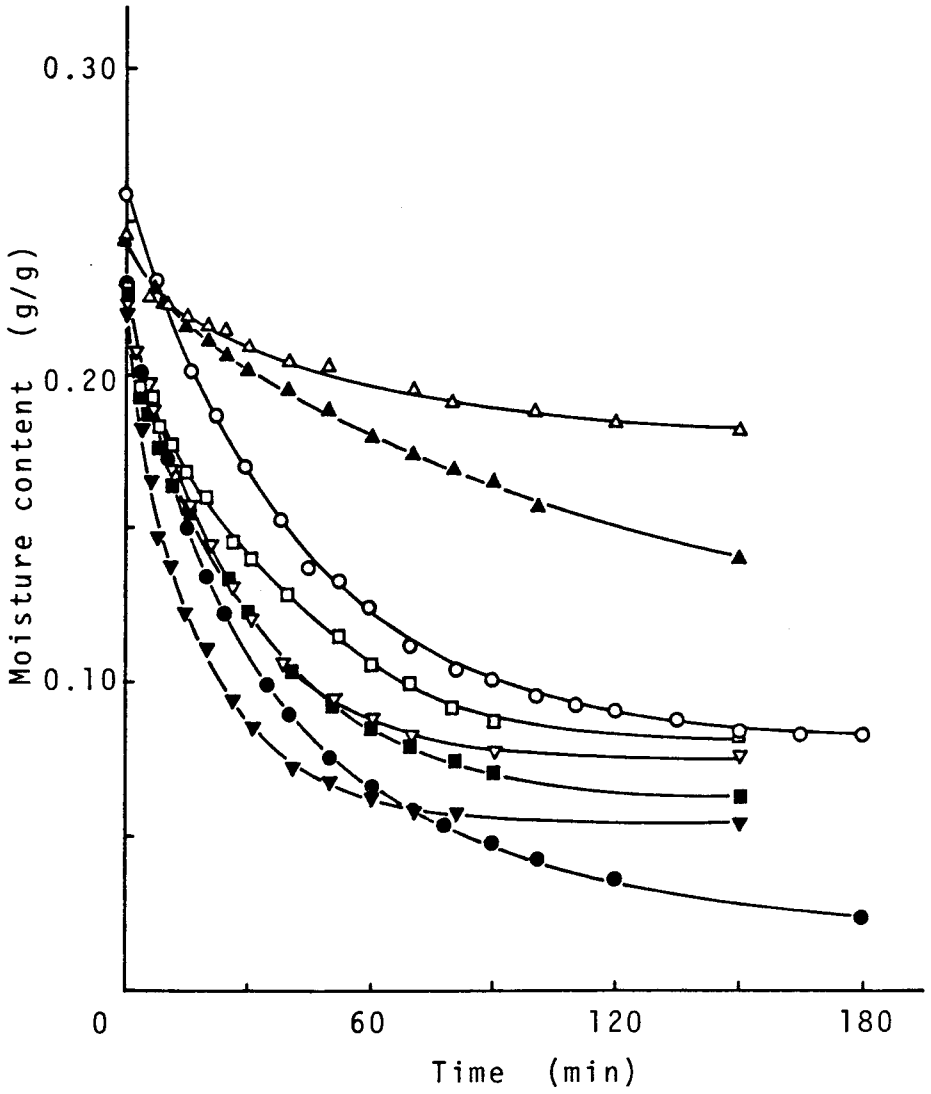


Fig.1.4 Drying curves

Drying conditions

△ : No.1, ▲ : No.2, ○ : No.3, ● : No.4,

□ : No.5, ■ : No.6, ▽ : No.7, ▼ : No.8.

shows the moisture distributions as a function of time for different drying temperatures. The same specimen was not used, and the average moisture content at time $t_M$ was not the same for each drying condition. Therefore, the moisture contents at positions of 0.0, 0.1, 0.2, 0.3, 0.4, and 0.5 cm from the wood

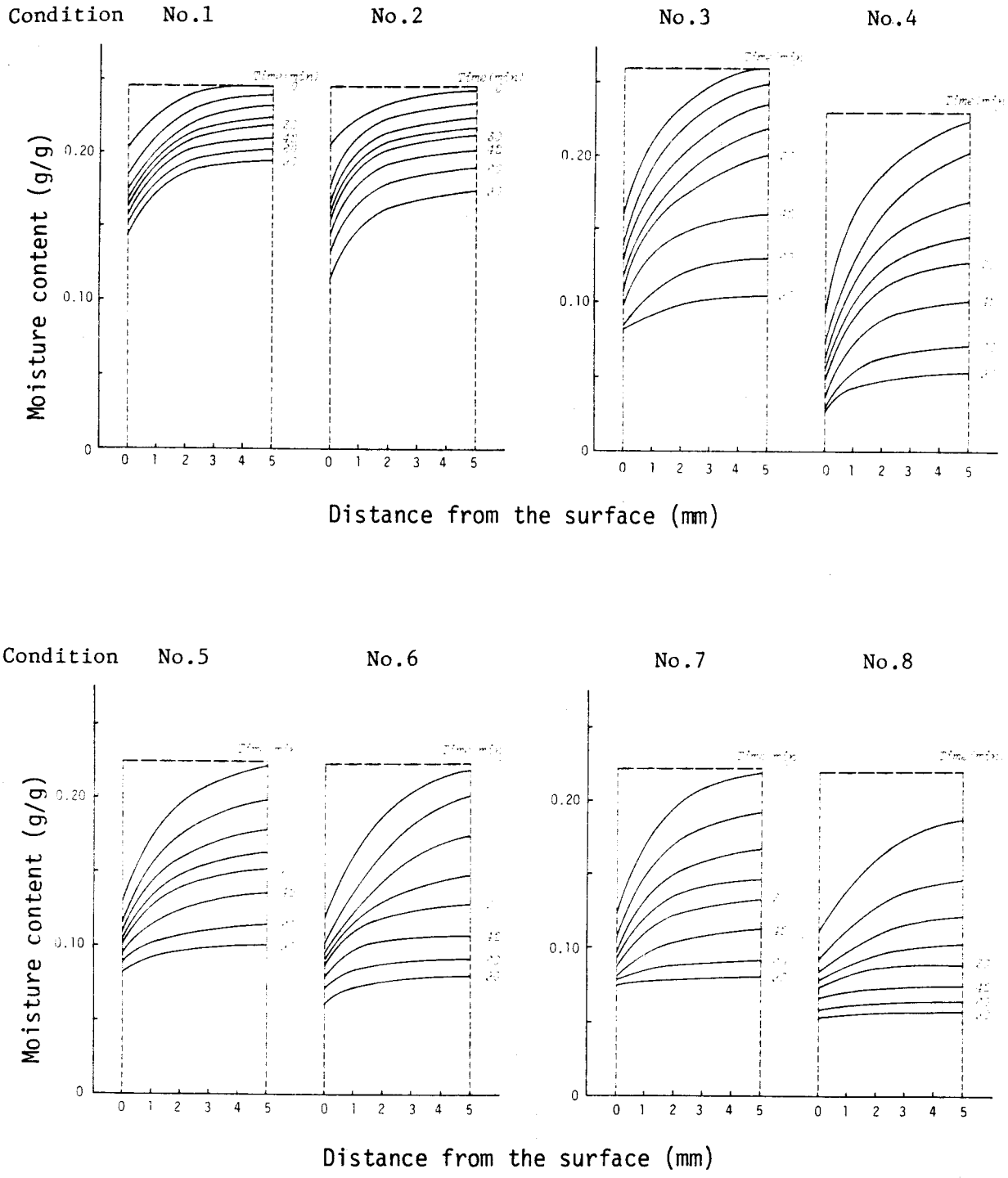


Fig.1.5 Moisture distributions at various times during drying at constant temperatures of 20, 40, 50, and 60°C dry bulb

surface were interpolated for the whole drying period, by use of the relationship between the average moisture content obtained by oven-dry method and the moisture content at each position obtained by soft X-ray densitometry. The figure shows the moisture distributions at 6 minutes intervals from the start of drying up to 30 minutes and thereafter at 42, 60, and 90 minutes. It is apparent from the figure that all the moisture distributions are parabolic curves. The surface moisture content decreases rapidly at the early stages of drying; the moisture gradient becomes steep. At temperatures of 40, 50, and 60°C, the core moisture content decreases faster than the surface moisture content, and the moisture gradient becomes less steep. The moisture content of the specimen then approaches equilibrium. On the other hand, at 20°C the rate of drying is extremely slow, and even the surface moisture content does not reach equilibrium in the time span of 90 min covered by the experiments. The moisture distribution from the surface to the core maintains a similar shape throughout, and the specimen is dried very gradually.

The main features of the measurement of moisture distribution by use of soft X-ray densitometry are as follows:

1) Specimens are not destroyed.
2) Continuous moisture distribution measurements in small specimens can be made.
3) The experimental error is evaluated to be less than 1% m.c., based on the average moisture content measured by oven-dry method and by soft X-ray densitometry. Moisture distributions can be obtained with adequate accuracy.

4) Errors in measurements of surface moisture content are rather great.

5) In this study, the same specimen could not be used during the entire drying period. To do this, the X-ray apparatus would have to be combined with the drying apparatus, and then further improvement of accuracy can be expected.

## 1-2. *Theory of Moisture Movement in Wood*

### 1-2.1. Fick's Law

Fick's law of diffusion is usually applied to describing diffusion phenomena in materials, and most of the studies of moisture movement in wood below the fiber saturation point have also been based on this law. For example, the diffusion coefficient of moisture in wood has been calculated in various moisture content and temperature ranges. These diffusion coefficients, as reported, do not always agree with each other, but most of them are calculated on the basis of the assumption that the moisture movement in wood obeys Fick's law. However, the validity of the application of Fick's law to the moisture diffusion in wood has not been proved and remains merely an assumption.

Fick's law of diffusion under a non-equilibrium state is derived as follows: Fig.1.6 shows a uni-dimensional flow in a small rectangular element of volume. It is assumed that the flux $F$ of mass per unit area and unit time is proportional to the concentration gradient $dC/dx$. Since the flux along the $x$-axis in the small body is given as the difference between the

inward flux and the outward flux during the time $dt$, the total rate of accumulation of mass is clearly

$$F_x = \{-D_c(x)\frac{\partial C}{\partial x} + D_c(x+dx)\frac{\partial}{\partial x}(C+\frac{\partial C}{\partial x}dx)\}dydzdt \qquad (1\text{-}2.1)$$

where $D_c$ is the diffusion coefficient. Subscript $x$ stands for the coordinate of the flow.

When the diffusion coefficient is independent of conentration and is a constant, then

$$D_c(x) = D_c(x+dx)$$

Therefore, Eq.(1-2.1) takes the form

$$F_x = D_c\frac{\partial^2 C}{\partial x^2}dxdydzdt \qquad (1\text{-}2.2)$$

When the diffusion coefficient is dependent on the concentration,

$$D_c(x+dx) = D_c(x) + \frac{\partial D_c}{\partial x}dx$$

Therefore, Eq.(1-2.1) takes the form

$$F_x = \{D_c\frac{\partial^2 C}{\partial x^2}dx + \frac{\partial D_c}{\partial x}\frac{\partial C}{\partial x}dx + \frac{\partial D_c}{\partial x}\frac{\partial^2 C}{\partial x^2}(dx)^2\}\,dydzdt$$

Since $(dx)^2 \simeq 0$,

$$F_x = \frac{\partial}{\partial x}(D_c\frac{\partial C}{\partial x})dxdydzdt \qquad (1\text{-}2.3)$$

On the other hand, the flux $F_x$ can be expressed as the change of concentration in time $dt$ in the small body. Then,

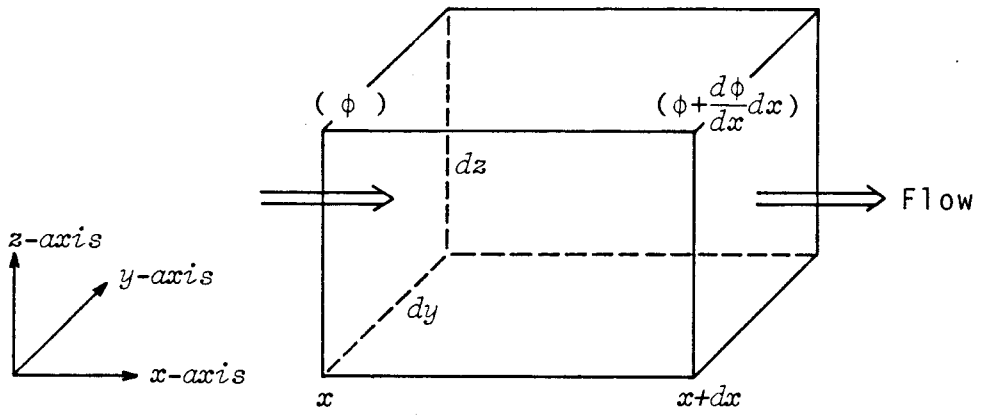


Fig.1.6 Element illustrating the unsteady-state flow of moisture

$$F_x = \frac{\partial C}{\partial t}\, dtdxdydz \tag{1-2.4}$$

From Eqs.(1-2.2) and (1-2.4),

$$\frac{\partial C}{\partial t} = D_c \frac{\partial^2 C}{\partial x^2} \tag{1-2.5}$$

And from Eqs.(1-2.3) and (1-2.4),

$$\frac{\partial C}{\partial t} = \frac{\partial}{\partial x}\left(D_c \frac{\partial C}{\partial x}\right) \tag{1-2.6}$$

For moisture movement in wood, the concentration $C$ is sometimes replaced by the moisture content $u$; Eqs.(1-2.5) and (1-2.6) take the forms

$$\frac{\partial u}{\partial t} = D_c \frac{\partial^2 u}{\partial x^2} \tag{1-2.7}$$

and

$$\frac{\partial u}{\partial t} = \frac{\partial}{\partial x}\left(D_c \frac{\partial u}{\partial x}\right) \tag{1-2.8}$$

Eqs.(1-2.5) and (1-2.7) correspond to Fick's second law of diffusion.

In 1855, when Adolf Fick[11] found his law (i.e., that the flux of the diffusion substance is proportional to the concentration gradient) in an experiment of diffusion using a very dilute salt solution, he expressed his law in a simple mathematical form:

$$F = -D_C \frac{\partial C}{\partial x} \tag{1-2.9}$$

where Fick defined the diffusion coefficient $D_C$ as "eine von der Natur der Substanzen abhängige Constante". The following assumptions are necessary in order that Fick's law of diffusion with a constant diffusion coefficient is valid[12]:

1) The motion of each particle is random and is unaffected by the presence of other particles.
2) Each successive jump is independent of previous jumps.
3) The mean jump length for a particle and the frequency of displacement do not vary with position or time.
4) No hydrodynamic flow exists in the system.
5) No forces exist that can give rise to a given direction of motion of the individual particles.

The moisture movement in wood below the fiber saturation point is governed by at least two different mechanisms: one is bound-water diffusion in the cell-wall substance, and the other is water-vapor diffusion in the cell lumen. Though the diffusion coefficient of the latter is much greater than that of former, the total flow rate appears to be controlled by the former mechanism.

Bound-water molecules are held on sorption sites with a certain distribution of the bonding energy that is known to be a function of moisture content. Molecular movement must depend on the distribution of the bond energy. Thus, for bound-water diffusion, which appears to be the rate-controlling process of moisture movement in wood, it is difficult to accept at least the first of the above-mensioned conditions of Fick's law. In fact, many experimental results have shown that the diffusion coefficient of moisture in wood is dependent on concentration. Therefore, Fick's second law,i.e., Eq.(1-2.5) and Eq.(1-2.7), are not applicable to moisture flow in wood.

On the other hand, Fick's first law,i.e., Eq.(1-2.9), is applicable to the moisture flow even if $D_C$ depends on concentration. In this case, the equation merely defines the conventional diffusion coefficient $D_C$ as the ratio of $F$ to $-dC/dx$. Eqs.(1-2.6) and (1-2.8) are valid when $D_C$ is a function of concentration, of mass density, and of the experimental temperature, but shows no dependence on the concentration gradient, on time and on position; they may be applicable to moisture flow in wood.

### 1-2.2. Some Modifications of Fick's Law

Recently, Bramhall [13], discussing bound-water diffusion in wood, tried to express his theory quantitatively. He stated that ".... bound-water diffusion occurs when water molecules bound to their sorption sites receive energy in excess of the bonding energy and migrate to the new sites. The number of molecules at any time with this excess energy is proportional

to the vapor pressure of water in wood at any given moisture content and temperature. Rate of diffusion is proportional to the concentration gradient of migrating molecules and this, in turn, is proportional to the vapor pressure gradient." Thus, he derived the next equation in place of Eq.(1-2.7).

$$\frac{\partial u}{\partial t} = D_p \frac{\partial^2 P}{\partial x^2} \qquad (1\text{-}2.10)$$

where $dP/dx$ is the vapor pressure gradient and $D_p$ is his diffusion coefficient dimensionally different from the conventional one.

Eq.(1-2.10) implies the constancy of $D_p$, while $D_p$ calculated by him in his report[13] varies with moisture content. Therefore, Eq.(1-2.10) should take more general form such as

$$\frac{\partial u}{\partial t} = \frac{\partial}{\partial x}\left(D_p \frac{\partial P}{\partial x}\right) \qquad (1\text{-}2.11)$$

Bramhall's discussion points out the basic difference between Fickian diffusion and bound-water diffusion in wood. His concept is based on the movement of water molecules in the gaseous state by successive evaporation and condensation. In this case, the height of energy barrier necessary for a bound water molecule to desorb from a sorption site and to migrate to another must equal the sum of the heat of wetting and the heat of evaporation. Careful consideration should be given to this mechanism, and it will be discussed later in connection with the relationship between the diffusion coefficient and the activation energy for bound-water diffusion in wood.

On the basis of thermodynamics of irreversible processes,

the driving force for diffusion is expressed by gradient of chemical potential[14]. The chemical potential $\mu_i$ of component $i$ in a phase, as well as temperature and pressure, is a thermodynamic intensive state variable and is defined as

$$\mu_i \equiv \left(\frac{\partial U}{\partial n_i}\right)_{S.V.n_{j\neq i}}$$

where $U$ is the energy of the phase, $S$ the entropy, $V$ the volume, $n_i$ the molar quantity of component $i$, and $n_{j\neq i}$ represents that $j$ other than $i$, if present in the phase, is constant. For any component in the system, the value of the chemical potential must be the same in every phase, when the system is in thermodynamic equilibrium,i.e., when the system is in phase equilibrium at uniform temperature. The relation between flux and driving force of moisture diffusion can be discussed without consideration of the sorption and diffusion mechanisms when the chemical potential of water in wood is considered.

At a temperature $T$, the chemical potential $\mu$ of the water in wood, which has equilibrium vapor pressure $P$, is expressed as[15]

$$\mu = \mu_{H_2O} + RT\ln(P/P_{H_2O}) \qquad (1\text{-}2.12)$$

where $\mu_{H_2O}$ is the chemical potential of liquid water at temperature $T$, and its vapor pressure is given as $P_{H_2O}$, and $R$ being the gas constant. In order to unify the unit of mass, the specific chemical potential $\tilde{\mu}$ of component $i$ is introduced instead of the chemical potential:

$$\tilde{\mu}_i \equiv \mu_i/M_i$$

where $M_i$ is the mass per unit mole of component $i$.

Using this potential, Eq.(1-2.12) results in

$$\tilde{\mu} = \tilde{\mu}_{H_2O} + \frac{RT}{M_{H_2O}} \ln(P/P_{H_2O}) \qquad (1\text{-}2.13)$$

The spatial derivative of the specific chemical potential of water in wood is

$$\frac{d\tilde{\mu}}{dx} = \frac{RT}{M_{H_2O}} \frac{d\ln P}{dx} \qquad (1\text{-}2.14)$$

When the specific chemical potential gradient is used in place of the concentration gradient, Eq.(1-2.8) becomes

$$\frac{\partial u}{\partial t} = \frac{\partial}{\partial x}\left(D'_{\mu} \frac{\partial \tilde{\mu}}{\partial x}\right) \qquad (1\text{-}2.15)$$

where $D'_{\mu}$ is a diffusion coefficient thought to be a constant which is independent of the chemical potential gradient and the concentration gradient. Eq.(1-2.15) can be transformed by use of Eq.(1-2.14). Then,

$$\frac{\partial u}{\partial t} = \frac{\partial}{\partial x}\left(D'_{\mu} \frac{RT}{M_{H_2O}} \frac{\partial \ln P}{\partial x}\right) \qquad (1\text{-}2.16)$$

Since $D_{\mu} \equiv D'_{\mu} RT/M_{H_2O}$ is also a constant independent of the chemical potential gradient and the concentration gradient, Eq. (1-2.16) can take the form

$$\frac{\partial u}{\partial t} = \frac{\partial}{\partial x}\left(D_{\mu} \frac{\partial \ln P}{\partial x}\right) \qquad (1\text{-}2.17)$$

### 1-2.3. Discussion of the Diffusion Equation

Table 1.2 shows the fluxes and the driving forces of various transport phenomena. In this table, electric potential is an intensive factor, constituting energy when multiplied by electric charge, the extensive factor. Similarly, velocity and momentum are intensive and extensive factors of energy, respectively. For an irreversible process in the system of uniform temperature, its driving force is expressed by the spatial derivative of the intensive factor, and its flux by the time derivative of the extensive factor.

For moisture movement in wood, the driving force comparable to those of other transport phenomena is the specific chemical potential gradient. The flux is expressed as mass flow per unit time and per unit area. And the product of mass and the potential gives energy. As Eq.(1-2.13) shows, the chemical potential $\tilde{\mu}$ is related to the equilibrium vapor pressure which is an essential factor in the mechanism of water sorption by wood.

The diffusion coefficients defined by Eqs.(1-2.8), (1-2.11), and (1-2.17) are related with each other:

$$D_{\mu} = PD_p = \frac{PD_c}{(\partial P/\partial u)} \qquad (1\text{-}2.18)$$

On the theoretical stand point, there is no reason to prefer one of these three coefficients rather than the other two. The reason must be experimental one that a simple relationship between diffusion coefficient and moisture content is observed.

Since it is clear from the sorption isotherm for water in

Table 1.2 Comparisons of water movement in wood (diffusion) with other transport processes

| Transport process | Flux | Driving force | Coefficient of proportionality | Equilibrium condition *1 |
|---|---|---|---|---|
| Diffusion | Mass flow | Specific chemical potential gradient | Diffusion coefficient | The specific chemical potential of the diffusing component is uniform. |
| Conduction of heat | Energy flow | Temperature gradient | Thermal conductivity | The temperature is uniform. |
| Electric conduction | Electric current | Electric potential gradient | Electric conductivity | The electric potential is uniform. |
| Viscose flow | Momentum flow | Velocity gradient | Viscosity | The velocity is uniform. |

*1 It is assumed that other transport processes in the system are in the dynamic equilibrium.

wood that $\partial P/\partial u$ and $\partial \ln P/\partial u$ vary with $u$, neither $D_p$ nor $D_\mu$ is proportional to $D_c$. The ratio of $D_\mu$ to $D_p$ equals $P$ which varies with $u$. Thus, if any of three coefficients is independent of $u$, others must depend on it. Furthermore, it is very possible that all the three depend on $u$.

According to Eq.(1-2.18), the dependence of $D_\mu$ on $u$ is distinguished from those of $D_c$ and $D_p$ in the neighborhood of $u=0$; in case that $D_\mu$ takes a finite value, values of $D_c$ and $D_p$ must become infinitive. On the other hand, in case that $D_c$ and $D_p$ take finite values, $D_\mu$ will vanish.

## 1-3. *Diffusion Coefficient*

### 1-3.1. Determination of the Diffusion Coefficient

Most diffusion coefficients for water in wood obtained heretofore are based on Fick's law of diffusion. The relation

of the diffusion coefficient of water in wood to concentration has been the subject of many studies, but the true nature of it is still unknown. One of the reasons is that the theoretical framework has been insufficient. Another reason is that each method to determine the diffusion coefficient has its own limitations. These make it difficult to compare the diffusion coefficients with each other and to consider the nature of diffusion.

Several methods are available for calculating the diffusion coefficient. The method are roughly divided into two groups: one type employs the steady-state, and the other the unsteady-state. Fig.1.7 illustrates a steady-state method. When the diffusion coefficient is independent of concentration, the concentration gradient keeps constant at any position, shown as a dot-and-dash line in the figure. Therefore, the diffusion coefficient can be expressed as

$$D_c = F/(\frac{C_0 - C_a}{a}) \qquad (1\text{-}3.1)$$

However, when Eq.(1-3.1) is used for a system in which the diffusion coefficient may be dependent upon concentration, the average diffusion coefficient is estimated over the concentration range measured.

For the system in which the diffusion coefficient is dependent on concentration, the diffusion coefficient is directly derived from Eq.(1-2.9):

$$D_c = F/(-\frac{dC}{dx}) \qquad (1\text{-}3.2)$$

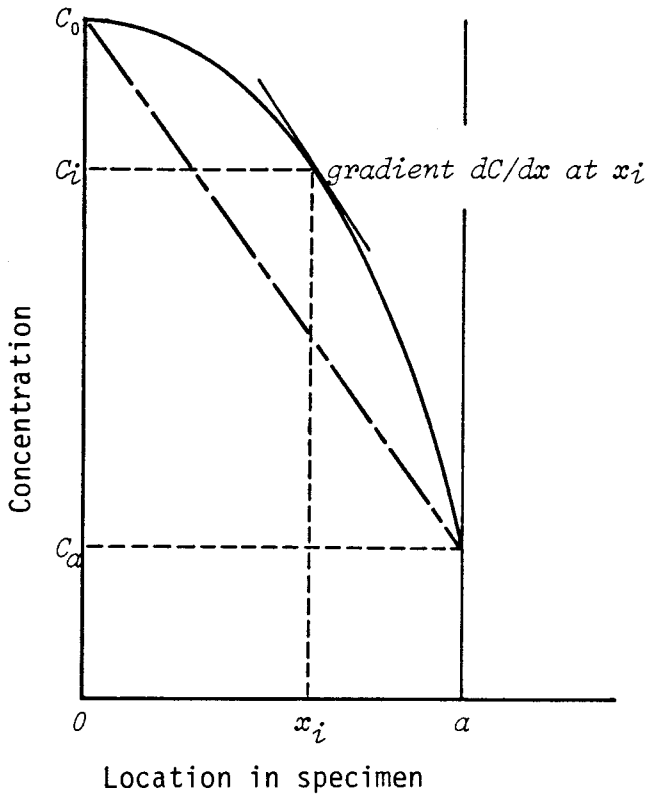


Fig.1.7 Measurement of the diffusion coefficient under steady-state water movement

where the concentration gradient at any position $x$ in the specimen can be determined by use of the moisture distribution shown in Fig.1.7 [16].

The steady-state method uses a rather simple diffusion equation, but has the practical disadvantage that considerable time is required to obtain a steady-state condition. On the other hand, the unsteady-state method can be used during the period before the steady-state condition is attained. Furthermore, the unsteady-state method gives a direct relation of the diffusion coefficient to the drying times of wood and to the moisture gradients responsible for the drying stresses. Its

main disadvantage is the mathematical complexity of the applicable equation. Therefore, Eqs.(1-2.7) or (1-2.8) is transformed into various more practical forms on the basis of certain simplifying assumptions[17)-20)], but initial- and boundary conditions, and types of function expressing the dependence of the diffusion coefficient on concentration are often limited.

For example, Plager and Long[21)] transformed Eq.(1-2.8) by use of Boltzmann's variable and derived the following equation:

$$\frac{M_t}{M_\infty} = \frac{4}{\sqrt{\pi}} \left(\frac{\bar{D}t}{d^2}\right)^{1/2} \qquad (1\text{-}3.3)$$

where $M_t$ : Amount of moisture adsorbed or desorbed (g),

$M\infty$ : Total amount adsorbed or desorbed at equilibrium (g),

$d$ : Thickness of the specimen (cm),

$t$ : Time (sec),

$\bar{D}$ : Diffusion coefficient ($cm^2/sec$).

This solution is subject to the following conditions:

1) The size of the specimen is semi-infinitive: the concentration at the center of the specimen does not change.
2) The surface of the specimen immediately reaches the equilibrium concentration.
3) The initial moisture content is uniformly distributed through the specimen thickness.
4) The diffusion coefficient is independent of the concentration in the range measured.

The diffusion coefficient obtained in Eq.(1-3.3) is in practice the average diffusion coefficient covering the range from initial to equilibrium moisture content when diffusion coefficient

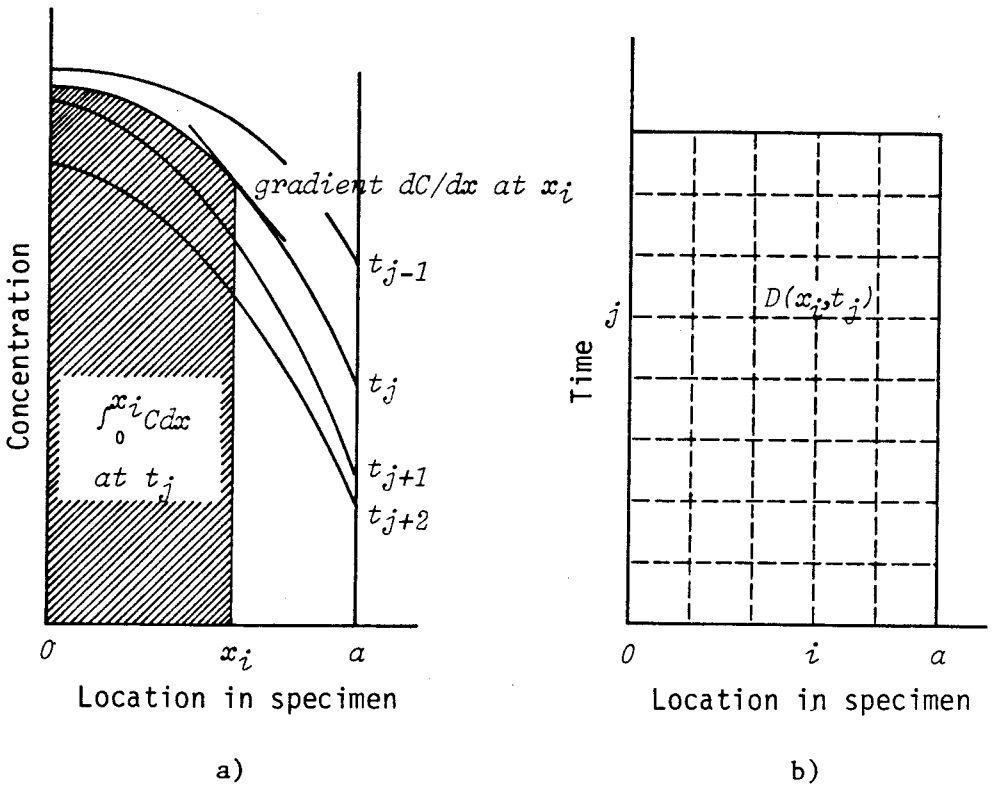


Fig.1.8 Measurement of the diffusion coefficient under unsteady-state water movement

a) Determination of the diffusion coefficient

b) $(x_i, t_j)$ matrix

is dependent on concentration.

Egner[22] derived the variable diffusion coefficient from Eq.(1-2.6) by means of integrating along the spatial coordinate $x$ as

$$D_c = \frac{\partial \int_0^{x_i} C dx}{\partial t} \Big/ \left(\frac{dC}{\partial x}\right) \qquad (1\text{-}3.4)$$

Egner's method requires a knowledge of the moisture distribution in a specimen at given time-intervals during drying, as Fig 1.8 a) shows. The integral $\int_0^{x_i} C dx$ for $x_i$ at time $t_j$ is the

hatched area in the figure. The integral $\int_0^{x_i} C dx$ for $x_i$ at time $t_{j+1}$ is calculated in the same way, so that the flux at position $x_i$ during the period $(t_{j+1}-t_j)$ is given as ( $\int_0^{x_i} C dx$ at $t_j$ - $\int_0^{x_i} C dx$ at $t_{j+1}$ ). Finally, a concentration gradient is obtained from the slope of the moisture distribution curve at time $t_j$ and position $x_i$.

By use of moisture content $u$ in place of concentration $C$ in Eq.(1-3.4),

$$D_c = \frac{\partial \int_0^{x_i} u dx}{\partial t} / (\frac{\partial u}{\partial x}) \qquad (1\text{-}3.5)$$

Thus the concentration-dependent diffusion coefficient corresponding to the $(x_i, t_j)$ matrix can be obtained, as Fig.1.8 b) shows.

Both Martley's method under steady-state conditions and Egner's method under unsteady-state conditions require determination of the moisture distribution with a certain technique, but do not require special limitations or assumptions. Therefore these methods have an advantage over other methods in obtaining the real concentration-dependent diffusion coefficient over the measured range.

In the present study, diffusion coefficients were determined on the basis of three diffusion equations,i.e.,(1-2.8), (1-2.11), and (1-2.17). A method of calculation similar to Egner's was used for the following reasons:

1) Egner's method provides concentration-dependent diffusion coefficients over the range measured.
2) Changes in moisture distribution during drying were

Table 1.3 Desorption moisture contents for Hinoki specimens at different relative vapor pressures

| Temp. (°C) | Saturated salt solution | Relative vapor pressure[9] | $\bar{X}_{e.m.c.}$ (g/g) | $\sigma$ | $\sigma/\bar{X}$ |
|---|---|---|---|---|---|
| 20 | $K_2SO_4$ | 0.975 | 0.233 | 0.0086 | 0.037 |
| | NaCl | 0.76 | 0.091 | 0.0032 | 0.035 |
| | $MgCl_2$ | 0.335 | 0.048 | 0.0049 | 0.100 |
| | LiCl | 0.12 | 0.026 | 0.0052 | 0.200 |
| 40 | $K_2SO_4$ | 0.97 | 0.212 | 0.0062 | 0.029 |
| | NaCl | 0.75 | 0.089 | 0.0020 | 0.023 |
| | $MgCl_2$ | 0.32 | 0.039 | 0.0021 | 0.053 |
| | LiCl | 0.11 | 0.018 | 0.0016 | 0.089 |
| 50 | $K_2SO_4$ | 0.965 | 0.206 | 0.0069 | 0.033 |
| | NaCl | 0.745 | 0.084 | 0.0037 | 0.044 |
| | $MgCl_2$ | 0.31 | 0.036 | 0.0019 | 0.052 |
| | LiCl | 0.11 | 0.015 | 0.0015 | 0.097 |
| 60 | $K_2SO_4$ | 0.96 | 0.191 | 0.0062 | 0.032 |
| | NaCl | 0.74 | 0.079 | 0.0020 | 0.025 |
| | $MgCl_2$ | 0.30 | 0.034 | 0.0018 | 0.053 |
| | LiCl | 0.105 | 0.014 | 0.0016 | 0.114 |

available from soft X-ray densitometry (Chapter 1-1).

3) By substituting the vapor pressure- and the logarithmic vapor pressure gradient discussed in Chapter 1-2 for $(\partial u/\partial x)$ in Eq.(1-3.5), the diffusion coefficients $D_p$ and $D_\mu$ could be determined in a similar manner to $D_c$.

For numerical calculation, moisture distribution curves of Chapter 1-1 were used in the time range from 0 to 90 minutes. The mesh size of $\Delta x$ and $\Delta t$ were 0.1 cm and 360 sec, respectively, for drying conditions at a temperature of 20°C. For drying

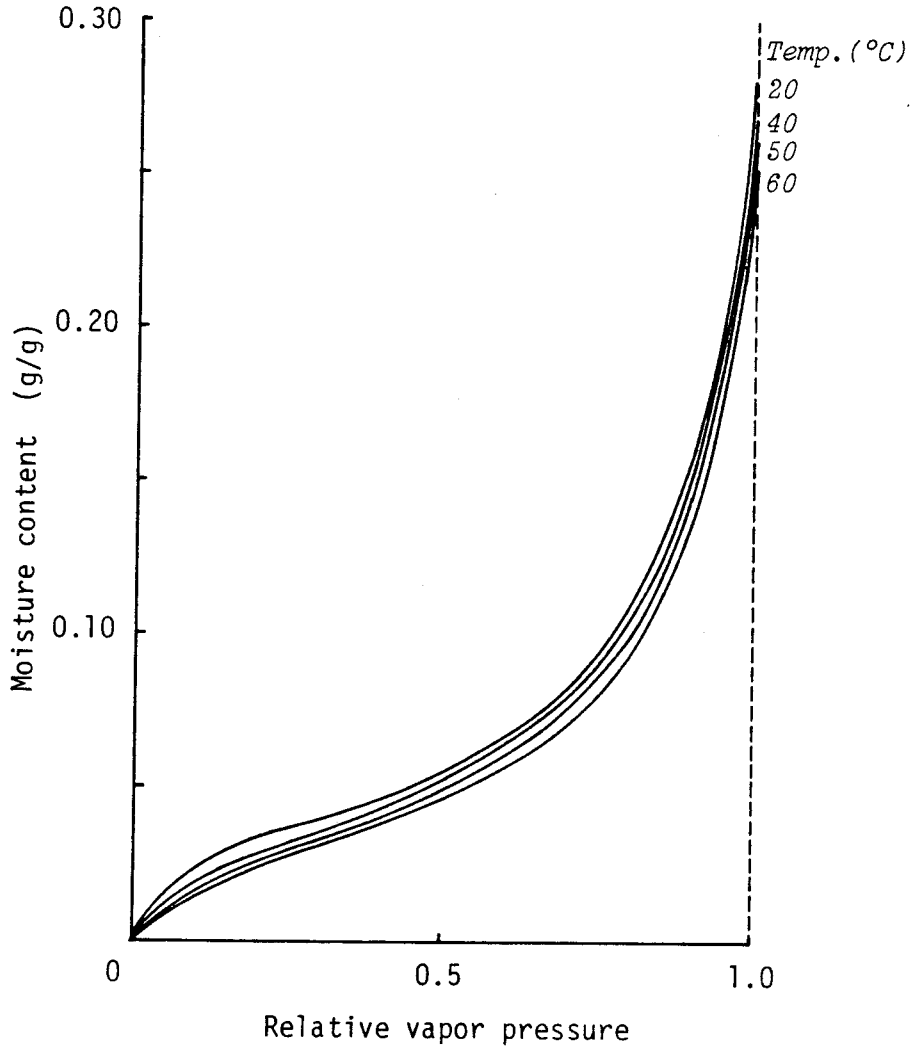


Fig.1.9 Desorption isotherms for water vapor by Hinoki specimens at different temperatures

conditions at a temperature of 40, 50, and 60°C, $\Delta x$ was chosen as 0.1 cm, and $\Delta t$ as 180 sec from the start of drying to 30 min, and thereafter as 360 sec.

In order to obtain the desorption isotherms necessary for calculating the vapor pressure gradient and the chemical potential gradient, moisture contents were measured when the specimens reached equilibrium with the saturated salt solutions

($K_2SO_4$, $NaCl$, $MgCl_2$, and $LiCl$) at the same temperatures as the drying experiments shown in Chapter 1-1. Six specimens were used for each condition, and Table 1.3 shows average values of the results. The data were approximated to the Hailwood-Horrobin equation [23] by least square methods.

Fig.1.9 shows the desorption isotherms obtained from the equations at the test temperatures. The equilibrium moisture content in the RH range from 50 to 80% are relatively low compared with the desorption isotherms reported by Stamm [24] and by Spalt [25]. However, the measured values show, as a whole, the sigmoid type which is common for sorption isotherms of water by wood. Further, the equilibrium moisture content in the drying experiments at the same conditions showed similar values. The desorption isotherms obtained are therefore assumed to be applicable to the specimens of the present study.

### 1-3.2. Results and Discussion

Fig.1.10 shows the dependence of the diffusion coefficient $D_c$ in Eq.(1-2.8) on moisture content at a temperature of 40°C. The degree of scatter is somewhat high in Fig.1.10, and there is no obvious dependence of $D_c$ on moisture content. Many investigators [26)-38)] have studied this relationship under various conditions of moisture content, temperature, and grain direction; some insist on a dependence of $D_c$ on moisture content, and others do not. Further, wood is a hygroscopic material and changes its structure with increasing or decreasing moisture content. Thus, different relationships between diffusion coefficient and moisture content have been observed when the

diffusion coefficients are determined by use of different methods, i.e., the adsorption, the desorption, and the steady-state methods[39) 40)]. However, their values of the diffusion coefficient are all in the range from $10^{-4}$ to $10^{-6}$ $cm^2/sec$. The value of $D_c$ in this study falls into the same range.

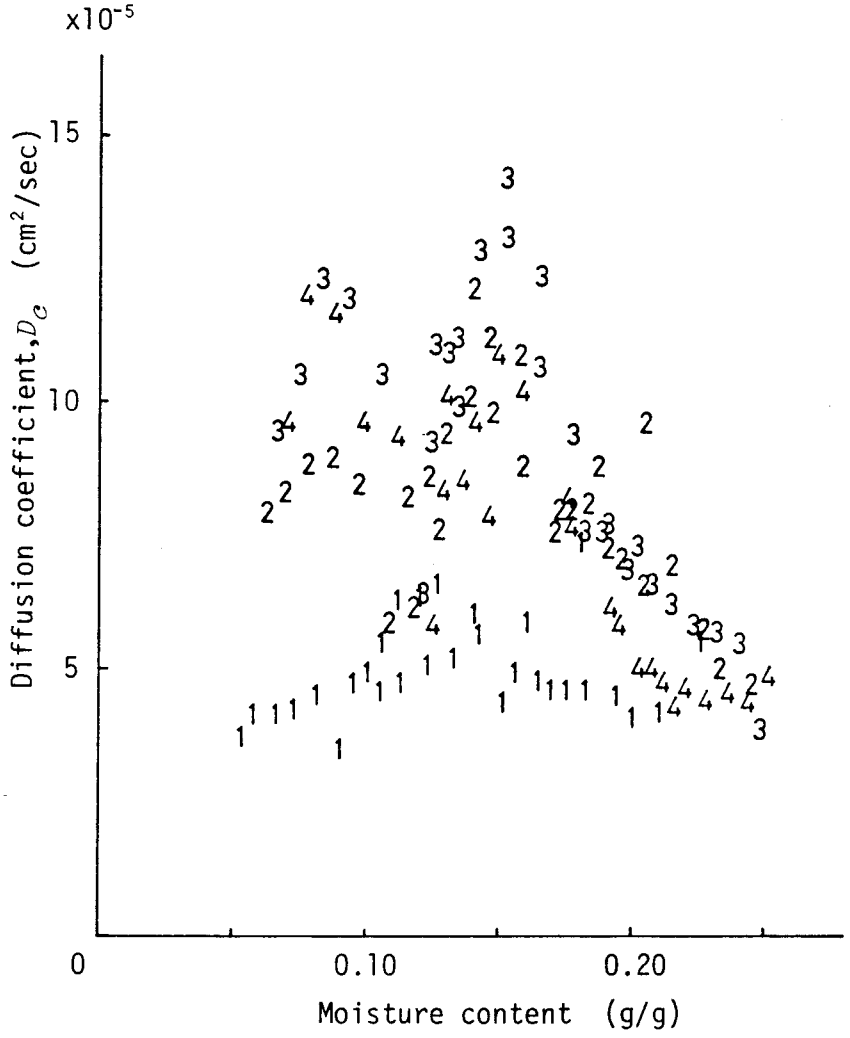


Fig.1.10 Dependence of the diffusion coefficient $D_c$ on moisture content at 40°C

Numbers show distance from the surface in mm.

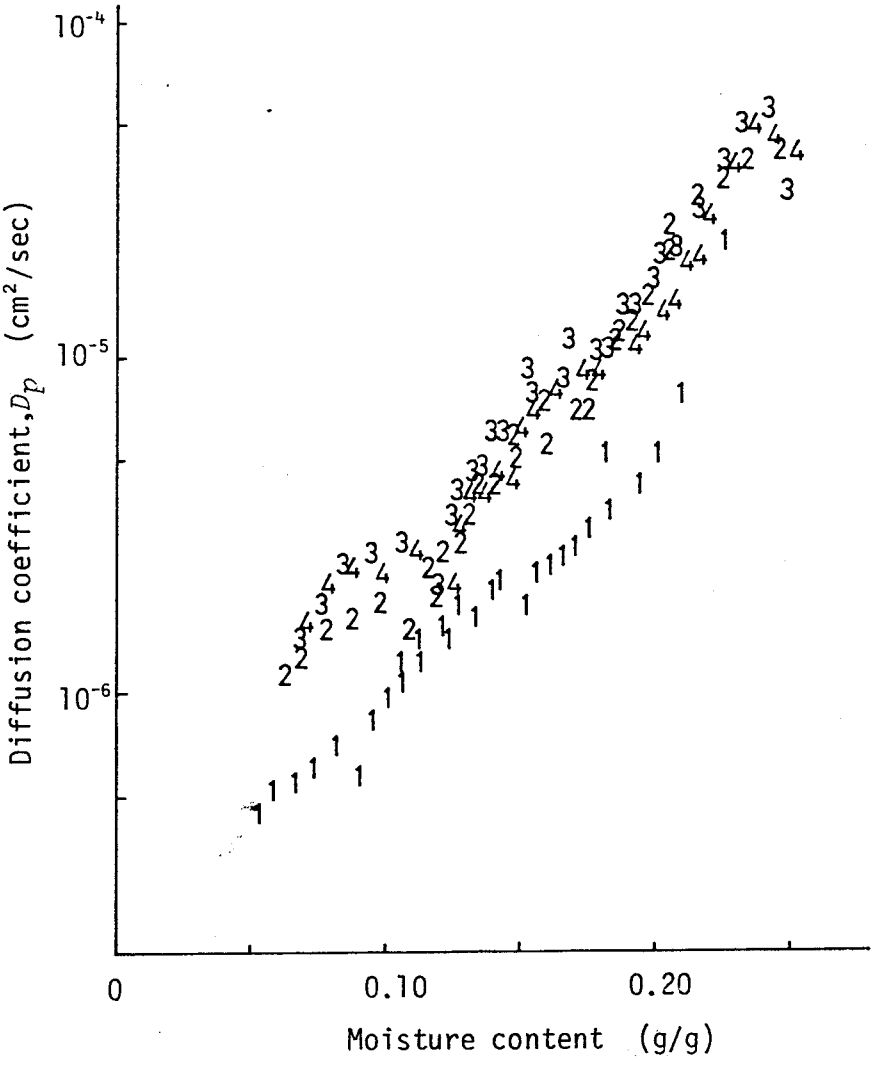


Fig.1.11 Dependence of the diffusion coefficient $D_p$ on moisture content at 40°C

Numbers show distance from the surface in mm.

Fig.1.11 shows the m.c. dependence of the diffusion coefficient $D_p$ in Eq.(1-2.11). $D_p$ is expressed in terms of the product of $D_p$ and $P_{H_2O}$ in order to unify the dimensions. $P_{H_2O}$ denotes saturated vapor pressure at a given temperature, being independent of moisture content. The diffusion coefficient $D_p$ increases exponentially with increasing moisture content. The

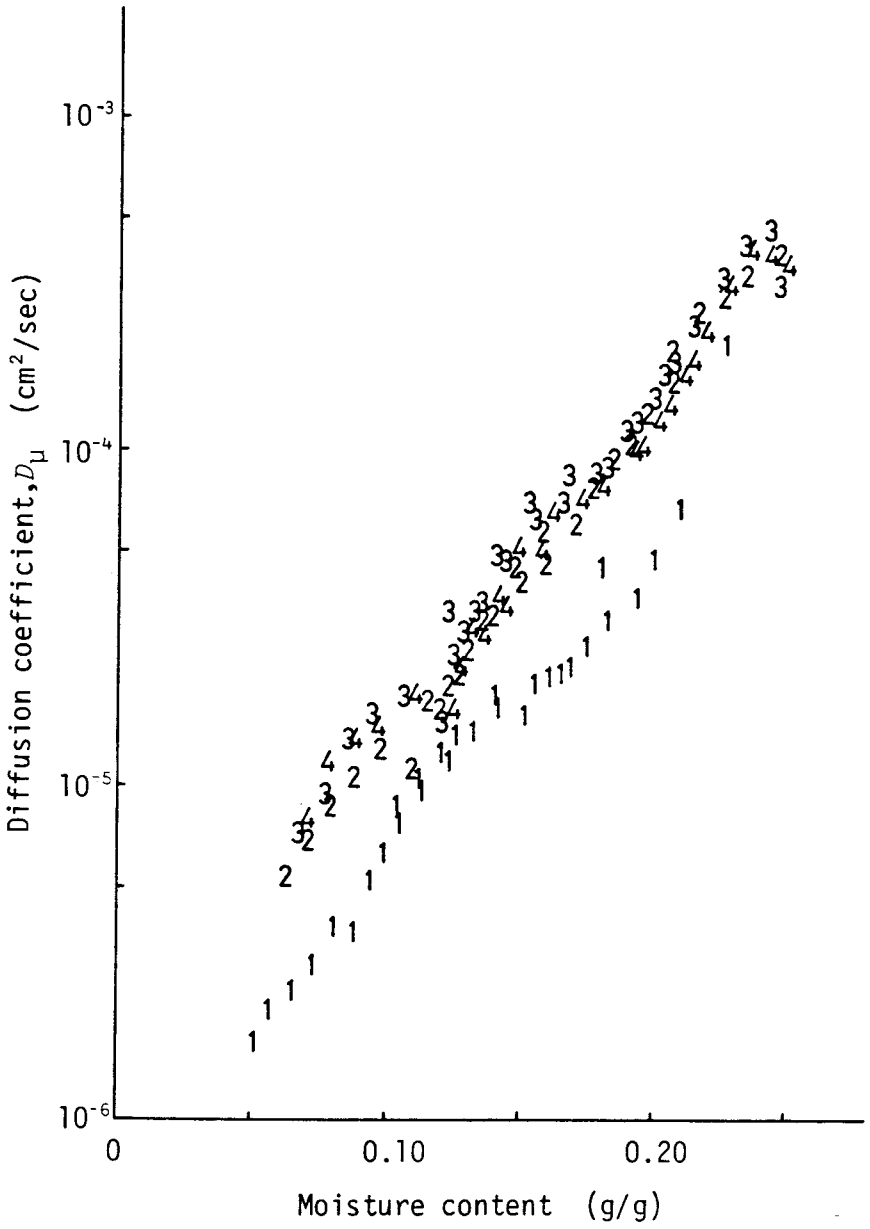


Fig.1.12 Dependence of the diffusion coefficient $D_\mu$ on moisture content at 40°C

Numbers show distance from the surface in mm.

diffusion coefficient $D_\mu$ increases in a similar manner to $D_p$, as shown in Fig.1.12.

These relationships were approximated by use of linear

Table 1.4 The fitness of regression lines between logarithmic diffusion coefficients and moisture content at 40°C

| Regression equation*1 | D.F. | M.S. | S.D. |
|---|---|---|---|
| $\log D_\mu = -5.80 + 9.8\,u$ | 83 | 0.0084 | 0.09 |
| $\log D_p = -6.32 + 7.4\,u$ | 83 | 0.0683 | 0.26 |

* The diffusion coefficients at position number 1 are excluded.

equations between logarithmic diffusion coefficients ($\log D_\mu$ and $\log D_p$ ) and moisture content with the method of least squares. The fitness was significantly better with $D_\mu$ than with $D_p$, as shown in Table 1.4. The standard deviations in the table show those of logarithmic diffusion coefficients, and the deviation of $D_\mu$ is about 20%, while that of $D_p$ is about 60%. In conclusion, the diffusion coefficient $D_\mu$ is preferred as the parameter in the diffusion equation.

The dependence of the diffusion coefficient $D_\mu$ on temperature may be seen in Fig.1.13 which shows isotherms of $D_\mu$ as a function of moisture content. The diffusion coefficients at position number 1 are not included in the figure because of their systematic error such as resulted from surface evaporation. The regression lines, indicated as solid lines in the figure, are as follows:

$\log D_\mu = -7.76 + 18.0\,u$ at 20°C,

$\log D_\mu = -5.80 + 9.8\,u$ at 40°C,

$\log D_\mu = -5.59 + 9.6\,u$ at 50°C,

and $\log D_\mu = -5.72 + 12.0\,u$ at 60°C.

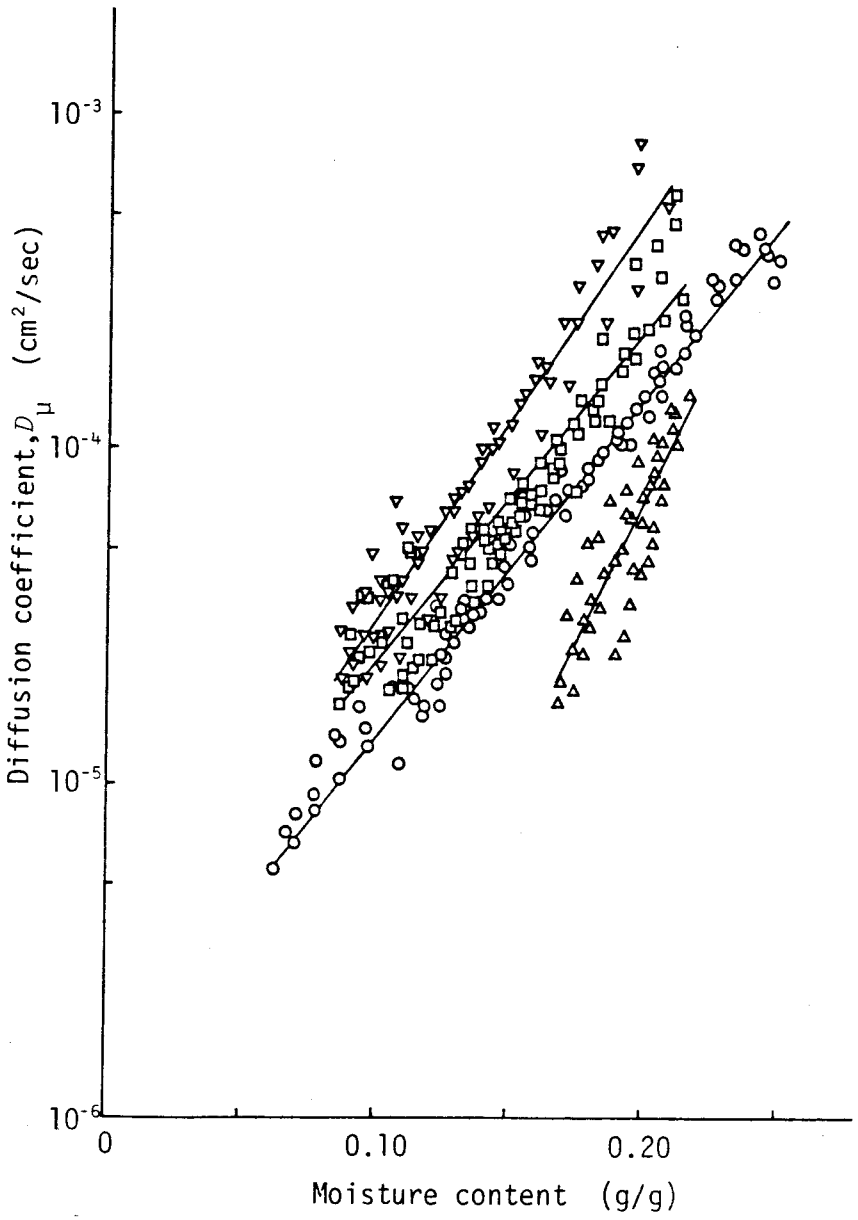


Fig.1.13 Dependence of the diffusion coefficient $D_\mu$ on moisture content at different temperatures

△: 20°C, ○: 40°C, □: 50°C, ▽: 60°C.

From Fig.1.13 it is evident that the diffusion coefficient at constant moisture content increases as the temperature rises. The slope of the regression line of $\log D_\mu$ and moisture content

is relatively large at 20°C, while those at temperatures of 40, 50, and 60°C have the similar values. This is assumed to reflect relatively error because of the narrow m.c. range in the experiment compared to the scatter of the diffusion coefficient.

If Arrhenius equation is adopted to express the temperature dependence of the diffusion coefficient $D_\mu$,

$$D_\mu = D_0 \exp(-E_a/RT) \tag{1-3.6}$$

where $D_0$ is the frequency factor, i.e., a constant which is independent of temperature, and $E_a$ Arrhenius activation energy, i.e., apparent activation energy. After the conversion of Eq. (1-3.6) to a natural logarithmic equation, the slope of $\ln D_\mu$ and the reciprocal of temperature can be obtained as

$$\frac{d(\ln D_\mu)}{d(1/T)} = -E_a/R \tag{1-3.7}$$

$D_\mu$ is an apparent diffusion coefficient defined as the product of $D_\mu'$ in Eq.(1-2.15) and some constants. Thus, if the diffusion coefficient $D_\mu'$ obeys Arrhenius equation, then

$$D_\mu \equiv D_\mu' \left(\frac{RT}{M_{H_2O}}\right) = \left(\frac{RT}{M_{H_2O}}\right) D_0 \exp(-E_a'/RT) \tag{1-3.8}$$

where $E_a'$ is Arrhenius activation energy for $D_\mu'$. In a similar manner,

$$\frac{d(\ln D_\mu)}{d(1/T)} = -T - (E_a'/R) \tag{1-3.9}$$

From Eqs.(1-3.7) and (1-3.9), the relationship between $E_a$ and $E_a'$ is obtained as

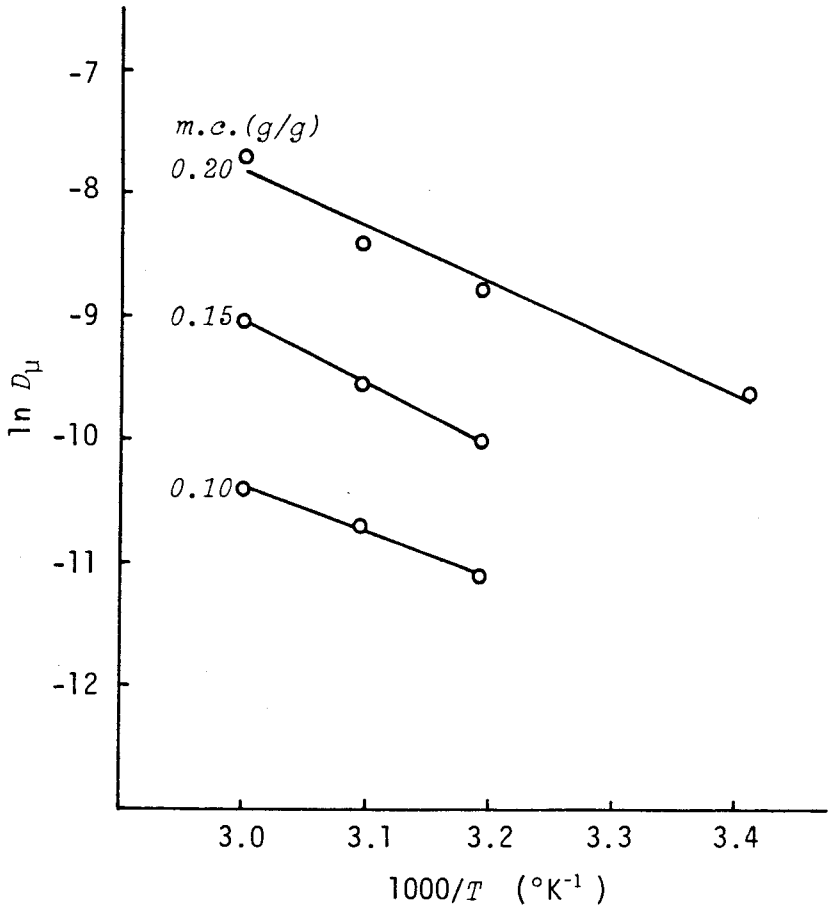


Fig.1.14 Effect of temperature on the diffusion coefficients of Hinoki specimens in the longitudinal direction

$$E_a = RT + E_a' \qquad (1\text{-}3.10)$$

In order to obtain Arrhenius activation energy, $\ln D_\mu$ is plotted as a function of $1/T$ at several levels of moisture content as shown in Fig.1.14. The relationships in the figure at moisture contents of 0.10, 0.15, and 0.20 are roughly linear, and their slopes are almost the same. The average activation energy $E_a$ is then calculated from these regression lines as 8.7 kcal/mol, while the activation energy $E_a'$ is estimated from

Eq.(1-3.10) as 8.1 kcal/mol. These values are in good agreement with that of 8.5 kcal/mol reported by Choong[41] who used the concentration gradient in Eq.(1-2.8) and that of 8.1 kcal/mol reported by Bramhall[42] who used the vapor pressure gradient in Eq.(1-2.11) with Voigt's data[43].

Fig.1.15 shows relative energy levels of water molecules in relation to the diffusion path in cell-wall substance in order to consider the diffusion mechanism of the bound-water molecules. There are two possible paths when a water molecule moves from a sorption site $W_1$ to a sorption site $W_2$, and the values of energy at these sites do not always coincide with each other.

Path I indicates that a water molecule leaving a sorption site $W_1$ overcomes the energy barrier completely and is free in the transition state. Thus, the activation energy would be estimated as the sum of the differential heat of sorption, the heat of evaporation, and the apparent activation energy for water-vapor diffusion. At 40°C, the differential heat of sorption is evaluated as about 30 to 70 cal/g[44] in the moisture content range from 0.20 to 0.10 and the heat of evaporation as 559 cal/g[45]. And the activation energy for water-vapor diffusion in bulk air is calculated by use of published data[46] as 1.2 kcal/mol. Thus, the activation energy for Path I is evaluated as about 11.8-12.5 kcal/mol, which is about 50% larger than the experimental value.

Path II indicates a similar idea to the migration mechanism based on surface diffusion which Kröll and others[26)47)-49)]

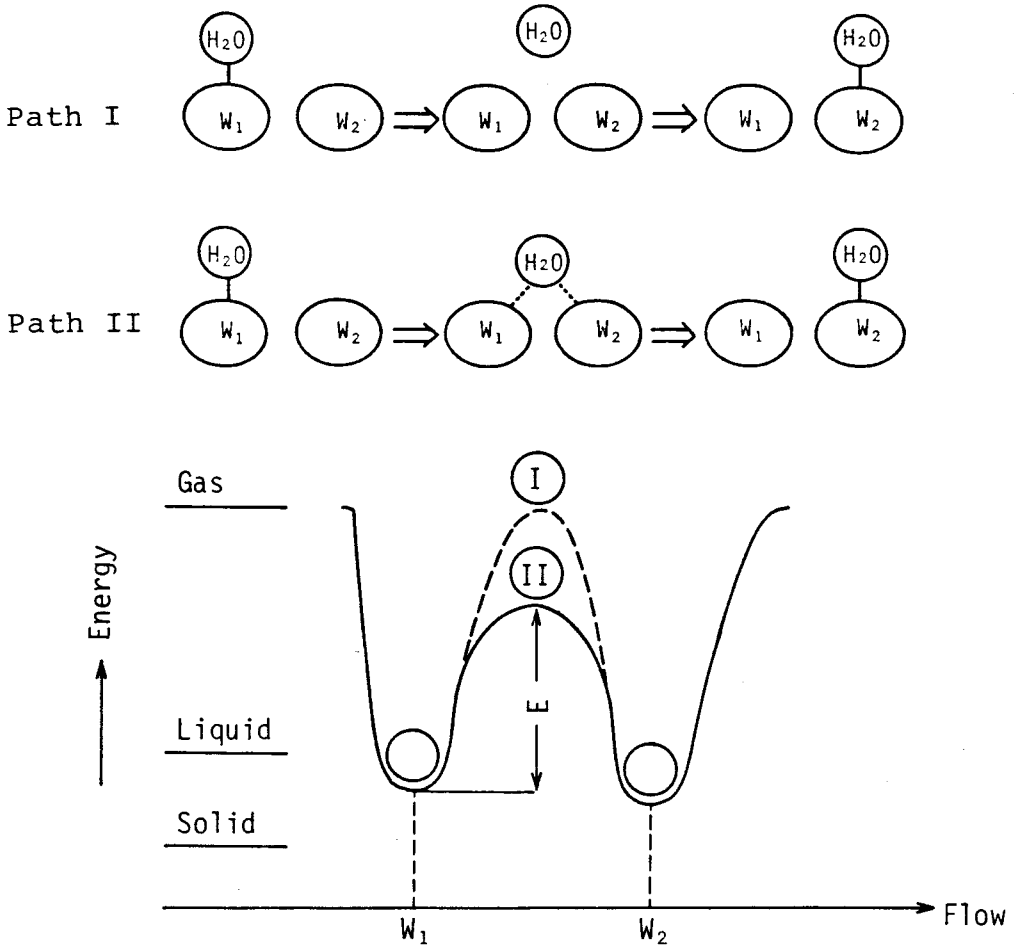


Fig.1.15 Schematic diagram showing relative energy levels of diffusing bound-water in relation to the migration mechanism

proposed. When the energy supplied is sufficient for the bound-water molecule to become free of local bonding, but is insufficient for it to desorb completely, the water-molecule migrates along the sorption surface. Thus, the water molecule does not need to be in the completely free state (such as vapor form) for migration, and the activation energy for Path II must be smaller than that for Path I. The activation energy obtained

in the experiments supports the migration mechanism of Path II, i.e., the surface diffusion of the bound-water molecules.

The diffusion coefficient $D_\mu$ increases with an increase of moisture content, as pointed out previously. If energy at transition state is constant regardless energies at sorption sites, the dependence of activation energy on moisture content is mainly determined by that of differential heat of sorption. Since the differential heat comprises only several percent of the total activation energy in the m.c. range of the experimental condition, the activation energy will vary only slightly with moisture content, as supported by the experiment.

On the contrary, the frequency factor $D_0$ must significantly depend on moisture content. This dependency may result from shrinkage of the specimen during drying. Shrinkage in the transverse plane of the cell-wall substance equals its volumetric shrinkage, since shrinkage in the longitudinal direction is negligible; the volumetric shrinkage $\alpha_v$ of the cell wall from moisture content $u$ to the ovendry condition is estimated as

$$\alpha_v = \frac{u \rho_s V_w}{1 + u \rho_s V_w} \qquad (1\text{-}3.11)$$

where $\rho_s$ is the density of the dry cell wall substance and $V_w$ the specific volume of the bound-water in the cell wall. Since $\rho_s$ and $V_w$ are estimated as 1.5 g/cm$^3$ and 0.91 cm$^3$/g, respectively [50], the total volumetric shrinkage from the fiber saturation point ( evaluated as 0.29 [51] ) to the ovendry condition is calculated as 0.29, which is far less in order to explain the exponetial dependency of the diffusion coefficient $D_\mu$ on

moisture content. Therefore, other reasons for it, which is now definitely unknown, will have to be sought.

Some scatter of $D_\mu$ is present at constant moisture content. The diffusion coefficients, for example, at position number 1 are consistently smaller than those at the other positions, mainly because of the effect of surface evaporation. The reasons for the scatter of $D_\mu$ are the heterogeneous structure of wood, the effect of temperature gradient and of drying stresses which arise in the specimen, and experimental and calculation errors. In order to consider the scatter of $D_\mu$, it is necessary to examine these factors, but they are difficult to analyze. Further investigation outside this study may be required.

## 1-4. *Summary*

The quantitative analysis for moisture movement in wood below the fiber saturation point was discussed. For this purpose, a new method for the continuous measurement of moisture distribution in wood during drying was developed, which made it possible to describe this phenomenon quantitatively. Then, the equation for representing moisture movement in wood was investigated. On the basis of thermodynamics of irreversible processes, a theoretical equation was derived. Finally, the proposed diffusion equation was examined in light of the experimental data. The results can be summarized as follows:

1) Changes in moisture distribution along the longitudinal direction were measured as a function of time during drying under various temperature and humidity conditions, by use of

serial specimens of Hinoki wood. Soft X-ray densitometry was used for this purpose, which made it possible to obtain continuous moisture distributions nondestructively. The moisture distributions obtained were parabolic, and the moisture content gradient near the surface at the initial stage of drying increased with increasing rate of drying.

2) In view of thermodynamics of irreversible processes, the relationship between mass flux and the driving force for moisture diffusion in wood was considered. Based on this theory, a diffusion equation was derived by use of the specific chemical potential gradient, i.e., a thermodynamic driving force. Then, the equation was compared with conventional ones.

3) In order to examine the proposed diffusion equation, the diffusion coefficients ($D_c$, $D_p$, and $D_\mu$) were calculated by use of the moisture distribution data. $D_c$ showed no obvious dependence on moisture content $u$, and the degree of scatter was rather high. On the other hand, $D_p$ and $D_\mu$ increased exponentially with increasing $u$, but the regression line of $D_\mu$ and $u$ showed better fit than that of $D_p$ and $u$. The dependence of the diffusion coefficient $D_\mu$ on temperature obeyed Arrhenius equation. The average value of Arrhenius activation energy calculated from experimental data suggested that the migration mechanism of bound water is surface diffusion in the cell-wall substance.

In conclusion, the diffusion coefficient $D_\mu$ is preferred as the parameter in the diffusion equation, and the proposed equation is valid for describing moisture movement in wood quantitatively.

# PART TWO

## PREDICTION OF MOISTURE DISTRIBUTION IN WOOD

Studies of moisture diffusion in wood belong to wood science, whereas prediction of moisture distribution in wood during drying is a step toward wood technology. The comparison of experimental moisture distributions with solutions of the diffusion equation provides the most direct evaluation of the theory of moisture movement in wood, while the knowledge of moisture distribution is indispensable for investigations of drying schedules and drying stresses in wood. Inspite of its importance, few scientists have investigated this field. The main reasons are probably that 1) it is difficult to obtain reliable experimental data of moisture distributions in wood during drying, and 2) the solution of Eq.(1-2.8) is very complex and often needs certain simplifying assumptions of the diffusion coefficient, and of initial and boundary conditions.

In the previous part, soft X-ray densitometry has been shown to be applicable to measuring the moisture distribution in wood during drying with adequate accuracy. In the present part, moisture distributions in wood are predicted by means of numerical solutions of the proposed diffusion equation (1-2.17), and the results are compared with experimental data.

## 2-1. *Theory for the Prediction of Moisture Distribution in Wood*

### 2-1.1. Numerical Solutions of the Proposed Diffusion Equation

General solutions of Fick's second law of diffusion,i.e., Eq.(1-2.7) were given by Newman and others[17) 34) 52) 53)] under various boundary conditions. On the other hand, Eq.(1-2.8) which applies to unsteady-state flow with a concentration-dependent diffusion coefficient is very complex, and there is no general solution for it. Crank[52)] obtained numerical solutions for Eq.(1-2.8) for some special cases where the diffusion coefficient varies in certain particular ways with concentration in a semi-infinite specimen.

When the assumptions that are implied by the general solutions are taken into account, it seems to be more useful for practical purposes to work with approximate solutions and to investigate their accuracy. Moschler and Martin[54)] used a finite difference technique for Eq.(1-2.8) in order to compare the theoretical solutions with experimental drying data. They assumed as a boundary condition that the sample surface was in equilibrium with the surrounding atmosphere, and took the diffusion coefficients and their concentration dependence from the literature. The results were then compared, and showed that these did not accurately describe the experimental wood drying they conducted.

A system of finite difference equations approximating Eq. (1-2.8) developed by von Neumann and Richtmyer[55)] was chosen for the present study[56)]. The system provides a numerical solution of partial differential equations of parabolic type with two

independent variables $x$ and $t$ :

$$\frac{\partial \Pi}{\partial t} = \delta \frac{\partial}{\partial x}\left(\eta \frac{\partial \Pi}{\partial x}\right) + \zeta \qquad (2\text{-}1.1)$$

where $\Pi$ is the dependent variable, and $\delta$, $\eta$, $\zeta$ are smooth functions of $x$, $t$, and $\Pi$. Fick's second law of diffusion,i.e., Eq.(1-2.8) corresponds to the case of $\delta=1$, and $\zeta=0$ in Eq.(2-1.1).

The system provides a numerical solution for equations such as the conventional diffusion equation with concentration-dependent coefficient $D_c$. Since equilibrium water-vapor pressure is related to wood moisture content by the sorption isotherm, and since the values of chemical potential can be numerically transformed into values of moisture content, the same system may be used for approximating Eq.(1-2.17) derived by the theory of moisture movement in wood. The system can be expressed as

$$\frac{MC(L,M+1)}{\Delta t} = \frac{MC(L,M)}{\Delta t} + \frac{1}{(\Delta x)^2}[D_\mu(L+1/2,M)\{CP(L+1,M)-CP(L,M)\} - D_\mu(L-1/2,M)\{CP(L,M)-CP(L-1,M)\}] \qquad (2\text{-}1.2)$$

Here a rectangular mesh of points $(x_L, t_M)$, where L=1,2,3,...: M=1,2,3,..., in the $x$-$t$ plane is chosen, as shown in Fig.2.1. $\Delta x$ and $\Delta t$ are the distance and the time increments, respectively. The value of moisture content at a mesh point $(x_L, t_M)$ is denoted by $MC(L,M)$ for brevity. $CP(L,M)$ is the value of $\ln P$ of the chemical potential in Eq.(1-2.17) at mesh point $(x_L, t_M)$. Similarly, $D_\mu(L+1/2,M)$ denotes the value of $D_\mu$ at a point midway between $(x_L, t_M)$ and $(x_{L+1}, t_M)$, and is taken as the mean of

$D_\mu$(L+1,M) and $D_\mu$(L,M).

2-1.2. Input Data for the Calculation of Moisture Distribution

The following input conditions must be considered in order to obtain numerical solutions by use of the difference equation (2-1.2) approximating the proposed diffusion equation (1-2.17).

a) The Size of $\Delta x$ and $\Delta t$

The actual distribution of mesh points can be determined by considerations of desired accuracy, rate of variation of $\eta(=D_\mu)$ with $x$ and $t$, and calculation time. However, the following stability condition must be satisfied for the system (2-1.2):[55]

$$2D_{max}\frac{\Delta t}{(\Delta x)^2} < 1 \qquad (2\text{-}1.3)$$

where $D_{max}$ is the maximum value of the diffusion coefficient over the moisture content range to which the estimating equation (2-1.2) is applied. If $\Delta x$ is chosen very small in the interest of accuracy, $\Delta t$ must be chosen much smaller yet in the interest of stability. Thus, it might happen that a prohibitively large number of steps $\Delta t$ would be required to complete the calculation by equation (2-1.2) over the desired domain of values of $\Delta t$.

b) Values of the Diffusion Coefficient

The diffusion coefficient of water in wood may be dependent on moisture content, temperature, and grain direction. When temperature and grain direction are taken into account, any concentration-dependent diffusion coefficient from the

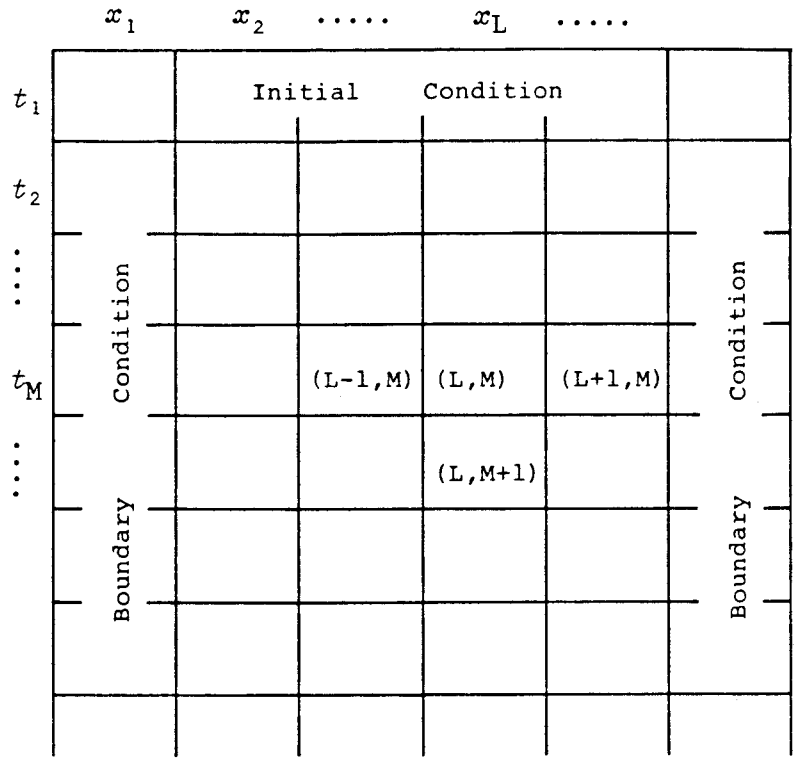


Fig.2.1 The rectangular mesh in the $x$-$t$ plane used in computation of the numerical solution

literature can be used if it is a smooth function of moisture content.

c) Initial Condition

The initial moisture content must be smoothly distributed, and its values must be known.

d) Boundary Conditions

The moisture content of the wood surfaces, or because of symmetry, of one surface and of the center of wood, during drying need to be known values.

For the solution of Eq.(1-2.8), it has usually been assumed that the wood surfaces immediately reach the equilibrium moisture

content.[34) 52) 53) 54)] It is apparent that this assumption is inapplicable to the actual drying process. To the author's knowledge, however, there are only two studies that have tried to evaluate the surface moisture content of wood during drying: one concerns Hart's method[57) 58)] of applying a psychrometric equation, and the other Ogura's method[59)] introducing the evaporating resistance pressure to the drying rate equation under a constant rate of drying. The disadvantage of the former is that the consideration of the consistency of constants is insufficient, while that of the latter is that the physical meaning of the evaporating resistance pressure is unclear. Neither of them has been sufficiently supported by experiments.

In the present paper, the surface moisture content is considered on the basis of the evaporation mechanism on the wood surface. Moisture movement in wood is a continuous diffusion process of water molecules, and its driving force is the chemical potential gradient, as discussed in the previous part, while evaporation on the wood surface is a phase-change process where water molecules on the wood surface evaporate to the surrounding atmosphere, and its driving force is assumed to be the vapor pressure difference. Thus, the drying rate equation can be expressed as

$$-\frac{d\Omega}{Adt} = \xi(P-P_e) \qquad (2\text{-}1.4)$$

where $-d\Omega/dt$ : Drying rate (g/sec),

$P$ : Vapor pressure of wood surface in equilibrium with the surface moisture content (mmHg),

$P_e$ : Vapor pressure of the surroundings (mmHg),

$\xi$ : Surface evaporating coefficient (g/sec.cm$^2$.mmHg),

$A$ : Surface area (cm$^2$).

Eq.(2-1.4) is a generalized drying rate equation in constant rate of drying. During the period of constant rate of drying, the temperature of the wood surface may be held to the wet bulb temperature, and the vapor pressure of the wood surface equals the saturated vapor pressure at the wet bulb temperature. Therefore, the vapor pressure difference ($P$-$P_e$) is kept constant, and a constant rate of drying results.

The surface vapor pressure is given by the transformation of Eq.(2-1.4) as

$$P = P_e - \frac{1}{\xi A}\frac{d\Omega}{dt} \qquad (2\text{-}1.5)$$

The vapor pressure of the surroundings and the conditions of the specimen are determined by means of the given conditions of drying. The surface evaporating coefficient is a constant depending on temperature and is chosen from the literature. As the drying rate $-d\Omega/dt$ can be measured experimentally, the surface vapor pressure $P$ is calculated on the basis of Eq. (2-1.5). The saturated vapor pressure $P_s$ which is a function of temperature is found in tables of water-vapor pressure vs. temperature, if the temperature of the wood surface is known. Then, the relative vapor pressure at the wood surface is calculated as

$$RH = P/P_s \qquad (2\text{-}1.6)$$

Finally, the surface moisture content is obtained by use of the desorption isotherm of water-vapor by the wood.

Though this method is the same as Hart's and Ogura's methods with respect to the estimation of the surface moisture content by use of the sorption isotherm, it requires neither constants based on theoretical assumptions nor factors of which the physical meaning is unclear. Furthermore, the equation used is very simple, and the data necessary for the calculation is obtained by use of conventional drying experiments.

The moisture content at the center of the specimen is calculated in each iteration of the program by using values near the center on the assumption that the moisture content is parabolically distributed and that the maximum values of the moisture distribution curves are at the center. Thus,

$$MC(L_{max},M) = 1/3\{4MC(L_{max}-1,M)-MC(L_{max}-2,M)\} \qquad (2\text{-}1.7)$$

where $MC(L_{max},M)$ is the center moisture content at time $t_M$, and $L_{max}$ stands for the maximum mesh point in the $x$-direction.

### 2-1.3. Programming - A Fortran Program -

Fig.2.2 shows a flow chart of the program for computation of moisture distribution in the specimen. New variables used for convenience of computation are as follows:

*CM*(L,M): Moisture content *MC*(L,M),

*DC*(L,I): Diffusion coefficient $D_\mu$(L,I),

*DC1*(L,I) and *DC2*(L,I): *DC*(L+½,I) and *DC*(L-½,I), respectively,

*BH* and *BK*: Mesh size $\Delta x$ and $\Delta t$, respectively,

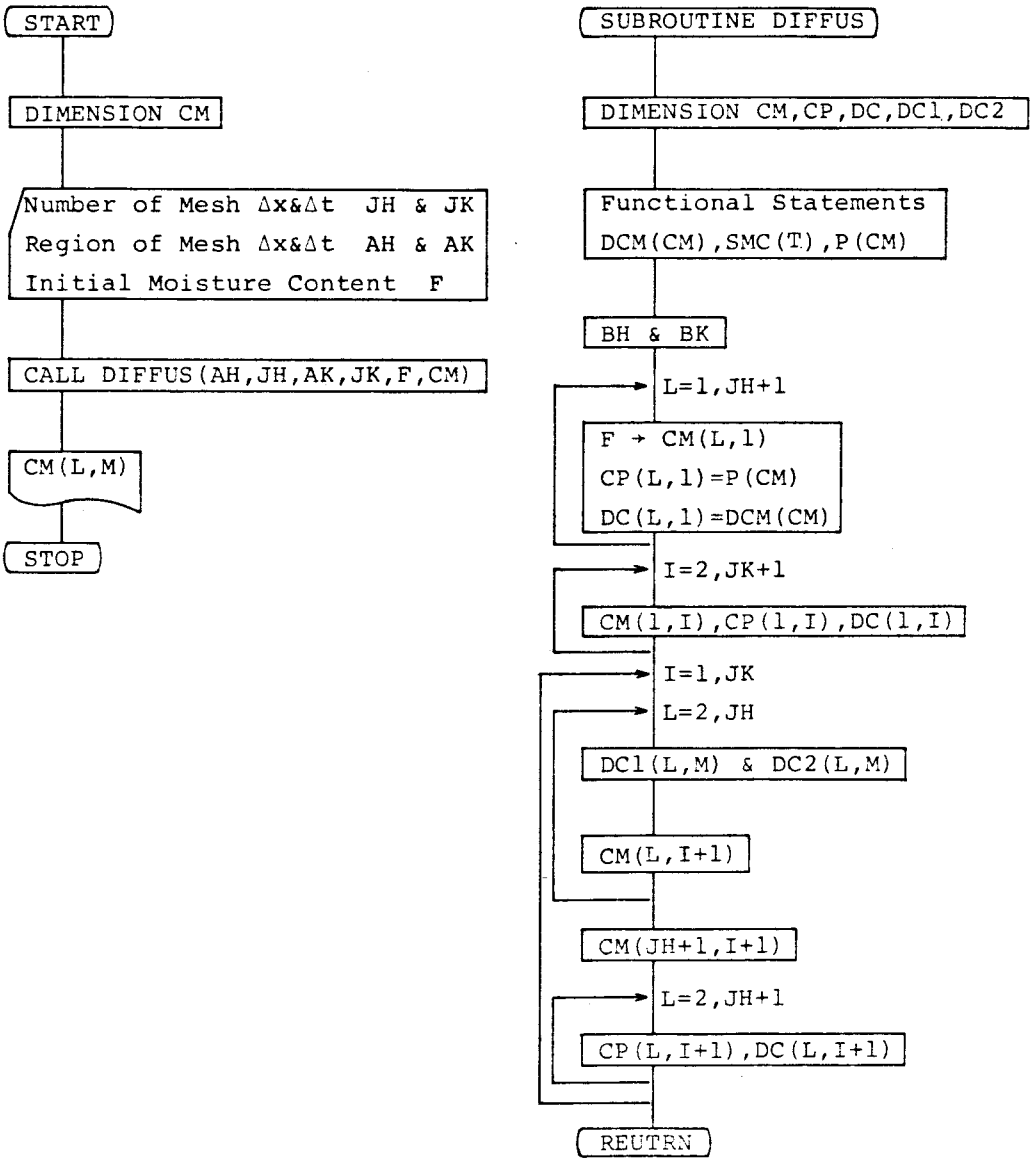


Fig.2.2 Flow chart for calculation of the moisture distribution

*DCM(CM)*: Diffusion coefficient $D_\mu$ as a function of moisture content,

*SMC(t)*: Surface moisture content as a function of time,

*P(CM)*: Desorption isotherm.

In the subroutine, the moisture content within wood is calculated for successive positions at time $t_M$ after the

computation of the initial and the surface moisture contents. The center moisture contents is calculated last.

## 2-2. *Application of the Method for Predicting Moisture Distributions in Wood*

### 2-2.1. Determination of the Input Data

The following drying conditions were chosen from the drying experiment data in Chapter 1-1 as examples for application:

i) Drying condition No.3 : An equilibrium moisture content (EMC) of 0.082 with an initial condition of 0.260 m.c.

ii) Drying condition No.4 : An EMC of 0.024 with an initial condition of 0.230 m.c.

The experiments were carried out at a constant temperature of 40°C dry bulb for both conditions. The wood species, the sample preparation, and the flow direction were described in Chapter 1-1. The moisture distributions were calculated in the time range from 0 to 90 minutes. Numerical values of the input conditions a, b, c, and d were determined as follows:

a) The Mesh Size $\Delta x$ and $\Delta t$

Taken into account the stability condition (2-1.3), the mesh size $\Delta x$ and $\Delta t$ were determined for each condition as

i) $\Delta x$=0.1 cm, and $\Delta t$=18 sec,

ii) $\Delta x$=0.1 cm, and $\Delta t$=36 sec.

b) Diffusion Coefficient $D_\mu$

The diffusion coefficient $D_\mu$ obtained in Chapter 1-3 was used. The data in Fig.1.12 were fitted to two different models by least square methods:

$\log D_{\mu}1 = -6.054 + 10.73(MC)$, and

$D_{\mu}2 = 0.2326\times10^{-3} - 0.4342\times10^{-2}(MC) + 0.1993\times10^{-1}(MC)^2$ .

c) Initial Conditions *IMC*

The specimens were conditioned to equilibrium with certain relative vapor pressures. And it was confirmed that the initial moisture content was uniformly distributed through the specimen thickness. The values for the drying conditions were

i) $IMC$=0.260, and

ii) $IMC$=0.230.

d) Boundary Conditions

In order to determine the surface moisture content, the drying rate $-d\Omega/dt$ was measured from the drying curves in Fig. 1.3. The surface evaporating coefficient $\xi$ was evaluated as $0.943\times10^{-6}$ g/sec.cm$^2$.mmHg on the basis of the drying rate at a constant rate of drying in the longitudinal direction at 40°C.[8] The value of $\xi$ was in good agreement with that of free water and those reported by other investigators.[59] The surface area $A$ of the specimen and the vapor pressure of the surroundings $P_e$ were determined by the given experimental conditions. The surface vapor pressure $P$ was then calculated by means of Eq.(2-1.5).

While the saturated vapor pressure $P_s$ is a function of the surface temperature of wood, the measurement of the surface temperature is not so easy. An estimation method of wood temperature by use of the heat-transfer equation has been reported,[57] but it is difficult to take into account the differential heat of sorption by this method. In the present study, wood temperature was measured by use of a thermocouple inserted into

Table 2.1 Calculation of surface moisture content of wood

| Time (min) | Flux ($g/cm^2sec$) | P (mmHg) | Temp. (°C) | $P_s$ (mmHg) | $P/P_s$ | MC (g/g) |
|---|---|---|---|---|---|---|
| Drying condition No.3 | | | | | | |
| 0 | - | - | - | - | - | 0.260 |
| 6 | $0.825 \times 10^{-5}$ | 48.04 | 38.9 | 52.17 | 0.921 | 0.161 |
| 12 | 0.759 | 47.34 | 39.3 | 53.31 | 0.888 | 0.138 |
| 18 | 0.686 | 46.58 | 39.5 | 53.88 | 0.865 | 0.127 |
| 24 | 0.678 | 46.46 | 39.7 | 54.46 | 0.853 | 0.122 |
| 30 | 0.660 | 46.29 | 39.8 | 54.75 | 0.845 | 0.118 |
| 36 | 0.617 | 45.83 | 39.9 | 55.04 | 0.833 | 0.114 |
| 42 | 0.530 | 44.91 | 39.9 | 55.04 | 0.816 | 0.108 |
| 48 | 0.455 | 44.12 | 40.0 | 55.34 | 0.797 | 0.102 |
| 54 | 0.381 | 43.33 | 40.0 | 55.34 | 0.783 | 0.097 |
| 60 | 0.318 | 42.66 | 40.0 | 55.34 | 0.771 | 0.094 |
| 66 | 0.248 | 41.92 | 40.0 | 55.34 | 0.757 | 0.090 |
| 72 | 0.168 | 41.07 | 40.0 | 55.34 | 0.742 | 0.087 |
| 78 | 0.131 | 40.68 | 40.0 | 55.34 | 0.735 | 0.085 |
| 84 | 0.111 | 40.46 | 40.0 | 55.34 | 0.731 | 0.083 |
| 90 | 0.082 | 40.16 | 40.0 | 55.34 | 0.726 | 0.083 |
| Drying condition No.4 | | | | | | |
| 0 | - | - | - | - | - | 0.230 |
| 6 | 1.594 | 25.75 | 31.4 | 34.47 | 0.747 | 0.090 |
| 12 | 1.107 | 20.59 | 33.5 | 38.81 | 0.531 | 0.056 |
| 18 | 0.903 | 18.42 | 35.2 | 42.65 | 0.432 | 0.048 |
| 24 | 0.707 | 16.34 | 36.4 | 45.56 | 0.359 | 0.041 |
| 30 | 0.577 | 14.97 | 37.3 | 47.85 | 0.313 | 0.038 |
| 36 | 0.508 | 14.23 | 38.1 | 49.97 | 0.285 | 0.035 |
| 42 | 0.446 | 13.59 | 38.7 | 51.62 | 0.263 | 0.033 |
| 48 | 0.397 | 13.06 | 39.3 | 53.31 | 0.245 | 0.031 |
| 54 | 0.342 | 12.48 | 39.6 | 54.17 | 0.230 | 0.029 |
| 60 | 0.262 | 11.63 | 39.8 | 54.75 | 0.212 | 0.028 |
| 66 | 0.196 | 10.88 | 39.9 | 55.04 | 0.197 | 0.027 |
| 72 | 0.138 | 10.32 | 40.0 | 55.34 | 0.186 | 0.026 |
| 78 | 0.111 | 10.03 | 40.0 | 55.34 | 0.181 | 0.026 |
| 84 | 0.091 | 9.81 | 40.0 | 55.34 | 0.177 | 0.025 |
| 90 | 0.036 | 9.24 | 40.0 | 55.34 | 0.167 | 0.024 |

Flux = $-d\Omega/Adt$

$P$ = Flux/$\xi$ + $P_e$, where $\xi$ is estimated as $0.943 \times 10^{6}$ g/sec.cm$^2$.mmHg, and $P_e$ as 39.32 and 8.85 mmHg for drying condition No.3 and 4, respectively.

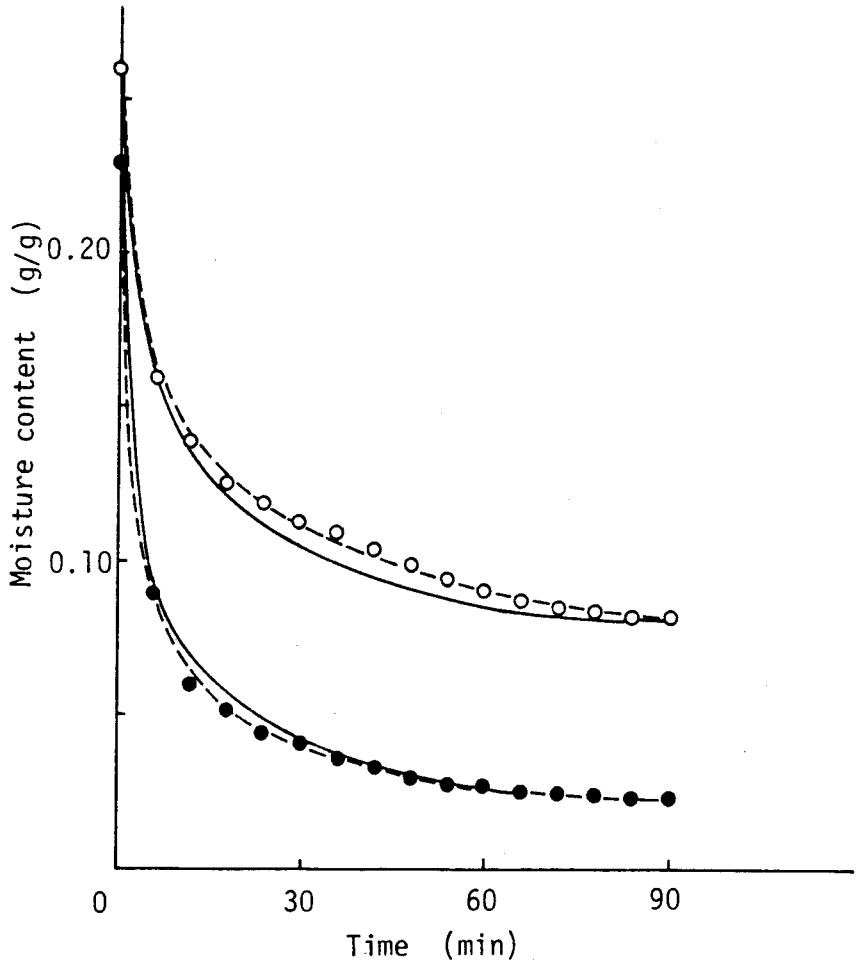


Fig.2.3 Surface moisture content during drying for drying conditions No.3 and No.4

○ : Calculated surface moisture content for drying condition No.3,

● : Calculated surface moisture content for drying condition No.4,

——: Drying data from soft X-ray measurements.

the center of specimen, on the assumption that the temperature was uniformly distributed.[60] This assumption may be reasonable, because in wood the thermal conductivity is much greater than the moisture diffusibility, and the specimens used were sufficiently small. Finally, the surface moisture content was

calculated by use of the desorption isotherm at 40°C shown in Fig.1.9. Table 2.1 shows the calculation of the surface moisture content, and Fig.2.3 shows the calculated surface moisture contents during drying by use of Eq.(2-1.4) in comparison with the experimental values obtained by means of soft X-ray densitometry. It is apparent from the figure that the calculated values for both drying conditions are in relatively good agreement with the experimental ones.

The moisture content at the center of the specimen was calculated in each iteration of the program by use of Eq.(2-1.7). From the mesh size chosen for this study, Eq.(2-1.7) becomes

$$MC(6,M) = 1/3\{4MC(5,M)-MC(4,M)\}$$

## 2-2.2. Calculation Results and Discussion

Fig.2.4 shows some solutions of the diffusion equation for condition i) as compared to measured distributions after several time intervals, and similar results for drying condition ii) are shown in Fig.2.5. Predicted and experimental moisture distributions in the early stage of drying for each condition show fairly good agreement with each other, but in the middle and the final stages of drying, the predicted values tend to be smaller than the actual ones, and the fit of the predicted moisture distributions to the experimental ones is rather poor.

The moisture distributions predicted by use of diffusion coefficient $D_\mu 1$(exponential form) shows generally better agreement with the experimental ones than those by use of diffusion coefficient $D_\mu 2$(polynominal form). The average difference

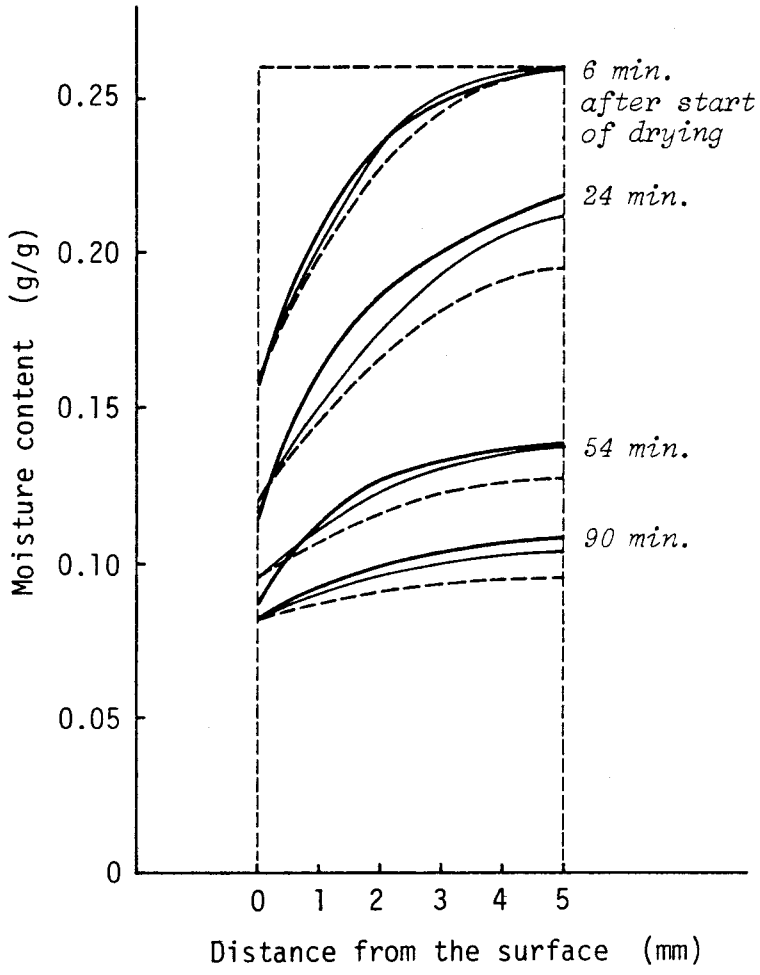


Fig.2.4 Predicted moisture distributions during drying for condition i) in comparison with the experimental data

——— : Experimental data,

——— : Predicted with $D_\mu 1$,

– – – – : Predicted with $D_\mu 2$.

between predicted and experimental values over all times and positions was 0.008 and 0.012 m.c. for $D_\mu 1$ and $D_\mu 2$, respectively. This confirms the exponential dependence of the diffusion coefficient on moisture content in the longitudinal direction of wood.

The maximum error between the predicted values for $D_\mu 1$

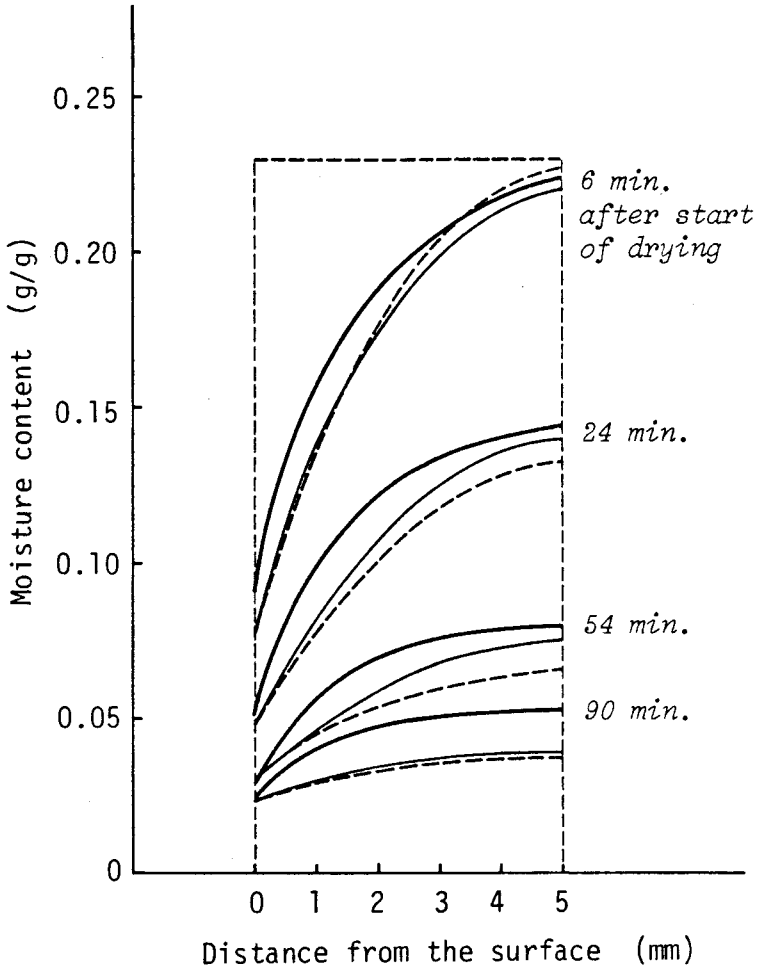


Fig.2.5 Predicted moisture distributions during drying for condition ii) in comparison with the experimental data

——— : Experimental data,

——— : Predicted with $D_{\mu}1$,

– – – – : Predicted with $D_{\mu}2$.

and the experimental ones is about 0.025 m.c. for the entire drying period. Several factors contributing to the error in the results can be considered. First is the experimental error, which was evaluated to be ±0.010 m.c. based on the average moisture content measured by the oven-dry method and by soft X-ray densitometry. This error imports an additional error to the

diffusion coefficient $D_\mu$, when it is calculated from the experimental data. However, it is not easy to evaluate the error in $D_\mu$, because it is also affected by other factors such as wood structure, wood temperature, and drying stresses. The second error occurs in calculation. In order to estimate this error, a half-size mesh was used for the calculation. The results showed only a slight improvement in moisture distributions, amounting to about 0.010-0.003 m.c. The third error is in estimating the boundary conditions. The surface moisture content calculated by use of Eq.(2-1.4) shows rather good agreement with the experimental data. As a boundary condition, however, it has an effect on the difference equation, which must be considered. Errors in the boundary condition in the early stages of drying, for example, are propagated in the iterative process, and the results appear in the middle or final stages of drying. The experimental data of surface and center moisture content were fitted to empirical equations, and these were used as boundary conditions. This reduced the maximum error to less than 0.020 m.c. Errors in the initial conditions are assumed to be small. Thus, the surface moisture content and the diffusion coefficient seem to be the significant factors which affect the accuracy of the approximate solutions.

In spite of these errors and factors, which should be investigated further in the future, the predicted moisture distributions estimated from the proposed diffusion equation agree fairly well with the experimental data. This suggests that the proposed equation represents a valid approach. The solution of Eq.(1-2.17) can thus be used for describing longitudinal

moisture movement below the fiber saturation point, and is valid for predicting the wood drying process.

## 2-3. *Summary*

Numerical solutions of the proposed diffusion equation were discussed in order to predict moisture distributions in wood during drying. Moisture distributions for two drying conditions were predicted, and the results were compared with experimental data. The investigation can be summarized as follows:

1) Numerical solutions of the proposed diffusion equation (1-2.17) by a finite difference technique were discussed. The input data necessary for the calculation,i.e, the mesh size, the diffusion coefficient, the initial- and the boundary conditions, were also discussed.

2) Moisture distributions in the longitudinal direction of wood were predicted for two drying conditions at 40°C, and the results were compared with the actual ones. The average difference between predicted and experimental values over all times and positions was 0.008 m.c., and the predicted moisture distributions showed good agreement with the experimental ones measured by use of soft X-ray densitometry. The effect of the input data on the accuracy of the approximation was also discussed. The surface moisture content as a boundary condition and the diffusion coefficient seemed to be the significant factors.

In conclusion, the proposed diffusion equation (1-2.17)

was shown to be valid for representing the moisture movement in wood below the fiber saturation point. Its numerical solutions can be used for predicting moisture distributions in wood during drying.

# PART THREE

## PREDICTION OF DRYING STRESSES IN WOOD

Internal drying stresses in wood during drying are of considerable interest to many wood scientists, because they cause drying defects such as checks, warp, and casehardening. Schniewind[61] has divided them systematically into two groups: one is the stress resulting from moisture gradients, and the other the stress resulting from inherent differences in shrinkage of structural components of wood. Apart from special usage of wood such as cross sectional discs for arts and crafts applications, the former type of drying stress may well be considered dominant for ordinary lumbers. Drying degrade can be mainly attributed to drying stresses resulting from moisture gradients, and thus they are the stresses that have usually been investigated.

However, there are no direct means for measuring the internal stresses. Drying stresses in wood occur internally in the absence of external loads, and change with time and position. Thus, drying stresses in wood are estimated by measuring the deformation of wood and then calculating the stresses from known values of the stiffness (modulus of elasticity) of wood.

The existence of drying stresses in wood became apparent

by means of the "prong test" devised by Tiemann[62]. Thereafter, McMillen[63)-65)] developed a method of determining drying stress distributions in a drying board from measurements of immediate dimensional changes of slices cut from such a board. A series of studies[66)-69)] applying this slicing technique succeeded in characterizing drying stresses, but could not go beyond the scope of quantitative discussions because of inadequate accuracy of the method.

Takemura[70) 71)] showed that the memory effect of wood during drying could be expressed as the superposition of nonsteady deformations corresponding to stresses applied independently. Taking into account this inelastic component, he then derived a fundamental equation in order to predict the drying stresses.[72)] Although the numerical solutions of this equation were calculated on the assumption that the moisture content is distributed linearly from the surface to the center of an isotropic board, the results did explain reversal patterns in drying stresses.[73) 74)] These occur when the surface layers in a board, formerly stressed in tension, become stressed in compression during drying with corresponding changes in the inner layers.

In the present part, a computing method for drying stresses in wood during drying is established. The constitutive equation for the drying stresses is derived on the basis of the theory of viscoelasticity and is combined with the prediction of moisture distributions in wood during drying by use of solutions of the diffusion equation[75)]. Then the predicted drying stresses under different drying conditions are compared with each other[76)].

## 3-1. *Theory for the Prediction of Drying Stresses in Wood during Drying*

### 3-1.1. Constitutive Equation for Drying Stresses in Wood

The constitutive equation for elastic materials can be expressed as

$$[\sigma] = [B^e][\varepsilon^e] \tag{3-1.1}$$

where $[\sigma]$ is the stress tensor, $[\varepsilon^e]$ the strain tensor, and $[B^e]$ the stiffness tensor. The three-dimensional stress components are expressed as

$$[\sigma] = \begin{bmatrix} \sigma_{11} & \sigma_{12} & \sigma_{13} \\ \sigma_{21} & \sigma_{22} & \sigma_{23} \\ \sigma_{31} & \sigma_{32} & \sigma_{33} \end{bmatrix} \tag{3-1.2}$$

where $\sigma_{jk}=\sigma_{kj}$ so that the stress tensor $[\sigma]$ is a symmetric tensor. For an orthotropic material Eq.(3-1.1) can be expressed as

$$\begin{Bmatrix} \sigma_x \\ \sigma_y \\ \sigma_z \\ \tau_{yz} \\ \tau_{zx} \\ \tau_{xy} \end{Bmatrix} = \begin{bmatrix} b_{11} & b_{12} & b_{13} & 0 & 0 & 0 \\ b_{12} & b_{22} & b_{23} & 0 & 0 & 0 \\ b_{13} & b_{23} & b_{33} & 0 & 0 & 0 \\ 0 & 0 & 0 & b_{44} & 0 & 0 \\ 0 & 0 & 0 & 0 & b_{55} & 0 \\ 0 & 0 & 0 & 0 & 0 & b_{66} \end{bmatrix} \begin{Bmatrix} \varepsilon_x^e \\ \varepsilon_y^e \\ \varepsilon_z^e \\ \gamma_{yz}^e \\ \gamma_{zx}^e \\ \gamma_{xy}^e \end{Bmatrix} \tag{3-1.3}$$

where $\sigma_x$, $\sigma_y$, $\sigma_z$ : Normal stress components,

$\tau_{yz}$, $\tau_{zx}$, $\tau_{xy}$: Shear stress components,

$\varepsilon_x^e$, $\varepsilon_y^e$, $\varepsilon_z^e$ : Normal strain components,

$\gamma_{yz}^e$, $\gamma_{zx}^e$, $\gamma_{xy}^e$: Shear strain components,

$b_{jk}$ : Stiffness matrix components.

As Eq.(3-1.3) shows, there is no cross-effect between the

normal components and the shear components, provided the $x$, $y$, and $z$ directions coincide with the principal structural axes of the material.

For visocoelastic materials, the total strain $\{\varepsilon\}$ may be assumed to consist of the elastic strain element $\{\varepsilon^e\}$ and the inelastic strain element $\{\varepsilon^f\}$ and is obtained as

$$\{\varepsilon\} = \{\varepsilon^e\} + \{\varepsilon^f\}$$

Thus,

$$\{\varepsilon^e\} = \{\varepsilon\} - \{\varepsilon^f\} \qquad (3\text{-}1.4)$$

By substitution of Eq.(3-1.4) into Eq.(3-1.1), the constitutive equation for viscoelastic materials can take the form

$$\{\sigma\} = [B^e]\{\varepsilon\} - [B^e]\{\varepsilon^f\} \qquad (3\text{-}1.5)$$

Wood can be considered an orthotropic and viscoelastic material. In order to use Eq.(3-1.5) in developing the constitutive equation for drying stresses resulting from moisture gradients in wood, one dimensional flow in the longitudinal direction of wood is considered for simplicity as shown in Fig. 3.1. During drying moisture gradients are formed along the longitudinal direction of wood, and plane stresses develop in planes normal to the longitudinal direction,i.e., in transverse planes. Thus,

$$\sigma_L=0, \text{ and } \tau_{TL}=\tau_{LR}=0$$

where the subscripts L, T, and R denote the three principal axes of wood. The components in Eq.(3-1.5) for the transverse

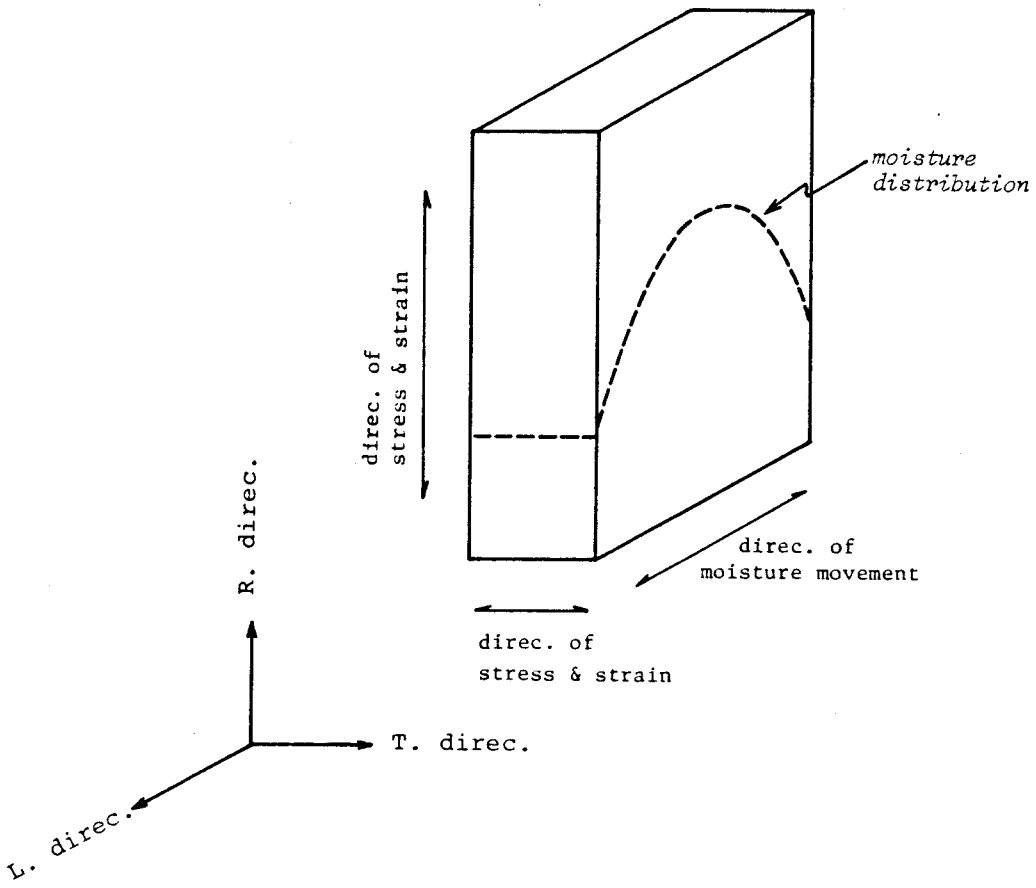


Fig.3.1 Schematic diagram showing the directions of moisture movement, drying stresses, and strains in wood

plane of wood are then derived as

$$\begin{Bmatrix} \sigma_R \\ \sigma_T \\ \tau_{RT} \end{Bmatrix} = \begin{bmatrix} b_{11} & b_{12} & 0 \\ b_{21} & b_{22} & 0 \\ 0 & 0 & b_{33} \end{bmatrix} \begin{Bmatrix} \varepsilon_R \\ \varepsilon_T \\ \gamma_{RT} \end{Bmatrix} - \begin{bmatrix} b_{11} & b_{12} & 0 \\ b_{21} & b_{22} & 0 \\ 0 & 0 & b_{33} \end{bmatrix} \begin{Bmatrix} \varepsilon_R^f \\ \varepsilon_T^f \\ \gamma_{RT}^f \end{Bmatrix} \qquad (3\text{-}1.6)$$

The components of the stiffness matrix $[B^e]$ in Eq.(3-1.6) are given by

$$\begin{aligned} b_{11} &= E_R/(1-\mu_{RT}\mu_{TR}) \\ b_{22} &= E_T/(1-\mu_{RT}\mu_{TR}) \\ b_{12} &= b_{21} = b_{11}\,\mu_{TR} = b_{22}\,\mu_{RT} \end{aligned} \qquad (3\text{-}1.7)$$

$b_{33} = G_{RT}$

where $E_R$ and $E_T$ are the moduli of elasticity in the radial and the tangential directions, respectively, $\mu_{RT}$ and $\mu_{TR}$ are Poisson's ratios, and $G_{RT}$ is the modulus of rigidity.

Wood shrinks with decreasing moisture content owing to its composition and structural organization. If wood is modelled by dividing it into layers along the longitudinal direction, and if these layers are thin enough, moisture distribution can be neglected in each layer. When wood is dried and has moisture gradients along the longitudinal direction, the layers try to shrink in the radial and the tangential directions to the potential deformations based on their moisture contents, shown as $\{dl_2\}$ in Fig.3.2. However, wood can be assumed to react as a unit body and the potential deformation in each layer is restrained to some extent by the adjacent layers. As a result, drying stresses develop in the wood layers.

Thus, by use of the symbols in Fig.3.2, the observed strain can be given as

$$\{\varepsilon^{OS}\} = \{\frac{dl_1}{l_g}\} \qquad (3\text{-}1.8)$$

where $\{dl_1\}$ is the observed deformation which can be measured during drying and $l_g$ the green dimension. The potential strain in each layer is given as

$$\{\varepsilon^{BS}\} = \{\frac{dl_2}{l_g}\} \qquad (3\text{-}1.9)$$

where $\{dl_2\}$ is the potential deformation in each layer. In

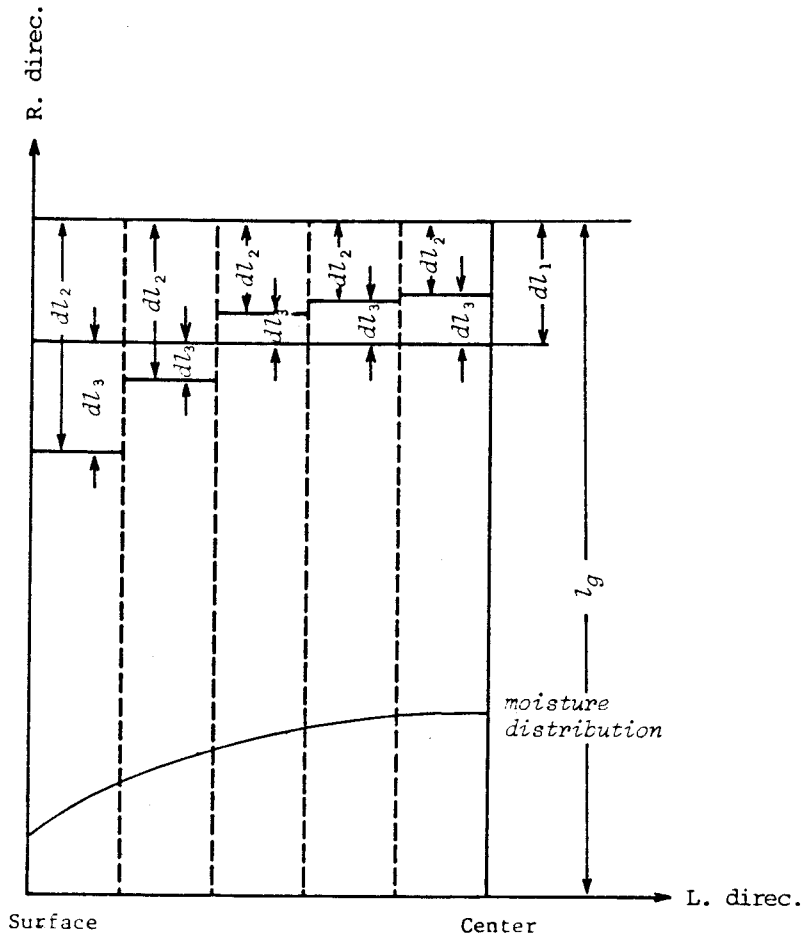


Fig.3.2 The deformation in the radial direction caused by the moisture distribution in relation to the observed deformation and the basic shrinkage(the potential deformation)

$l_g$: The green dimension, $dl_1$: The observed deformation, $dl_2$: The potential deformation, $dl_3$: The restrained deformation.

wood science, these strains are often expressed as shrinkages which are positive quantities. The observed strain and the potential strain are thus expressed in this paper as the observed shrinkage $\{\varepsilon^{OS}\}$ and the basic shrinkage $\{\varepsilon^{BS}\}$, respectively.

Therefore, the total strain $\{\varepsilon\}$ in Eq.(3-1.5) caused by the drying stress is defined as the restrained strain in each

layer and is obtained from Fig.3.2 as

$$\{\varepsilon\} = \{\frac{dl_3}{l_g}\} \tag{3-1.10}$$

where $\{dl_3\}$ is the restrained deformation. Eq.(3-1.10) may thus take the form

$$\{\varepsilon\} = \{\varepsilon^{BS}\}-\{\varepsilon^{OS}\} \tag{3-1.11}$$

where tensile strain is positive and compressive strain negative. Substitution of Eq.(3-1.11) into Eq.(3-1.5) yields the constitutive equation for drying stresses in wood as

$$\{\sigma\} = [B^e]\{\varepsilon^{BS}\}-[B^e]\{\varepsilon^{OS}\}-[B^e]\{\varepsilon^f\} \tag{3-1.12}$$

The components in Eq.(3-1.12) for the transverse plane(R-T plane) of wood are written as

$$\begin{Bmatrix}\sigma_R\\ \sigma_T\\ \tau_{RT}\end{Bmatrix} = \begin{bmatrix}b_{11} & b_{12} & 0\\ b_{12} & b_{22} & 0\\ 0 & 0 & b_{33}\end{bmatrix}\begin{Bmatrix}\varepsilon_R^{BS}\\ \varepsilon_T^{BS}\\ \gamma_{RT}^{BS}\end{Bmatrix} - \begin{bmatrix}b_{11} & b_{12} & 0\\ b_{12} & b_{22} & 0\\ 0 & 0 & b_{33}\end{bmatrix}\begin{Bmatrix}\varepsilon_R^{OS}\\ \varepsilon_T^{OS}\\ \gamma_{RT}^{OS}\end{Bmatrix} - \begin{bmatrix}b_{11} & b_{12} & 0\\ b_{12} & b_{22} & 0\\ 0 & 0 & b_{33}\end{bmatrix}\begin{Bmatrix}\varepsilon_R^{f}\\ \varepsilon_T^{f}\\ \gamma_{RT}^{f}\end{Bmatrix} \tag{3-1.13}$$

### 3-1.2. Input Data for the Calculation of Drying Stresses

In order to calculate the drying stresses in wood by use of the constitutive equation, the following input data are necessary.

a) Mechanical Properties of the Wood

Modulus of elasticity and Poisson's ratio of wood are functions of moisture content, grain direction, density, temperature and so on. Since in this study drying is carried out at

constant temperature and since serial sections are used, only the effects of moisture content and grain direction must be taken into consideration. Below the fiber saturation point, the moduli of elasticity increase with decreasing moisture content. The Poisson's ratios $\mu_{RT}$, $\mu_{TR}$, and $\mu_{LT}$ increase with increasing moisture content. However, the Poisson's ratio $\mu_{LR}$ decreases with increasing moisture content.[77]

b) Basic Shrinkage $\{\varepsilon^{BS}\}$

Basic shrinkage is the inherent shrinkage of wood due to the loss of moisture from the swollen cell wall. A linear relationship is generally found between moisture content and shrinkage from the fiber saturation point to the oven-dry state. The relationship is obtained by a drying experiment where the moisture gradient in the specimen thickness can be neglected during drying. This condition is almost satisfied in very slow drying of very thin specimens where the thickness is the moisture flow direction.

In the previous part, it became possible to predict moisture distributions in wood during drying. Thus, the basic shrinkage $\{\varepsilon^{BS}\}$ in each layer can be calculated by use of the predicted moisture contents, when the functional relationship between moisture content and basic shrinkage is known. The basic shrinkage $\{\varepsilon^{BS}\}$ during drying is calculated as a function of position $x_L$ and time $t_M$.

c) Observed Shrinkage $\{\varepsilon^{OS}\}$

Observed shrinkage is obtained by the measurement of deformation under a given drying condition. Since the wood specimen

is assumed to react as a unit body, the observed shrinkage $\{\varepsilon^{OS}\}$ takes the same values at any position $x_L$ and is a function of time $t_M$.

d) Inelastic Strain $\{\varepsilon^f\}$

Takemura[78) 79)] derived the creep compliance of wood during drying from his relaxation theory[80)] as

$$J = J_0(J'/J_0')(1+\kappa\Delta MC) \tag{3-1.14}$$

where $J$ and $J_0$ : Creep and elastic compliances during drying, respectively,

$J'$ and $J_0'$ : Creep and elastic compliances, respectively, at moisture equilibrium,

$\Delta MC$ : Moisture content change,

$\kappa$ : Parameter.

He showed that the memory effect of wood during drying can be expressed as the superposition of non-steady deformations corresponding to stresses applied independently.[70) 71)]

$$\{\varepsilon\} = \int_{-\infty}^{t} \frac{\{d\sigma\}}{dt'}\{J\}dt' \tag{3-1.15}$$

where $\{\varepsilon\}$ is the total strain, $\{d\sigma\}$ the stress increment, $dt'$ the time increment, and $\{J\}$ the creep compliance of wood during drying, as expressed in terms of (3-1.14). Thus, the inelastic strain $\{\varepsilon^f\}$ was expressed as

$$\{\varepsilon^f\} = \int_{0}^{t} \frac{\{d\sigma\}}{dt'}\{J-J_0\}dt' \tag{3-1.16}$$

Fig.3.3 shows an outline of the computation of drying stresses

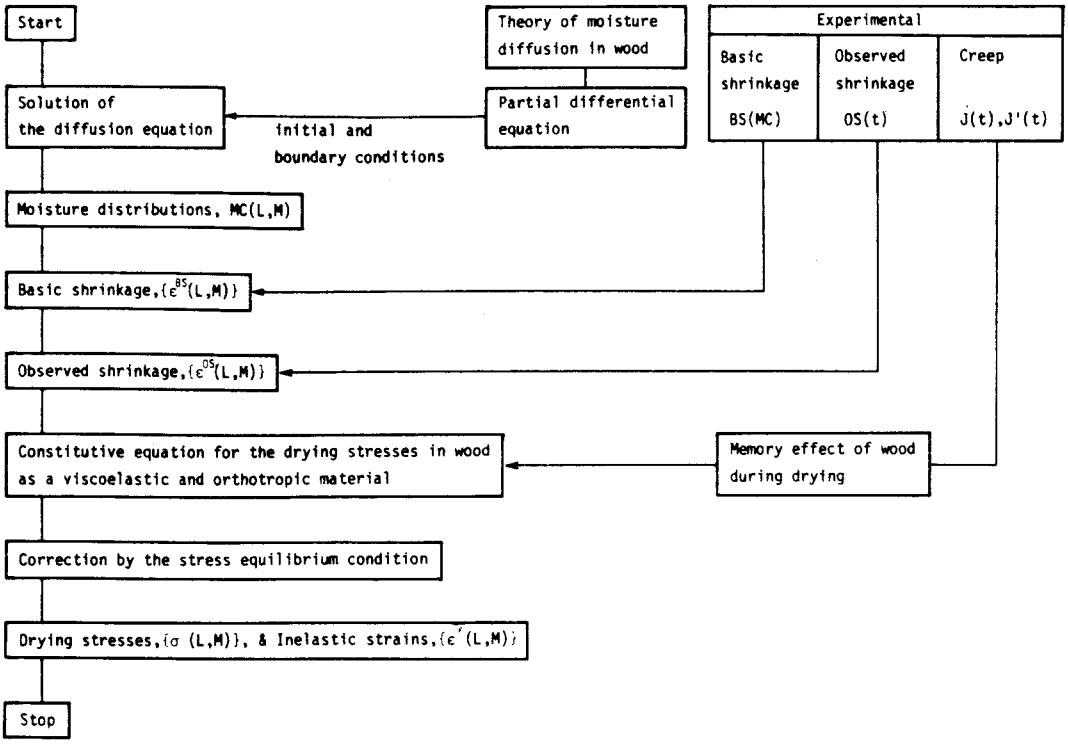


Fig.3.3 Outline of the computation of drying stresses in wood during drying

in wood during drying. The first step is the numerical solution of the proposed diffusion equation (1-2.17) by use of the finite difference technique in order to predict moisture distributions $MC(L,M)$ at position $x_L$ and time $t_M$. Basic shrinkage and observed shrinkage experimentally obtained as a function of moisture content and time, respectively, are used in computing the basic shrinkage $\{\varepsilon^{BS}(L,M)\}$ and the observed shrinkage $\{\varepsilon^{OS}(L,M)\}$, respectively. Then the drying stresses $\{\sigma(L,M)\}$ in the transverse plane of wood are calculated from the constitutive equation (3-1.12). Since external forces do not exist, the sum of the internal stresses at time $t_M$ must be zero, and as the last step the predicted drying stresses are corrected

on the basis of this stress equilibrium condition.

### 3-1.3. Programming - A Fortran Program -

The constitutive equation (3-1.13) and the necessary data for the calculation of drying stresses in wood were considered in previous sections. Programming for the numerical calculations according to Eq.(3-1.13) are discussed below.

The normal stress components in the transverse plane of wood for longitudinal flow are given by Eq.(3-1.13) as

$$\sigma_R = \frac{E_R}{1-\mu_{RT}\mu_{TR}}\{(\varepsilon_R^{BS}-\varepsilon_R^{OS}-\varepsilon_R^{f})+\mu_{TR}(\varepsilon_T^{BS}-\varepsilon_T^{OS}-\varepsilon_T^{f})\}$$

and (3-1.17)

$$\sigma_T = \frac{E_T}{1-\mu_{RT}\mu_{TR}}\{\mu_{RT}(\varepsilon_R^{BS}-\varepsilon_R^{OS}-\varepsilon_R^{f})+(\varepsilon_T^{BS}-\varepsilon_T^{OS}-\varepsilon_T^{f})\}$$

Since the moisture distribution of wood during drying is a function of position $x_L$ and time $t_M$ as shown in Eq.(2-1.2), the drying stresses computed by use of Eq.(3-1.17) are also functions of them. Thus, Eq.(3-1.17) is written in the same way as Eq.(2-1.2), and variables are transformed for convenience of computation as

$$\begin{aligned} SR(L,M) &= \frac{ER(L,M)}{1-PR\times PT}[\{BSR(L,M)-OSR(L,M)-FSR(L,M)\} \\ &\qquad +PT\{BST(L,M)-OST(L,M)-FST(L,M)\}] \\ ST(L,M) &= \frac{ET(L,M)}{1-PR\times PT}[PR\{BSR(L,M)-OSR(L,M)-FSR(L,M)\} \\ &\qquad +\{BST(L,M)-OST(L,M)-FST(L,M)\}] \end{aligned} \qquad (3\text{-}1.18)$$

where $SR(L,M)$ and $ST(L,M)$: Stress components $\sigma_R$ and $\sigma_T$, respectively,

*BSR*(L,M) and *BST*(L,M): Basic shrinkage components $\varepsilon_R^{BS}$ and $\varepsilon_T^{BS}$, respectively,

*OSR*(L,M) and *OST*(L,M): Observed shrinkage components $\varepsilon_R^{OS}$ and $\varepsilon_T^{OS}$, respectively,

*FSR*(L,M) and *FST*(L,M): Inelastic strain components $\varepsilon_R^f$ and $\varepsilon_T^f$, respectively,

*ER*(L,M) and *ET*(L,M): Moduli of elasticity $E_R$ and $E_T$, respectively,

*PR* and *PT*: Poisson's ratios $\mu_{RT}$ and $\mu_{TR}$, respectively.

Poisson's ratios are assumed to be constant (although they are a function of moisture content), and Eq.(3-1.18) is again transformed to

$$\begin{aligned} SR(L,M) &= \frac{ER(L,M)}{P}[SSR(L,M)-FSR(L,M)-PT\times FST(L,M)] \\ ST(L,M) &= \frac{ET(L,M)}{P}[SST(L,M)-PR\times FSR(L,M)-FST(L,M)] \end{aligned} \tag{3-1.19}$$

where $SSR(L,M)$: $\{BSR(L,M)-OSR(L,M)\}+PT\{BST(L,M)-OST(L,M)\}$,

$SST(L,M)$: $\{BST(L,M)-OST(L,M)\}+PR\{BSR(L,M)-OSR(L,M)\}$,

$P$ : $1-PR\times PT$.

Substitution of Eq.(3-1.16) into Eq.(3-1.19) yields the following:

$$\begin{aligned} SR(L,M) &= \frac{ER(L,M)}{P}[SSR(L,M)-\int_0^t WR(L,M)\frac{dSR(L,M)}{dt'}\,dt' \\ &\qquad -PT\int_0^t WT(L,M)\frac{dST(L,M)}{dt'}\,dt'] \\ ST(L,M) &= \frac{ET(L,M)}{P}[SST(L,M)-PR\int_0^t WR(L,M)\frac{dSR(L,M)}{dt'}\,dt' \\ &\qquad -\int_0^t WT(L,M)\frac{dST(L,M)}{dt'}\,dt'] \end{aligned} \tag{3-1.20}$$

where $dSR(L,M)$ and $dST(L,M)$ are the incremental stress components $d\sigma_R$ and $d\sigma_T$, respectively, and $WR(L,M)$ and $WT(L,M)$ the creep functions $(J-J_0)$ in the radial and the tangential directions, respectively. By the application of incremental theory to Eq.(3-1.20), the integro-differential equation (3-1.20) can be written as

$$SR(L,M) = \frac{ER(L,M)}{P}\left[SSR(L,M) - \sum_{N=1}^{M} WR(L,M,N)\,\Delta SR(L,N) - PT\sum_{N=1}^{M} WT(L,M,N)\,\Delta ST(L,N)\right]$$

$$ST(L,M) = \frac{ET(L,M)}{P}\left[SST(L,M) - PR\sum_{N=1}^{M} WR(L,M,N)\,\Delta SR(L,N) - \sum_{N=1}^{M} WT(L,M,N)\,\Delta ST(L,N)\right] \qquad (3\text{-}1.21)$$

$$N = 1,2,\ldots,M$$

where $\sum_{N=1}^{M} \Delta SR(L,N) = SR(L,M)$,

$\sum_{N=1}^{M} \Delta ST(L,N) = ST(L,M)$.

Eq.(3-1.21) indicates that the submatrices $WR(M,N)$ and $WT(M,N)$ are triangular matrices. And

$WR(M,N)=0$

$WT(M,N)=0$ when M=N

Since incremental stress component matrices $[\Delta SR]$ and $[\Delta ST]$ in Eq.(3-1.21) are unknown variables and the others are known variables, the constitutive equation for drying stresses in wood is expressed as two systems of simultaneous linear equations, shown as

$$
\begin{aligned}
&[\underset{L\times M\times N}{A1}]\,[\underset{L\times M}{\Delta SR}] + [\underset{L\times M\times N}{A2}]\,[\underset{L\times M}{\Delta ST}] = [\underset{L\times M}{SSR}] \\
&[\underset{L\times M\times N}{A3}]\,[\underset{L\times M}{\Delta SR}] + [\underset{L\times M\times N}{A4}]\,[\underset{L\times M}{\Delta ST}] = [\underset{L\times M}{SST}]
\end{aligned}
\qquad (3\text{-}1.22)
$$

where $[\,A1\,] = \sum_{N=1}^{M}\{P/ER(L,M)+WR(L,M,N)\}$,

$[\,A2\,] = \sum_{N=1}^{M}\{PT\times WT(L,M,N)\}$,

$[\,A3\,] = \sum_{N=1}^{M}\{PR\times WR(L,M,N)\}$,

$[\,A4\,] = \sum_{N=1}^{M}\{P/ET(L,M)+WT(L,M,N)\}$.

Thus, the incremental stress components are obtained as

$$
\begin{aligned}
[\Delta SR] &= \frac{[A2]\,[SST]-[A4]\,[SSR]}{[A2]\,[A3]\;-\;[A1]\,[A4]} \\
[\Delta ST] &= \frac{[A3]\,[SSR]-[A1]\,[SST]}{[A2]\,[A3]\;-\;[A1]\,[A4]}\,,
\end{aligned}
\qquad (3\text{-}1.23)
$$

and the inelastic strain components as

$$
\begin{aligned}
DR(L,M) &= \sum_{N=1}^{M} WR(L,M,N)\,\Delta SR(L,N) + PT\sum_{N=1}^{M} WT(L,M,N)\,\Delta ST(L,N) \\
DT(L,M) &= \sum_{N=1}^{M} WT(L,M,N)\,\Delta ST(L,N) + PR\sum_{N=1}^{M} WR(L,M,N)\,\Delta SR(L,N)
\end{aligned}
\qquad (3\text{-}1.24)
$$

Fig.3.4 shows a flow chart of the program for the computation of drying stresses in wood during drying. New variables used for convenience of computation are as follows:

$G = CM(L,M)-CM(L,N)$,

$FF = 1+\kappa G$,

$YR$ and $YT$ = Creep compliances in the radial and the tangential directions $JR$ and $JT$, respectively,

$XR(L,M)$ and $XT(L,M)$ = $\Delta SR(L,M)$ and $\Delta ST(L,M)$, respectively,

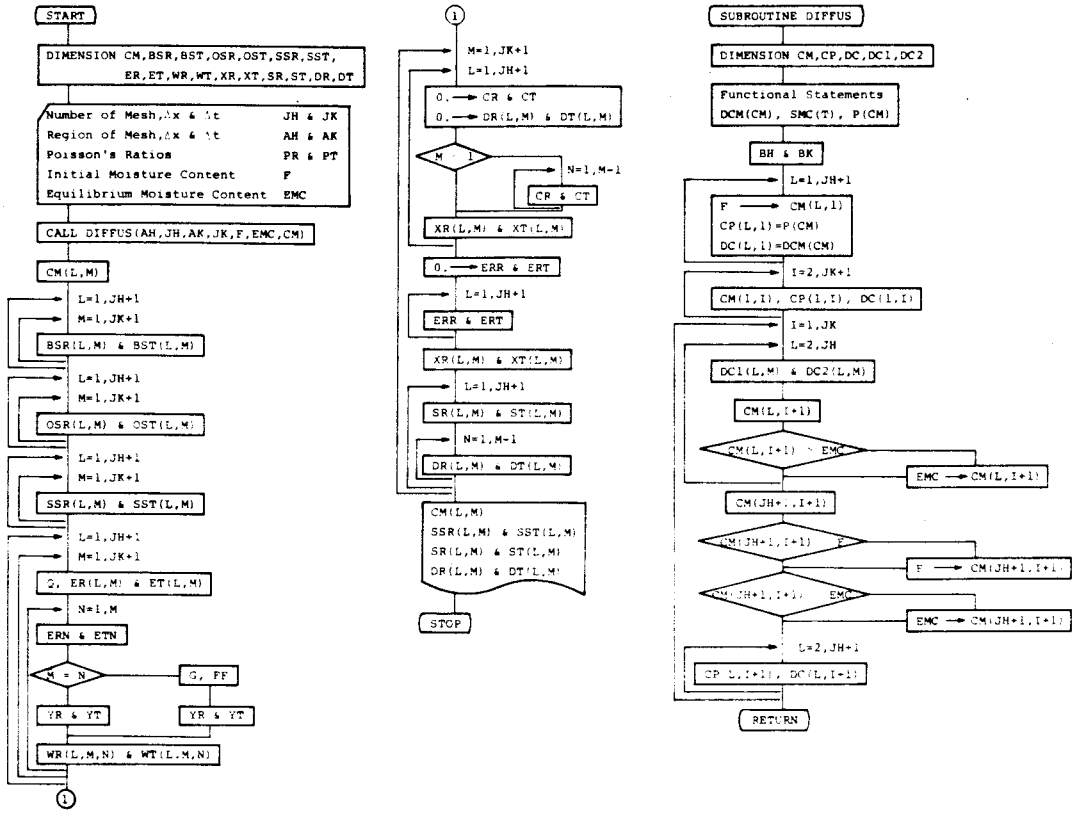


Fig.3.4 Flow chart for the calculation of drying stresses

$$CR \text{ and } CT = \sum_{N=1}^{M-1} A1(L,M,N)\times XR(L,N) + \sum_{N=1}^{M-1} A2(L,M,N)\times XT(L,N) \text{ and}$$
$$\sum_{N=1}^{M-1} A3(L,M,N)\times XR(L,N) + \sum_{N=1}^{M-1} A4(L,M,N)\times XT(L,N), \text{ respec-}$$

tively,

$$ERR \text{ and } ERT = \sum_{L=1}^{JH+1} XR(L,M) \text{ and } \sum_{L=1}^{JH+1} XT(L,M), \text{ respectively,}$$

$EMC$ = Equilibrium moisture content.

In the section from "START" to "1" as shown in Fig.3.4, the data are input, and the moisture content $CM(L,M)$ is calculated in Subroutine DIFFUS. The same program as described in Section 2-1.3 can be used for this, and the variables used are expressed in terms of the same symbols. However, the moisture

content is controlled to be less than the initial moisture content and to be larger than the equilibrium moisture content by use of an IF statement. It is also designed to make corrections during each iteration based on the average moisture content measured experimentally during drying. When the mesh size of $\Delta x$ and $\Delta t$ of the main program and the subroutine are different, the moisture content *CM*(L,M) must be rearranged in the appropriate order. The basic shrinkage *BSR*(L,M) and *BST*(L,M), the observed shrinkage *OSR*(L,M) and *OST*(L,M), and the elastic strain components *SSR*(L,M) and *SST*(L,M) are calculated in order. *WR*(L,M,N) and *WT*(L,M,N) are then obtained. In the section from "1" to "STOP", the stress increments *XR*(L,M) and *XT*(L,M) are obtained and corrected by the stress equilibrium condition. Finally, the drying stress *SR*(L,M) and *ST*(L,M) and the inelastic strains *DR*(L,M) and *DT*(L,M) are calculated and then obtained as output.

The method is based on piecewise linear theory, and the constitutive equation is also described in incremental form in the program. Therefore, the method is valid only on condition that the linear incremental relation can be assumed and that the material does not reach rupture. Further, calculation of the constitutive equation is very complex and is almost impossible without a computer.

## 3-2. *Application of the Method for Predicting Drying Stresses in Wood*

### 3-2.1. Determination of Input Data

a) Experimental

Table 3.1 Experimental conditions for determining the input data

| Type of measurement | | Experimental condition |
|---|---|---|
| Basic shrinkage | | Drying rate 1%m.c./day<br>i.m.c. 0.50 |
| Observed shrinkage | I | Under drying at 40°C,74%RH<br>i.m.c. 0.214 |
| | II | Under drying at 40°C,32%RH<br>i.m.c. 0.219 |
| | III | Under drying at 40°C,11%RH<br>i.m.c. 0.230 |
| Creep<br>(cantilever beam) | I | Under drying at 40°C,74%RH<br>i.m.c. 0.214 |
| | | At equilibrium state of moisture<br>e.m.c. 0.100 |
| | II | Under drying at 40°C,32%RH<br>i.m.c. 0.219 |
| | | At equilibrium state of moisture<br>e.m.c. 0.051 |
| | III | Under drying at 40°C,11%RH<br>i.m.c. 0.231 |
| | | At equilibrium state of moisture<br>e.m.c. 0.031 |

The experiments outlined in Table 3.1 were carried out in order to obtain the necessary data for calculation.

Specimens were taken as serial sections in the longitudinal direction from the heart wood of Hinoki (*Chamaecyparis Obtusa* Endl.) of oven-dry density of 0.39. Specimens for determining observed shrinkage were prepared to the dimensions of 100(R)×10(T) mm for measurements in the randial direction and of 50(T)×10(R) mm for measurements in the tangential direction. In both types the thickness was 10 mm in the longitudinal direction. For

basic shrinkage and creep experiments the dimensions of the specimens in cross section were the same as those for observed shrinkage, but the dimension in the longitudinal direction was kept to 2 mm because effects of drying stresses resulting from moisture gradients were undesirable in these cases.

The radial and the tangential surfaces of the specimens were sealed with adhesive tape so that drying was limited to the cross section. Specimens for measuring shrinkage had pin markers inserted on the cross section. Specimens for the measurement of observed shrinkage and creep under drying were conditioned at the same temperature as that of the drying experiments to approximately 0.22 m.c. There were no weight changes of the specimens during the last few days of conditioning, and it was confirmed by X-ray densitometry that there was uniform moisture distribution through the specimen thickness.

Basic shrinkage as a function of moisture content was obtained by drying experiments using a very slow drying rate (about 1% m.c./day) at room temperature with specimens initially conditioned to about 50% m.c. During drying, changes in dimension and in weight of the specimens were measured by use of a travelling microscope and an analytical balance, respectively. The relationship obtained between shrinkage and moisture content was regarded as the basic shrinkage curve.

Observed shrinkage was determined as a function of time. Changes in dimension and in weight of the specimens during drying were measured by use of a travelling microscope and a load cell, respectively. The drying apparatus was the same as used for the measurement of moisture distribution as shown in

Fig.1.1. The specimens were dried at a constant temperature of 40°C dry bulb with three relative humidity conditions. These were maintained by use of saturated salt solutions selected on the basis of stability with respect to temperature. The following drying conditions were used:

I) 40°C dry bulb, and 74%RH ($NaCl$),

II) 40°C dry bulb, and 32%RH ($MgCl_2$),

III) 40°C dry bulb, and 11%RH ($LiCl$).

Creep was measured using cantilever beams within the linear range. Creep under drying was obtained under conditions I, II, and III as used for observed shrinkage. Creep at moisture equilibrium was obtained with specimens initially conditioned to equilibrium moisture contents corresponding to drying conditions I, II, and III.

Wood temperature during drying was measured by use of a thermocouple inserted into the center of the specimen in order to evaluate surface moisture content which is necessary for the calculation of moisture distribution. Three or four specimens were used for each experiment.

b) Input Data

Fig.3.5 shows basic shrinkage curves as a function of moisture content. The shrinkage for both the radial and the tangential directions starts at about 0.30 m.c. which is usually considered to be the fiber saturation point. An almost linear relationship is observed between basic shrinkage and moisture content from about 0.15 to zero moisture content. Since the drying rate was extremely slow and since thin wafers

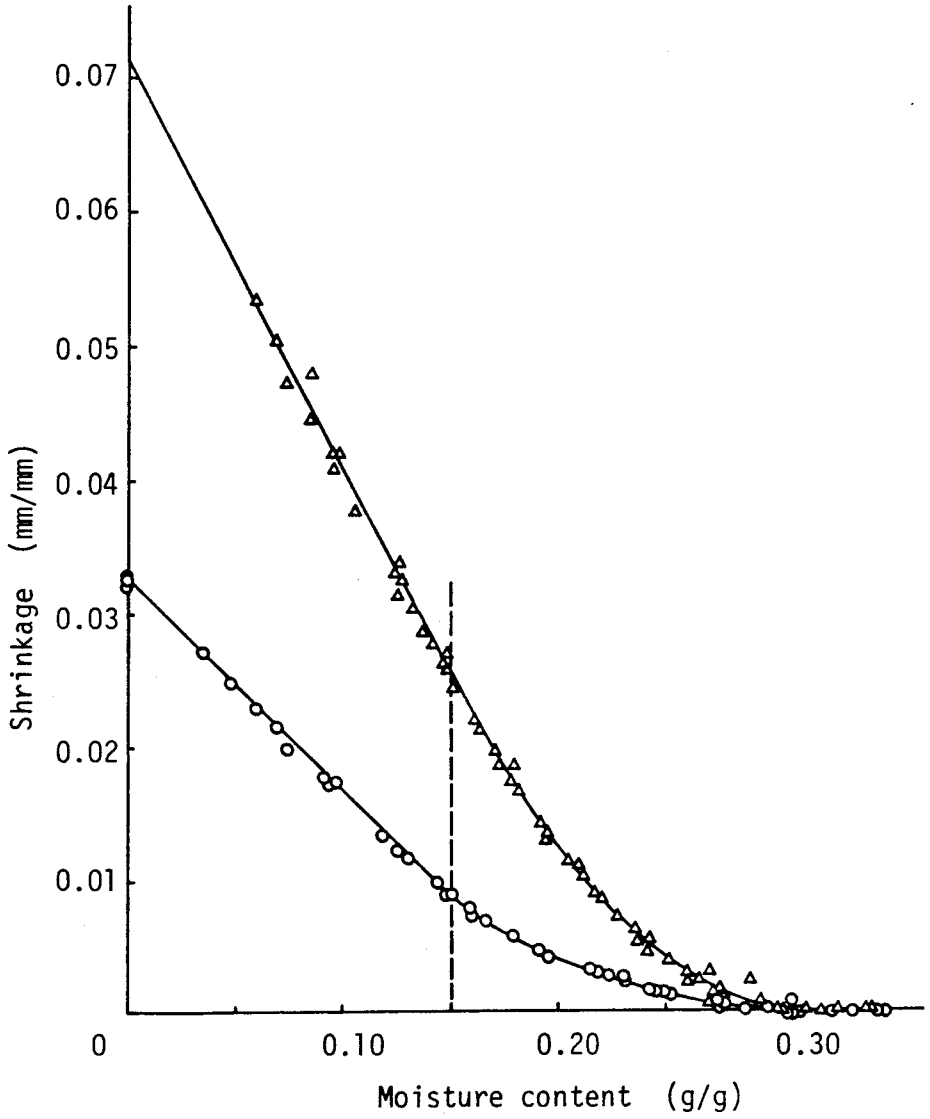


Fig.3.5 Basic shrinkage

○ : Radial direction, △ : Tangential direction

were used, the assumption that the moisture distribution was uniform during drying was probably satisfied. Therefore, it was assumed that moisture distribution did not affect shrinkage. The shrinkage curves obtained as a function of moisture content can thus be considered basic shrinkage curves,i.e., curves showing the inherent hygroscopic shrinkage of wood due to loss of

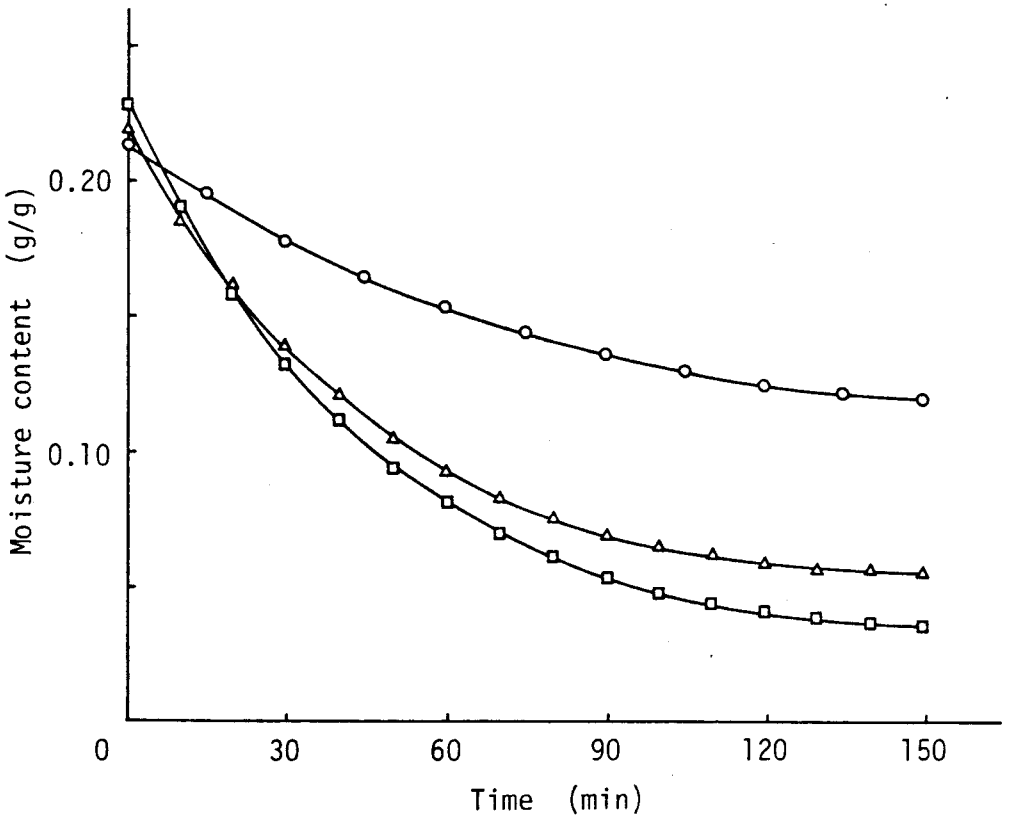


Fig.3.6 Average drying curves
○ : Condition I (74%RH), △ : Condition II (32%RH),
□ : Condition III (11%RH).

moisture from the swollen cell wall as a function of m.c.

Fig.3.6 shows average drying curves for drying conditions I, II, and III. Specimens were approaching equilibrium after 150 minutes of drying at EMC levels of 0.120, 0.055, and 0.036 for drying conditions I, II, and III, respectively. Fig.3.7 shows observed shrinkage as a function of time. Since a stress-free state is assumed at the start of drying, the green dimensions $l_g$ in Eq.(3-1.8) can be estimated by use of the initial dimensions and the basic shrinkage corresponding to the initial moisture content.

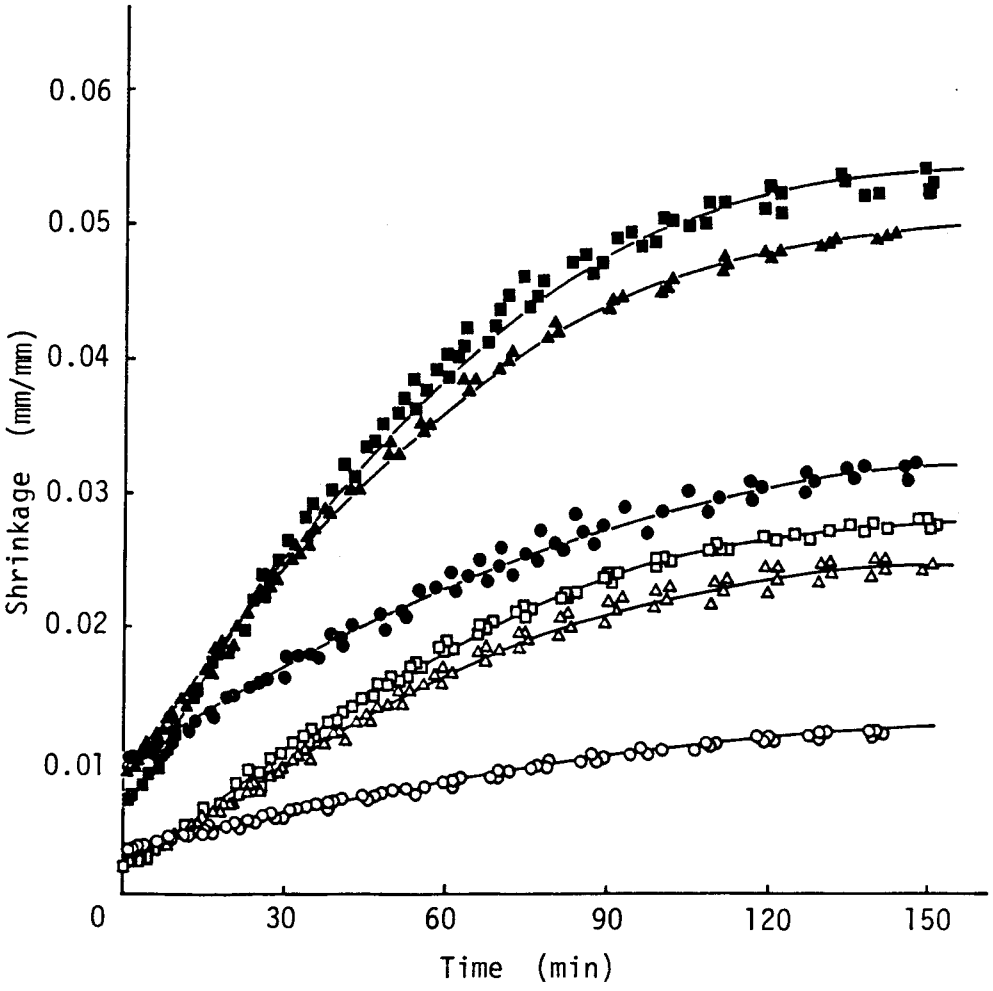


Fig.3.7 Observed shrinkage

○ : Condition I (74%RH) in the radial direction,

● : Condition I (74%RH) in the tangential direction,

△ : Condition II (32%RH) in the radial direction,

▲ : Condition II (32%RH) in the tangential direction,

□ : Condition III (11%RH) in the radial direction,

■ : Condition III (11%RH) in the tangential direction.

Fig.3.8 shows the results of creep experiments for condition II as an example. It is well-known that creep is much larger under drying than at an equilibrium state of moisture.[81)-85)] Its mechanism has been investigated by Suzuki, Armstrong, and

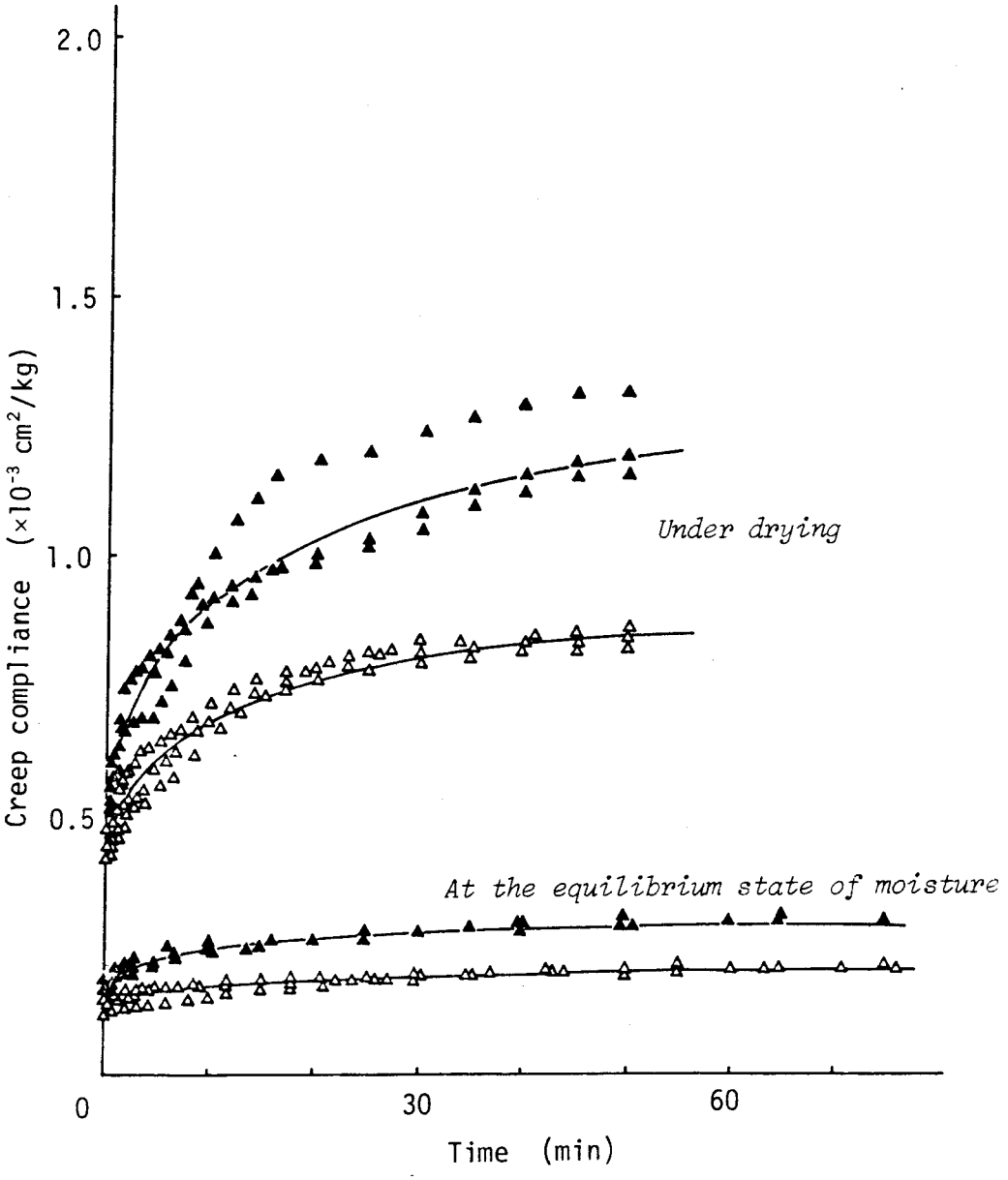


Fig.3.8 Creep compliance for condition II (32%RH)
△ : Radial direction, ▲ : Tangential direction.

others.[86)-90)] Solid lines in the figure are the creep compliances $J(t)$ at time $t$(min) approximated with power functions using least square methods. Table 3.2 shows creep compliances as functions of time for the given drying conditions.

Table 3.2 Creep compliances approximated by power functions by least square methods

| Drying condition | Creep compliance ($cm^2/kg$) |
|---|---|
| I | $JR = 0.5715\times10^{-3}\times t^{0.2263}$<br>$JR' = 0.1741\times10^{-3}\times t^{0.09373}$ |
| | $JT = 0.6855\times10^{-3}\times t^{0.2198}$<br>$JT' = 0.2381\times10^{-3}\times t^{0.1188}$ |
| II | $JR = 0.4786\times10^{-3}\times t^{0.1522}$<br>$JR' = 0.1347\times10^{-3}\times t^{0.1027}$ |
| | $JT = 0.6067\times10^{-3}\times t^{0.1760}$<br>$JT' = 0.1884\times10^{-3}\times t^{0.1149}$ |
| III | $JR = 0.7586\times10^{-3}\times t^{0.09170}$<br>$JR' = 0.1349\times10^{-3}\times t^{0.04505}$ |
| | $JT = 0.7568\times10^{-3}\times t^{0.2244}$<br>$JT' = 0.1603\times10^{-3}\times t^{0.07826}$ |

$JR$ and $JT$ : Creep compliances under drying in the radial and the tangential directions, respectively,

$JR'$ and $JT'$: Creep compliances at the equilibrium state of moisture in the radial and the tangential directions, respectively,

$t$ (>0.1) : Time (min).

Elastic compliances for drying conditions were obtained approximately from $J(0)=J(0.1)$.

The parameter $\kappa$ in Eq.(3-1.14) can then be determined as

$$\Psi = \kappa \Delta MC \qquad (3\text{-}2.1)$$

where $\Psi = (J/J_0)/(J'/J_0')-1$, and

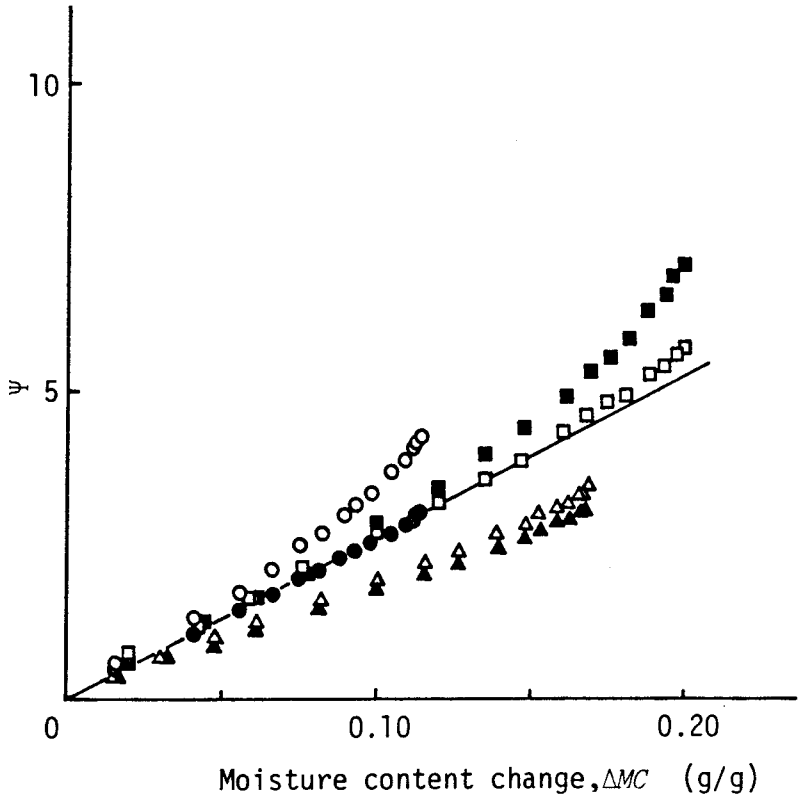


Fig.3.9 Determination of constant κ based on Takemura's theory

○ : Condition I (74%RH) in the radial direction,

● : Condition I (74%RH) in the tangential direction,

△ : Condition II (32%RH) in the radial direction,

▲ : Condition II (32%RH) in the tangential direction,

□ : Condition III (11%RH) in the radial direction,

■ : Condition III (11%RH) in the tangential direction.

$\Delta MC$ = Moisture content change (g/g).

According to Eq.(3-2.1), the variable Ψ is linearly related to the moisture content change $\Delta MC$ , as expressed by a straight line passing through the origin. Fig.3.9 shows how this relationship is obtained from the creep data at the given drying conditions. A linear relationship between the variables Ψ and $\Delta MC$ is apparently realized for each condition, although some

scatter is observed in the region where the moisture content approaches equilibrium. The parameter $\kappa$ depends on oven-dry weight per unit volume and modulus of elasticity according to Takemura[80]. Since serial sections were used for these experiments, wood density can be assumed to be constant. Since the initial moisture content for each condition was almost the same, the modulus of elasticity can also be considered the same after a moisture content change of $\Delta MC$. Therefore, the parameter $\kappa$ in Eq.(3-2.1) should only depend on grain direction. However, the dependence of the parameter on grain direction is unclear, and some scattering according to drying condition can be observed from the figure. Therefore, a common value of $\kappa$ was determined for both radial and tangential directions by use of all the plots. The regression line is

$$\Psi = 26.6\Delta MC - 0.0212$$

Thus, the parameter $\kappa$ equals 26.7 which is in good agreement with the published value[80].

The dependence of the moduli of elasticity in the radial ($E_R$(kg/cm$^2$)) and the tangential ($E_T$(kg/cm$^2$)) directions on moisture content was determined by use of reciprocals of elastic compliances obtained by creep experiments under both drying and moisture equilibrium conditions. A linear relationship between modulus of elasticity and moisture content was assumed in the moisture content range used. The regression lines are

$$E_R = 10332 - 35031 \times MC, \text{ and}$$

$$E_T = 8253 - 26567 \times MC.$$

Poisson's ratios were chosen as $\mu_{RT}=0.54$ and $\mu_{TR}=0.32$, which are average values of softwoods from the literature.[91)]

Table 3.3 shows approximate equations of basic shrinkage as a function of moisture content, and observed shrinkage and creep compliance as a function of time, for two grain directions measured and for the drying conditions used.

Table 3.3 Approximate equations of basic shrinkage, observed shrinkage, and creep compliance under drying in both the radial and the tangential directions

| Factor | | Unit | Value |
|---|---|---|---|
| Basic shrinkage | | mm/mm | $BSR = 0.03198-0.1547\times MC$<br>$BST = 0.07101-0.3078\times MC$ $(MC < 0.15)$ |
| | | | $BSR = 0.03176-0.1995\times MC+0.3136\times MC^2$<br>$BST = 0.08990-0.5612\times MC+0.8738\times MC^2$ $(MC \geq 0.15)$ |
| Observed shrinkage | I | mm/mm | $OSR = 0.3359\times10^{-2}+0.9872\times10^{-4}\times t-0.2422\times10^{-6}\times t^2$<br>$OST = 0.9322\times10^{-2}+0.2794\times10^{-3}\times t-0.8459\times10^{-6}\times t^2$ |
| | II | | $OSR = 0.1457\times10^{-2}+0.3093\times10^{-3}\times t-0.1012\times10^{-5}\times t^2$<br>$OST = 0.9903\times10^{-2}+0.5282\times10^{-3}\times t-0.1704\times10^{-5}\times t^2$ |
| | III | | $OSR = 0.6508\times10^{-3}+0.3597\times10^{-3}\times t-0.1198\times10^{-5}\times t^2$<br>$OST = 0.8246\times10^{-2}+0.6076\times10^{-3}\times t-0.1964\times10^{-5}\times t^2$ |
| Creep compliance under drying | I | $cm^2/kg$ | $JR = 1.1892\times1/ER\times t^{0.09373}(1+26.7\times\Delta MC)$<br>$JT = 1.3324\times1/ET\times t^{0.1188}(1+26.7\times\Delta MC)$ |
| | II | | $JR = 1.1479\times1/ER\times t^{0.1027}(1+26.7\times\Delta MC)$<br>$JT = 1.2993\times1/ET\times t^{0.1149}(1+26.7\times\Delta MC)$ |
| | III | | $JR = 1.2468\times1/ER\times t^{0.04505}(1+26.7\times\Delta MC)$<br>$JT = 1.1909\times1/ET\times t^{0.07826}(1+26.7\times\Delta MC)$ |

*BSR* and *BST* : Basic shrinkage in the radial and the tangential directions, respectively,

*OSR* and *OST* : Observed shrinkage in the radial and the tangential directions, respectively,

*JR* and *JT* : Creep compliance under drying in the radial and the tangential directions, respectively,

$t$ : Time (min),

*MC* and $\Delta MC$ : Moisture content (g/g) and moisture content change (g/g), respectively.

### 3-2.2 Results of Calculation and Discussion

The first step is the calculation of moisture distribution in Subroutine DIFFUS. Since the ranges of position and time were given as 0.5 cm and 150 min, respectively, and since the number of increments of $x$ and $t$ as 5 and 900, respectively, the mesh size of $\Delta x$ and $\Delta t$ became 0.1 cm and 10 sec, respectively. As the drying temperature was the same in Chapter 2-2, the same concentration-dependent diffusion coefficient was used. Initial conditions as given in Table 3.1 for drying conditions I, II, and III were assumed to be uniform distributions. Surface moisture contents were estimated from measurements of drying rate and wood temperature during drying with the method described in Section 2-1.2. Moisture distributions were then calculated by numerical solution of the proposed diffusion equation. Fig.3.10 shows moisture distributions during drying for conditions I, II, and III. The moisture distributions were corrected in each iteration based on the average moisture content during drying. The calculated moisture content $CM$(L,M) was rearranged before the calculation of drying stresses,i.e., mesh size $\Delta t$ was chosen as 10 sec for the first 10 minutes and thereafter as 60 sec. This is necessary since the moisture gradients at the surface increase rapidly during the first 10 minutes of drying, and a larger increment $\Delta t$ would cause instability of the system.

Since all the results showed the same stress patterns, drying stresses for condition II in the tangential direction as a function of time are shown as an example in Fig.3.11. Numbers show the distance from the wood surface in millimeters.

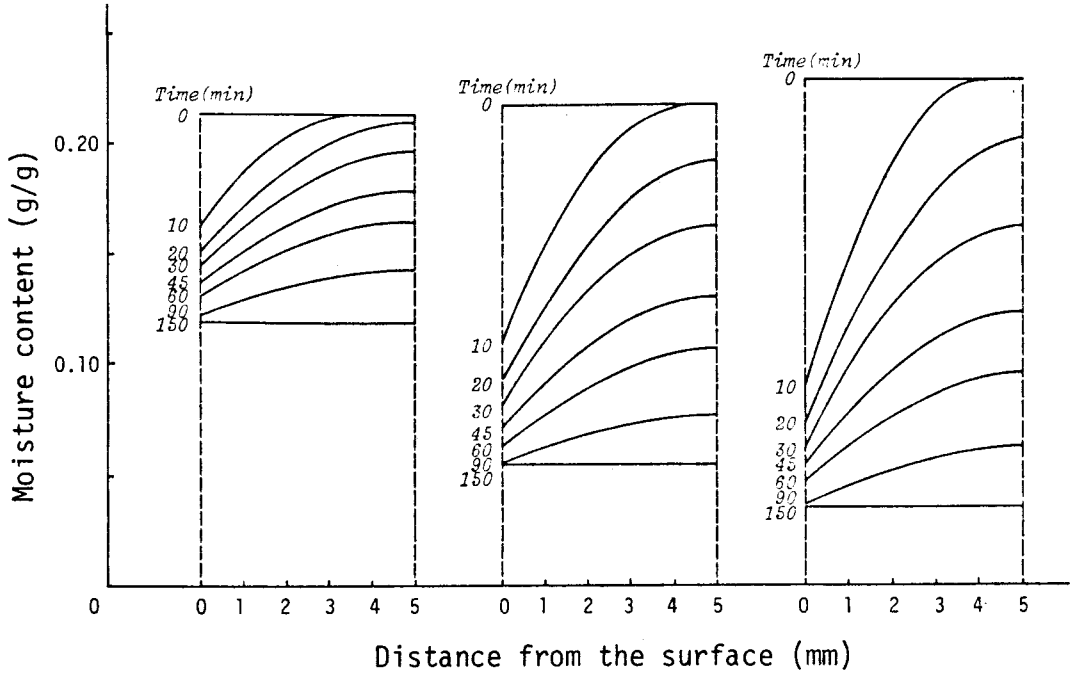


Fig.3.10 Moisture distribution through the specimen thickness calculated by the diffusion equation
Left: Condition I (74%RH),
Middle: Condition II (32%RH),
Right: Condition III (11%RH).

At the very early stages of drying, tensile stresses develop rapidly at the wood surface (number 0) and reach a maximum of 23.8 kg/cm$^2$, while the internal parts are under compression.

The second stage is the stress reversal period. The surface tensile stress decreases and becomes zero at the 13 minute point. The outer zone (number 1) which is slightly stressed in compression in the early stages has almost the same pattern as the surface. The inner zones (number 2-5) reach maxima of compressive stress, which then becomes zero in one layer after another.

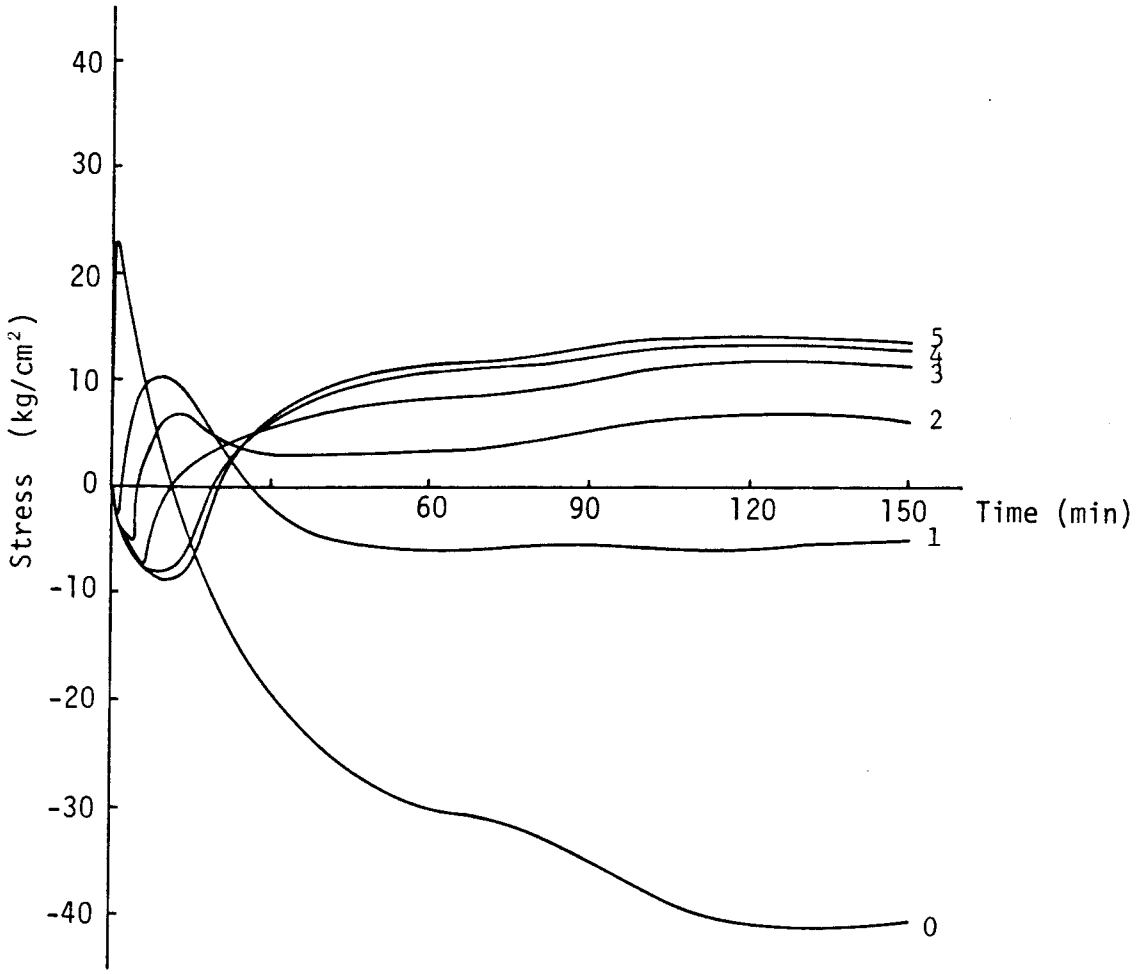


Fig.3.11 Calculated drying stresses for condition II in the tangential direction as a function of drying time

Numbers show distance from the surface (mm).

The third stage is the period after the reversal in stress. The surface compressive stress increases rather fast up to 90 minutes of drying. Then it gradually reaches a maximum of 40.9 kg/cm$^2$ at the 132 minute point, and thereafter decreases slightly. On the other hand, the compressive stress in the outer zone reaches its maximum much faster and then tends to decrease slightly. The inner zones stressed in tension after the reversal

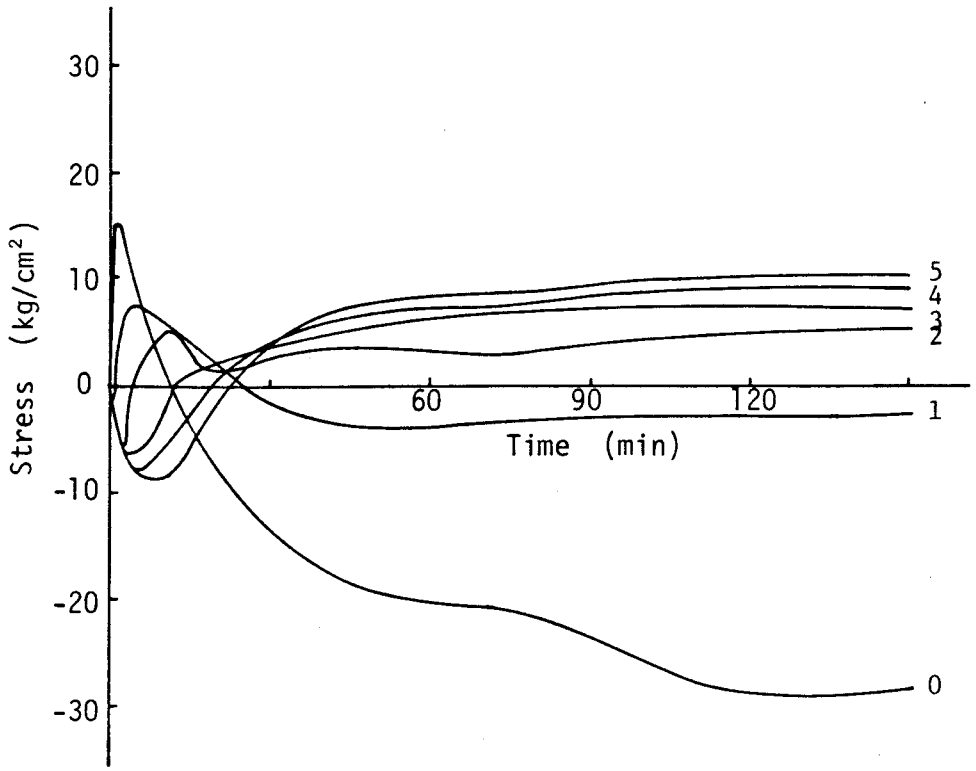


Fig.3.12 Calculated drying stresses for condition II in the radial direction as a function of drying time

Numbers show distance from the surface (mm).

in stress keep rather flat stress patterns and finally show residual stresses in tension. Among the inner zones, the maxima of compressive and of tensile stresses are largest at the center of the wood.

Fig.3.12 shows the drying stresses in the radial direction for condition II, which have the same patterns as in the tangential direction. However, the maximum tensile and compressive stresses at the surface are 15.9 and 28.9 kg/cm$^2$, respectively, or some 30% lower than those in the tangential direction. In general, it is known that wood is stronger in the radial than

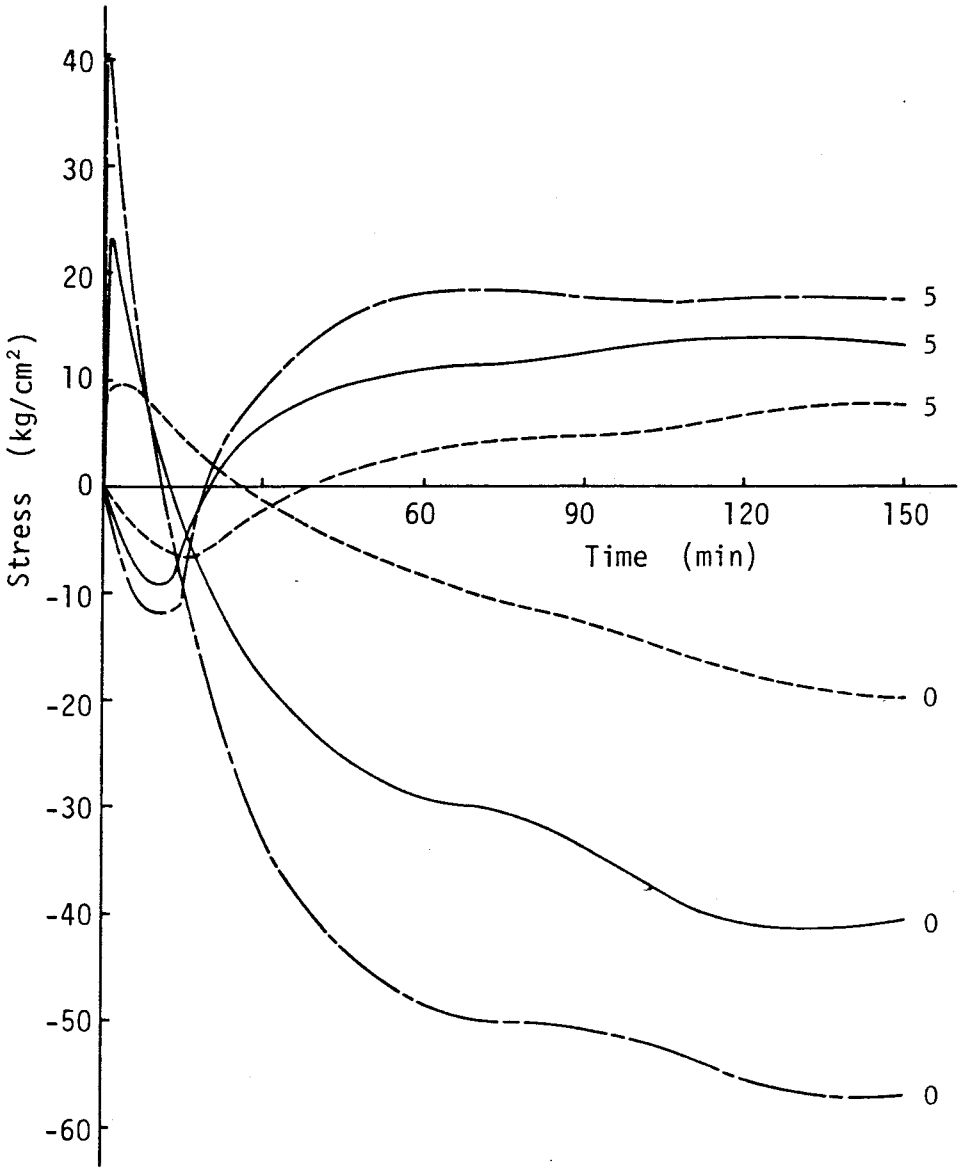


Fig.3.13 Comparison of the drying stresses in condition I,II, and III in the tangential direction
Numbers show distance from the surface (mm).
----: Condition I, ———: Condition II,
—·—·—: Condition III.

in the tangential direction because of the presence of ray tissue. The results obtained indicate that drying checks in the transverse plane of wood should occur by cleavage in the

radial plane because of the low strength and high stresses in the tangential direction.

Fig.3.13 shows drying stresses at the surface and the center in the tangential direction for each condition, in order to discuss the effect of relative humidity conditions during drying on drying stresses. It is apparent from the figure that the magnitude of the drying stresses increases with decreasing relative humidity. The maximum tensile stresses at the surface at the early stage of drying (which is the period of danger with respect to surface checks), for example, are 9.8, 23.8, and 40.8 $kg/cm^2$ for drying conditions I, II, and III, respectively. The decrease of relative humidity causes a faster drying rate. This leads to steeper moisture gradients especially at the early stage of drying as shown in Fig.3.10. The moisture gradients at the surface, for example at the 1 minute point, for the conditions I, II, and III are 0.222, 0.559, and 0.823 m.c./cm, respectively, which is almost in proportion to the magnitude of the maximum tensile stress at the surface. Although the time when the tensile stress of the surface reaches maximum is a little different for each condition, this discussion suggests that the moisture gradients of the surface at that time strongly affect the drying stresses at the early stage.

On the other hand, no distinct difference in moisture gradient among drying conditions I, II, and III is evident after 90 minutes of drying. However, the magnitude of the drying stresses at both the surface and the center in the later stage of drying indicates an obvious difference among the drying

conditions just as in the early stage. The shrinkage of the outer portions is restrained more at the early stage with steeper moisture gradients. As a result, after the reversal in stress when the core tries to shrink it is restrained more and larger drying stresses develop. Thus, the moisture gradients at the early stage of drying seem to play the most important role in the occurence of the drying stresses throughout the drying period.

In order to consider the effect of the inelastic strain component on drying stresses, drying stresses were calculated with the maximum and the minimum observed values of the parameter $\kappa$ in Eq.(3-2.1). The results showed the same stress patterns, and showed that changes of $\kappa$ had only little effect on the maximum tensile stress of the surface at the early stage. However, the muximum compressive stress at the later stage increased or decreased about 20-30% using the minimum or maximum value of the parameter $\kappa$.

Changes of Poisson's ratio by some 10% changed the drying stresses by only a few percent.

Fig.3.14 shows inelastic strains for condition II in the tangential direction as a function of time. The tensile inelastic strain at the surface reaches a maximum at the 13 minute point which coincides with the time of reversal in stress. The other portions which show a compressive inelastic strain at the early stage successively develop tensile inelastic strains. At the final stage of drying, the inelastic strains of all portions are tensile. Thus, tension set occurs through the entire thickness of the specimen.

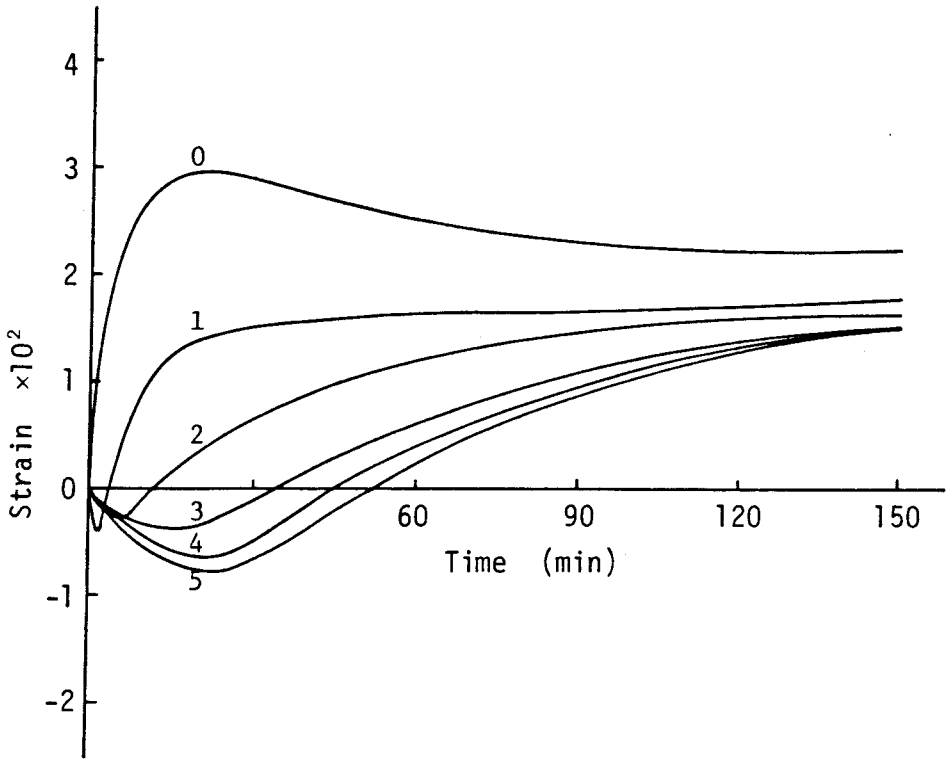


Fig.3.14 Calculated inelastic strains for condition II in the tangential direction as a function of drying time. Numbers show distance from the surface (mm).

Fig.3.15 shows a comparison of the inelastic strains of drying conditions I, II, and III. It indicates that the magnitude of the maximum tensile inelastic strain at the surface and of the maximum compressive inelastic strain at the center increase with increasing rate of drying, and that the tension set at the final stage increases also with increasing rate of drying. Because specimens were dried at a constant temperature of 40°C for all the experiments, the drying conditions do not affect the viscous properties of wood. Eq.(3-1.24) for the inelastic strains suggests that larger stresses cause larger inelastic strains if the viscous properties of wood are unchanged.

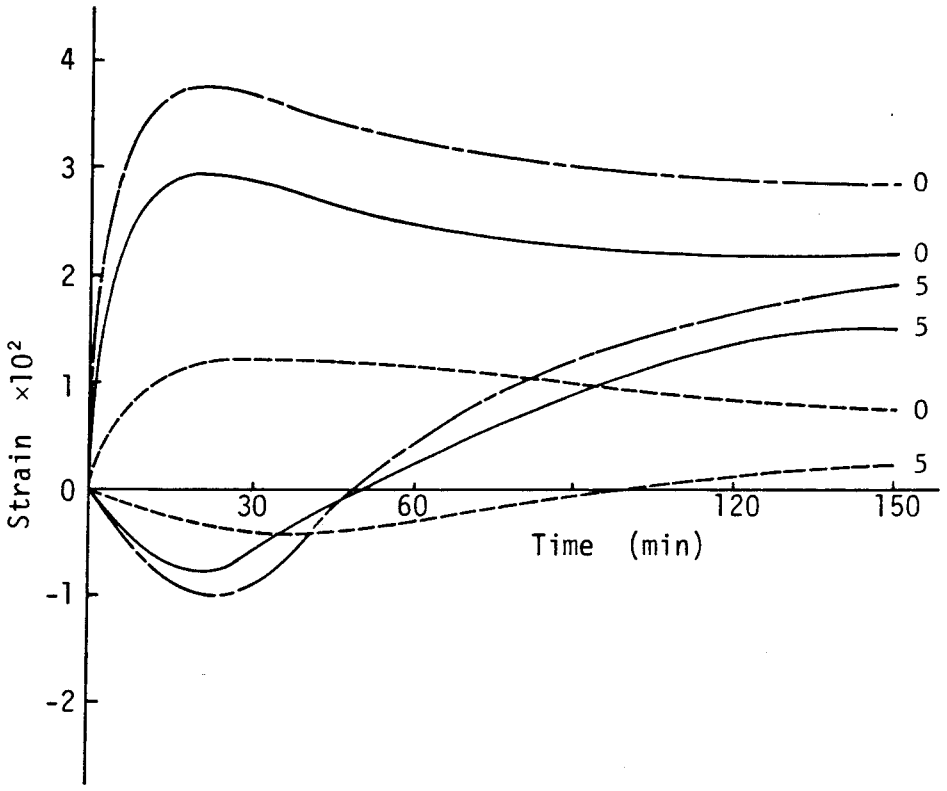


Fig.3.15 Comparison of the inelastic strains in condition I, II, and III in the tangential direction

Numbers show distance from the surface (mm).

– – – –: Condition I, ———: Condition II,

——·——: Condition III.

The above discussion explains that drying defects occur more often when the rate of drying increases. Such comparisons of the drying stresses under various conditions make it possible to predict the magnitude of drying defects such as surface checks and casehardening, and the stage of drying when they occur. Quantitative estimation and prediction of drying stresses of this kind will give useful information for studies of drying schedules and drying defects.

## 3-3. *Summary*

Numerical solutions of the proposed diffusion equation made it possible to predict moisture distributions in wood during drying, as shown in Part 2. In this part, a method of computing drying stresses resulting from moisture gradients in wood during drying was discussed. The drying stresses in the transverse plane of wood under given drying conditions were estimated, and the results were compared with each other. The results may be summarized as follows:

1) A method for calculating the drying stresses of wood during drying was established, where wood was dealt with as a viscoelastic and orthotropic material. A constitutive equation was derived for stresses in the transverse plane owing to moisture flow in the longitudinal direction of wood. The equation was then combined with the predictive method for moisture distribution by solution of the diffusion equation. Given the necessary information on basic shrinkage, the viscoelastic properties of wood, and observed shrinkage, the drying stresses could be estimated.

2) Drying stresses in the transverse plane of wood under the drying conditions used,i.e., a constant temperature of 40°C and relative humidity conditions of 74, 32, and 11%RH, were calculated. The calculated drying stresses showed the common reversal patterns in stress and increased with an increase in drying rate which is a major factor in the variation of moisture distribution. The moisture gradients at the surface at the early stage of drying seemed to play the most important

role in the development of the drying stresses through the whole drying period.

# CONCLUSION

Moisture movement and drying stresses in wood are fundamental subjects in wood science and wood technology, respectively, and both are closely related with each other. However, few studies have been found which deal with these phenomena using a consolidated theory that can describe them quantitatively.

The present study deals with the quantitative analysis of moisture movement in wood below the fiber saturation point and of drying stresses in wood resulting from moisture gradients during drying. The results of each part are summarized as follows:

1) The equation for representing moisture movement in wood was considered in view of thermodynamics of irreversible processes. Based on this theory, the following equation was derived instead of the conventional Fick's law of diffusion.

$$\frac{\partial u}{\partial t} = \frac{\partial}{\partial x}\left(D_{\mu}\frac{\partial \ln P}{\partial x}\right) \qquad (1\text{-}2.17)$$

where $u$ is the moisture content, $D_{\mu}$ the diffusion coefficient, and $P$ the equilibrium vapor pressure.

Changes in moisture distribution in the longitudinal direction of Hinoki wood were measured during drying by means of

soft X-ray densitometry. By use of three diffusion equations, the diffusion coefficients $D_c$, $D_p$, and $D_\mu$ were determined from the moisture distribution data. $D_c$ showed no obvious dependence on moisture content $u$, and the degree of scatter was rather high. On the other hand, $D_p$ and $D_\mu$ increased exponentially with increasing moisture content $u$, but the regression line of $D_\mu$ and $u$ showed better fit than that of $D_p$ and $u$. Thus, it was concluded that the diffusion coefficient $D_\mu$ is preferred as the parameter in the diffusion equation, and the proposed equation is valid for describing moisture movement in wood quantitatively.

The dependence of the diffusion coefficient $D_\mu$ on temperature obeyed Arrhenius equation. The average value of Arrhenius activation energy was calculated from experimental data as 8.7 kcal/mol. This supported the view that the migration mechanism of bound-water molecules is surface diffusion in the cell-wall substance.

2) Numerical solution of the proposed diffusion equation made it possible to predict moisture distributions in wood during drying with sufficient accuracy: the average difference between predicted and measured moisture content over all drying times and positions was 0.008 m.c. Among the input data, the surface moisture content as a boundary condition and the diffusion coefficient seemed to be the significant factors which affected the accuracy of the approximation.

3) A computing method for predicting drying stresses resulting from moisture gradients in wood during drying was established. Wood was dealt with as a viscoelastic and orthotropic material, and the constitutive equation for the stresses in

the transverse plane was combined with the method for predicting moisture distribution in wood during drying.

The calculated drying stresses showed the common reversal patterns, and they increased with increasing rate of drying. The moisture gradients at the surface in the early stages of drying seemed to play the most important role in the occurence of drying stresses through the whole drying period. All of the results showed good agreement with present knowledge of drying and drying stresses, which supports the validity of the predictive method for drying stresses.

Although moisture movement and drying stresses in wood in the past have been investigated independently in wood science and in wood technology, respectively, the present study has succeeded in relating them to each other. There are still many subjects to be investigated: they are, for example, 1) free water movement in wood, and 2) moisture movement in wood under the unsteady-state of temperature. Further studies in these fields are needed and can be expected in the future.

## ACKNOWLEDGEMENT

The author wishes to express his sincerest appreciation to Professor Kanji Nakato, Department of Wood Science and Technology, Faculty of Agriculture, Kyoto University, for his direction and encouragement during the entire course of the present study.

The author is also deeply grateful to Professor Hajime Okamoto and Dr. Takeshi Sadoh, Department of Wood Science and Technology, Faculty of Agriculture, Kyoto University, and to Professor Hikaru Sasaki, Wood Research Institute, Kyoto University, for their advice and suggestions.

Special thanks are due to Professor Arno P. Schniewind, Forest Products Laboratory, College of Natural Resources, University of California, for his counsel and critical reading of the manuscript.

The author expresses his appreciation to the members of the Laboratory of Wood Technology, Department of Wood Science and Technology, Faculty of Agriculture, Kyoto University, for their kind assistance and suggestions.

## REFERENCES


1) S.Enomoto and K.Kojima: *Mokuzai Gakkaishi*, 13, 87 (1967)

2) H.Polge and P.Luts: *Holztechnologie*, 10, 75 (1969)

3) N.Takamura: *Mokuzai Gakkaishi*, 17, 415 (1971)

4) T.Sadoh, K.Nakato, K.Shimada, and S.Asahara: *Bull. Kyoto Univ. Forests*, 47, 159 (1975)

5) P.R.Steiner, L.A.Jozsa, M.L.Parker, and S.Chow: *Wood Science*, 11, 48 (1978)

6) M.L.Parker and L.A.Jozsa: *Wood and Fiber*, 5, 192 (1963)

7) H.Polge: *Wood Science and Technology*, 12, 187 (1978)

8) S.Kawai, K.Nakato, and T.Sadoh: *Mokuzai Gakkaishi*, 22, 649 (1976)

9) A.Schneider: *Holz als Roh- und Werkstoff*, 18, 269 (1960)

10) S.Kawai: M.S.Thesis, Kyoto Univ., p.38 (1976)

11) A.Fick: *Annln Phys.*, 94, 594 (1855)

12) R.McGregor:"Diffusion and Sorption in Fibers and Films", Academic Press, p.17 (1974)

13) G.Bramhall: *Wood Science*, 8, 153 (1976)

14) S.R.de Groot and P.Mazur:"Non-equilibrium Thermodynamics", North-Holland Pub. Co., p.23 (1969)

15) S.Kawai, K.Nakato, and T.Sadoh: *Mokuzai Gakkaishi*, 24, 273 (1978)

16) J.F.Martley: *For. Prod. Res. Tech. Paper No.2*, Dept. Sci. and Indust. Res., (Gt.Britain) London
[ C.Skaar: *Journal of FPRS*, 1954, 403 ]

17) A.B.Newman: *Trans. Amer. Inst. Chem. Engin.*, 27, 310 (1931)

18) C.Matano: *Japanese Jour. Physics*, 8, 109 (1933)

19) J.Crank and M.E.Henry: *Trans. Faraday Soc.*, 45, 636 (1949)

20) J.Crank and M.E.Henry: *Trans. Faraday Soc.*, 45, 1119 (1949)

21) S.Prager and F.A.Long: *Jour. Amer. Chem. Soc.*, 73, 4072 (1951)

22) K.Egner:"Forschungsberichte Holz", Heft 2, 91pp, illus. Berlin (1934)
[ C.Skaar: *Journal of FPRS*, 1954, 403 ]

23) A.J.Hailwood and S.Horrobin: *Trans. Faraday Soc.*, 42B, 84 (1946)

24) A.J.Stamm:"Wood and Cellulose Science", Ronald Press, p.152 (1964)

25) H.A.Spalt: *For. Prod. Jour.*, 8, 288 (1958)

26) A.J.Stamm: *For. Prod. Jour.*, 9, 27 (1959)

27) A.J.Stamm: *Jour. Physical Chemistry*, 60, 76 (1956)

28) A.J.Stamm: *Jour. Physical Chemistry*, 60, 83 (1956)

29) A.J.Stamm: *For. Prod. Jour.*, 10, 644 (1960)

30) T.Yokota: *Mokuzai Gakkaishi*, 5, 143 (1959)

31) T.Ogura: *Bull. Government For. Experiment Station*, 45, 55 (1945)

32) T.Ogura: *Bull. Government For. Experiment Station*, 54, 165 (1954)

33) T.Ogura and M.Umehara: *Mokuzai Gakkaishi*, 3, 51 (1957)

34) T.Maku: *Wood Research*, 13, 81 (1954)

35) E.T.Choong: *For. Prod. Jour.*, 13, 489 (1963)

36) E.T.Choong and P.J.Fogg: *For. Prod. Jour.*, 18, 66 (1968)

37) E.M.Martin and W.W.Moschler: *Wood Science*, 2, 186 (1970)

38) H.N.Rosen: *Wood Science*, 8, 174 (1976)

39) G.L.Comstock: *For. Prod. Jour.*, 13, 97 (1963)

40) C.A.Hart: *For. Prod. Jour.*, 14, 207 (1964)

41) E.T.Choong: *For. Prod. Jour.*, 15, 21 (1965)

42) G.Bramhall: *Wood Science*, 9, 149 (1977)

43) H.Voigt, O.Krischer, and H.Schauss: *Hol als Roh- und Werkstoff*, 3, 305 (1940)

44) A.J.Stamm and W.K.Loughborough: *Jour. Physical Chemistry*, 39, 121 (1935)

45) R.C.Wheast ed.:"Handbook of Chemistry and Physics 55th ed." CRC Press, E-18 (1974)

46) A.J.Stamm:"Wood and Cellulose Science", Ronald Press, p.437 (1964)

47) K.Kröll: *Holz als Roh- und Werkstoff*, 9,176 (1951)

48) H.Kübler: *Holz als Roh- und Werkstoff*, 15, 453 (1957)

49) O.Kisselof: *Hoz als Roh- und Werkstoff*, 27, 245 (1969)

50) A.J.Stamm:"Wood and Cellulose Science", Ronald Press, p.50 (1964)

51) A.J.Stamm: *Wood Science*, 4,114 (1971)

52) J.Crank:"The Mathematics of Diffusion", Oxford Univ. Press, (1956)

53) T.Ogura: *Bull. Government For. Experiment Station*, 54, 173 (1954)

54) W.W.Moschler and R.E.Martin: *Wood Science*, 1, 47 (1968)

55) J.Neumann and R.D.Richtmyer:"John von Neumann, Corrected Works, vol.5", Pergamon Press, p.652 (1963)

56) S.Kawai, K.Nakato, and T.Sadoh: *Mokuzai Gakkaishi*, 24,520 (1978)

57) C.A.Hart: *Wood Science*, 9, 194 (1977)

58) W.S.McNamara and C.A.Hart: *Wood Science*, 4, 37 (1971)

59) T.Ogura: *Bull. Government For. Experiment Station*, 51, 61 (1951)

60) G.Bramhall *Wood Science*, 7, 137 (1974)

61) A.P.Schniewind: *Holzforschung*, 14, 161 (1960)

62) H.D.Tiemann:"Wood Technology", Pitman Publ.Co.,p.316 (1942)

63) J.M.McMillen: *U.S.For. Prod. Lab.*, Rep.No.1652 (1957)

64) J.M.McMillen: *For. Prod. Jour.*, 15, 71 (1955)

65) J.M.McMillen: *For. Prod. Jour.*, 15, 230 (1955)

66) R.L.Youngs and C.B.Norris: *For. Prod. Jour.*, 9, 367 (1949)

67) R.L.Youngs: *For. Prod. Jour.*, 7, 315 (1957)

68) R.L.Youngs and B.A.Bendtson: *For. Prod. Jour.*, 14, 113 (1964)

69) M.Y.Cech: *For. Prod. Jour.*, 14, 69 (1964)

70) T.Takemura: *Mokuzai Gakkaishi*, 16, 108 (1970)

71) T.Takemura: *Mokuzai Gakkaishi*, 16, 115 (1970)

72) T.Takemura: *Mokuzai Gakkaishi*, 18, 1 (1972)

73) T.Takemura: *Mokuzai Gakkaishi*, 18, 105 (1972)

74) T.Takemura: *Zairyo*, 22, 943 (1973)

75) S.Kawai, K.Nakato, and T.Sadoh: *Mokuzai Gakkaishi*, 25, 103 (1979)

76) S.Kawai, K.Nakato, and T.Sadoh: *Mokuzai Gakkaishi*, 25, 272 (1979)

77) F.P.Kollmann and W.A.Côté: "Principles of Wood Science and Technology vol.1", Springer Verlag, p.311 (1968)

78) T.Takemura: *Memoirs of the Coll. Agri., Kyoto Univ.*, 88, 31 (1966)

79) T.Takemura: *Mokuzai Gakkaishi*, 13, 77 (1967)

80) T.Takemura: *Mokuzai Gakkaishi*, 14, 406 (1968)

81) K.Takeyama: *Trans. Inst. of Japanese Architects*, 33, 6 (1944)

82) Y.Suzuki: *Jour. Japanese For. Soc.*, 31, 188 (1949)

83) L.D.Armstrong and R.S.T.Kingston: *Nature*, 185, 4716 (1960)

84) L.D.Armstrong and G.N.Christensen: *Nature*, 191, 4791 (1961)

85) L.D.Armstrong and R.S.T.Kingston: *Aust. Jour. Appl. Sci.*, 13, 257 (1962)

86) Y.Suzuki: *Trans. Japanese For. Soc.*, 61, 210 (1962)

87) K.Okusa, S.Hayashi, and Y.Kosako: *Bull. Shimane Agri. Coll.* 4, 93 (1956)

88) K.Okusa and S.Hayashi: *Mokuzai Gakkaishi*, 2, 5 (1956)

89) L.D.Armstrong: *Wood Science*, 5, 81 (1972)

90) P.U.A.Grossman: *Wood Sci. and Tech.*, 10, 163 (1976)

91) R.F.S.Hearmon: *For. Prod. Res.*, Special Rep.No.7, 6 (1948)